Applied Catalysis B: Environment and Energy 355 (2024) 124197

Contents lists available at ScienceDirect

Applied Catalysis B: Environment and Energy

journal homepage: www.elsevier.com/locate/apcatb

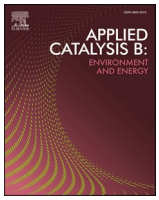

Unlocking the potential of hydrogen evolution: Advancements in 3D nanostructured electrocatalysts supported on nickel foam

Chengzhi Xiao [a,b,1], Tongzhou Hong [a,b,1], Jin Jia [b,*], Haowen Jia [b], Jiajia Li [b], Yuanyuan Zhu [b], Shanhai Ge [c,*], Conghu Liu [b], Guang Zhu [a,b,**]

[a] School of Mechanics and Optoelectronics Physics, Anhui University of Science and Technology, Huainan 232001, China
[b] Key Laboratory of Spin Electron and Nanomaterials of Anhui Higher Education Institutes, Suzhou University, Suzhou 234000, China
[c] Department of Mechanical Engineering, The Pennsylvania State University, University Park, PA 16802, USA

ARTICLE INFO

Keywords:
Nickel foam
Electrocatalysts
Water splitting
Hydrogen evolution reaction
Self-supporting electrodes

ABSTRACT

Electrochemical water splitting is crucial for sustainable energy, enabling hydrogen fuel conversion, storage, and energy transfer. This review focuses on innovative approaches to replace costly precious metal catalysts with earth-abundant elements, known for their high catalytic activity and durability in alkaline hydrogen evolution reactions. Designing self-supporting electrodes, particularly using three-dimensional (3D) nickel foam (NF) substrates, has emerged as an effective strategy to enhance electrocatalyst performance and stability. The continuous porous structure of 3D NF ensures excellent electrical conductivity and a larger active surface area. This review extensively catalogs emerging nanostructured materials directly grown on 3D NF, including sulfides, phosphides, layered double hydroxides, nitrides, oxides, selenides, and alloys. Emphasis is placed on their cutting-edge achievements in structural design, controllable synthesis, performance optimization, and elucidation of catalytic mechanism. These insights facilitate the selection and fabrication of high-performance self-supporting electrodes, accelerating the commercialization and scalability of water electrolysis technology.

1. Introduction

The energy crisis looms as one of the most pressing challenges of contemporary society [1–3]. With escalating economic growth and a concomitant surge in energy demand, the reliance on non-renewable fossil fuels such as natural gas, crude oil, and coal increasingly highlights the sustainability issues inherent in our current energy infrastructure. The depletion of fossil fuel reserves [2,4–6] and the subsequent global carbon dioxide emissions from their combustion, which contribute to around 70% of total emissions [7,8], present an environmental dilemma that cannot be ignored. As a result, the need for sustainable energy systems and the exploration of alternative solutions has become paramount [9–11]. Among the various alternative energy sources, hydrogen stands out for its cleanliness and high efficiency, emerging as a potential game-changer [12–15]. While contemporary industrial production of hydrogen — primarily through methods such as steam reforming of hydrocarbons, gasification of natural gas or coal, and fermentation of organic wastewater — accounts for over 95% of the global supply, it is evident that these practices not only consume substantial fossil resources but also contribute to environmental pollution and CO_2 emissions [16–18]. In contrast, renewable electricity-driven water electrolysis, as a route for hydrogen production, has garnered widespread attention for its potential to address both energy and environmental concerns [19–21]. However, the high cost associated with electrolytic hydrogen production remains a significant barrier to its widespread adoption, currently constituting a mere 4% of hydrogen generation [9,22,23]. Therefore, investigating avenues to reduce the costs of water electrolysis and catalyze the transition towards hydrogen energy production has become an urgent priority.

In the mainstream of commercial water electrolysis, precious metal catalysts such as Pt, Ir, and Ru are extensively employed owing to their high catalytic efficiency in the hydrogen evolution reaction (HER) and oxygen evolution reaction (OER) [24–27]. Despite their efficacy, the prohibitive cost of these materials significantly constrains their

* Corresponding authors.
** Corresponding author at: School of Mechanics and Optoelectronics Physics, Anhui University of Science and Technology, Huainan 232001, China.
E-mail addresses: jiajin@ahszu.edu.cn, ifc_jiaj@ujn.edu.cn (J. Jia), sug13@psu.edu (S. Ge), guangzhu@ahszu.edu.cn (G. Zhu).
[1] Chengzhi Xiao and Tongzhou Hong are co-first authors and contributed equally to this study.

https://doi.org/10.1016/j.apcatb.2024.124197
Received 28 February 2024; Received in revised form 28 April 2024; Accepted 10 May 2024
Available online 12 May 2024
0926-3373/© 2024 Elsevier B.V. All rights are reserved, including those for text and data mining, AI training, and similar technologies.

feasibility for large-scale application [28–30]. This challenge has prompted researchers to explore cost-effective, non-precious metal catalysts that leverage the Earth's abundant transition metal resources to reduce costs while maintaining or surpassing the catalytic performance of existing materials. Various studies have demonstrated that non-precious metal materials, including transition metal oxides, sulfides, phosphides, layered double hydroxides, selenides, and nitrides, exhibit significant catalytic activity in OER and HER [31–33]. However, these materials often exhibit higher overpotential compared to precious metal catalysts, and achieving long-term stability remains a research bottleneck. In light of this, the development of novel electrocatalytic materials that offer low cost, high efficiency, superior activity, and enduring stability is of strategic significance to advance the efficiency and economic viability of water splitting technologies [34–36].

Recent research has synthesized an array of electrocatalysts for the HER [37–39], broadly categorized into binder-loaded and self-supported types. Binder-loaded catalysts, although immobilized on conductive substrates via binders like Nafion, inevitably introduce additional interfacial resistance and can obstruct active sites (Fig. 1**a**), potentially reducing the catalyst's HER activity and stability [40]. In contrast, self-supported catalysts, exemplified in Fig. 1**b** [41], directly constructed on conductive substrates, present significant advantages [42–45]: (1) robust anchoring and dispersion of active catalysts on the substrate enhance effective loading and number of active sites; (2) circumventing polymer binders and conductive additives exposes more catalytic active sites; (3) nanoengineering with zero-dimensional (0D), one-dimensional (1D), two-dimensional (2D), or three-dimensional (3D) structures amplifies the electrochemically active surface area and facilitates rapid electron and mass transfer, optimizing reaction kinetics; (4) strong adhesion and high integration between catalysts and substrates ensure stability under sustained high current density water splitting; (5) surface wettability engineering allows for tailored nano-catalyst deposition based on composition and structure, where superhydrophilic surface design promotes intimate contact between catalytic active sites and electrolyte, enhancing catalytic activity, while superhydrophobic electrode surfaces aid in bubble detachment, preventing bubble accumulation under high current densities and protecting active catalysts from detachment, thereby minimizing interfacial resistance; (6) the simplified fabrication process of self-supported catalysts and the obviation of additional polymer binders and conductive additives offer cost reduction potential, showcasing immense prospective application potential in hydrogen production to meet anticipated energy demands [46, 47]. Compared to traditional powder catalysts, self-supported catalysts are more suited for industrial applications. Although significant progress toward practicality in self-supported electrodes, overcoming the challenges to meet industrial standards and enhance electrocatalyst performance for HER remains a daunting task, with current levels insufficient for commercialization [48–50]. At high current densities, the primary challenge for electrocatalysts is the stringent requirement for efficient electron and mass transfer. Consequently, the rational design of electrocatalytic electrodes with optimal morphologies and structures is critical for enhancing electron conductivity, exposing active sites, facilitating ion diffusion rates, improving reaction kinetics, and ensuring mechanical stability. All of which decisively influence HER performance at high current densities. Thus, the development of efficient and stable self-supported electrocatalysts is urgently required for industrial water electrolysis hydrogen production [51–53].

In the current research paradigm, commonly employed substrates encompass a variety of metals, carbonaceous materials, and other conductive media, such as carbon fiber paper (CFP) [54–56], carbon cloth (CC) [57–59], graphite plates [60–62], and metallic foams (e.g., Ni, Co, Ni/Co, Ni/Cu foam) [63–65], metallic meshes (such as Fe mesh, Ti/Cu mesh) [66–68], metallic plates/foils (including Ti plate and W/Mo/Cu foils) [69–71], and F-doped tin oxide (FTO) [72–74]. Novel 3D porous metallic materials, with their expansive specific surface area and hierarchically porous architecture, effectively shorten ion diffusion pathways, thereby enhancing ionic and electronic conductivity and attracting widespread attention [75–77]. Nickel foam (NF), in particular, with its superior electronic conductivity, optimized 3D porous structure, and high specific surface area, has emerged as the material of choice for electrode substrate and support frameworks [78–81]. For instance, Du et al. [82] developed a superhydrophilic self-supported Ni/Y_2O_3 heterostructure catalyst that exhibits exceptional durability and performance in alkaline HER. This catalyst remained stable and maintained a current density of 1 A cm^{-2} over 500 h, significantly outperforming the conventional Pt/C (20%) electrode. Additionally, Qian et al.[83] successfully drove the evolution of grain boundaries in a Cu-mediated NiMo bimetallic oxide (MCu-BNiMo), establishing its application in industrial alkaline electrolyzers. The $MCu_{0.10}$-BNiMo catalyst achieved a current density of 0.5 A cm^{-2} at 2.12 V and 0.1 A cm^{-2} at 1.79 V, which is approximately five times higher than that of the state-of-the-art HER catalyst (Pt/C). These strategies provide valuable insights into scaling high-efficiency HER catalysts for industrial hydrogen production.

The development of efficient, stable, and cost-effective catalysts is crucial for the long-term progression of water splitting technologies [84–86]. In acidic electrolytes, catalysts often exhibit superior HER activity due to the high concentration of protons (or hydrated hydrogen ions). However, NF materials display suboptimal stability in such acidic solutions, making them prone to oxidative corrosion. Extracting hydrogen from pure water under neutral conditions poses a significant challenge due to reduced conductivity and reactivity, with the technology still largely confined to laboratory research. In contrast, hydrogen production via alkaline electrolysis is the most mature and longest-established industrial technology. In alkaline media, NF demonstrates enhanced stability, avoiding corrosion and dissolution, thereby revealing greater potential for application. Additionally, it is noteworthy that in acidic media, the diffusion of gases might produce acid mists, compromising the purity of the produced hydrogen. Alkaline

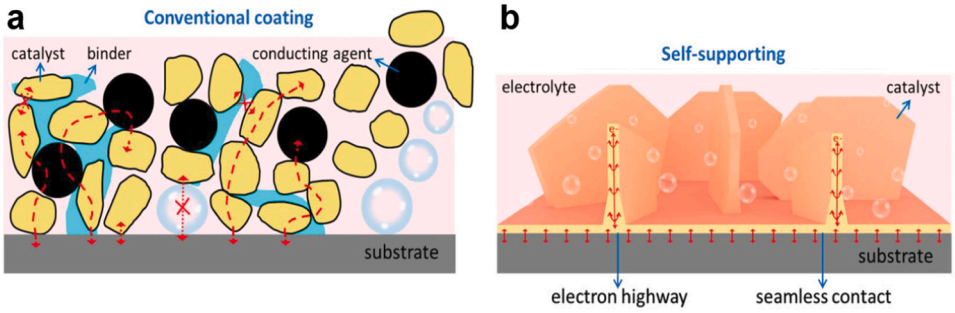

Fig. 1. Schematic illustration of the structural and electrochemical features of: (a) conventional powdery catalysts coated on current collectors with polymer binder and carbon additives, and (b) self-supported electrode with *in situ* grown catalysts on the substrates. (a) and (b) Reproduced with permission [41]. Copyright 2019, Wiley-VCH.

water electrolysis circumvents this issue, making it a more economically viable and safer green hydrogen production technology. Catalysts grown on NF substrates are considered an effective strategy to enhance the activity of the HER in alkaline media. Based on this, precision engineering of the crystallography and architecture of electrocatalytic materials can optimize electron transport efficiency, the exposure of active sites, ion diffusion rates, reaction dynamics, and mechanical stability, thereby substantially augmenting electrocatalytic performance.

Despite considerable interest and numerous research achievements in the use of Ni-based electrocatalysts for the HER, recent review literature has predominantly focused on the performance of various self-supported substrates for HER or has centered on studies of electrocatalysts for both HER and OER on NF carriers. However, there has been a noticeable lack of comprehensive, systematic reviews specifically addressing HER electrocatalysts on NF substrates. Addressing this research gap is crucial, as it involves delving into electrocatalysts on NF platforms for the HER, which holds significant practical importance. This endeavor aims to identify and promote promising self-supported electrocatalytic materials for practical HER applications. This review will encapsulate the latest research advances of NF-based electrocatalysts under alkaline conditions (Fig. 2), offering not only an overview of the HER mechanisms and the evaluation metrics for electrocatalyst performance but also emphasizing systematic studies on their structural design, electrode fabrication processes, and catalytic efficiencies. The spectrum of NF-based electrocatalytic materials discussed includes sulfides, layered double hydroxides, selenides, phosphides, nitrides, oxides, and alloys. Finally, the review delves into the prospective challenges and future outlook for NF-based electrocatalysts.

2. Electrochemical HER

2.1. Mechanism of HER

The electrolysis of water involves a non-spontaneous process with a positive Gibbs free energy (ΔG), requiring energy input from an external power source to induce spontaneity ($\Delta G < 0$) [87, 88]. The theoretical decomposition voltage (E_0) of water is calculated to be 1.23 V, based on the equation $\Delta G = -n \times E_0 \times F$, where F denotes the Faraday constant and n represents the number of electrons transferred during the electrode reaction. The cathode undergoes a reduction reaction, producing hydrogen gas, while the anode undergoes an oxidation reaction, releasing oxygen. Due to low conductivity of pure water, electrolytes such as H_2SO_4, NaOH, or KOH are commonly added to reduce the ohmic resistance of the electrolyte and enhance the conductivity of the system, ensuring smooth progression of electrolysis [89].

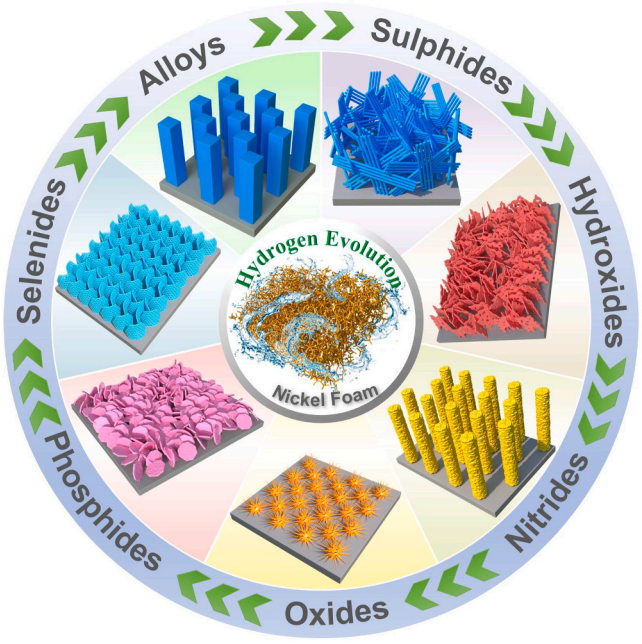

Fig. 2. Schematic illustrating the design of NF-based materials for efficient electrocatalysts.

In acidic environments, the HER proceeds through a series of two consecutive steps. Initially, in the Volmer step (Eq. 1), protons (H^+) are electrochemically adsorbed at active sites on the catalyst surface to form adsorbed hydrogen atoms (H*). Subsequently, these adsorbed hydrogen atoms (H*) can react with another proton and an electron in the Heyrovsky step (Eq. 2), leading to the formation of H_2 through an electrochemical desorption process. Alternatively, the Tafel step (Eq. 3), a purely chemical desorption process, occurs when two adsorbed hydrogen atoms (H*) combine on the surface of the electrocatalyst to produce H_2.

Volmer step:

$$H^+ + e^- + * \rightarrow H^* \quad (1)$$

Heyrovsky step:

$$H^+ + e^- + H^* \rightarrow H_2 + * \quad (2)$$

Tafel step:

$$2H^* \rightarrow H_2 + 2^* \quad (3)$$

The mechanism of HER under alkaline conditions has been thoroughly analyzed in the scholarly domain (Fig. 3**a**). In an alkaline medium, the HER process initially involves the dissociation of H_2O into adsorbed hydrogen (H*) and hydroxide ions (OH^-) due to the scarcity of protons. Subsequent reaction steps involve water molecules serving as the proton donor, encompassing the Volmer and Heyrovsky steps [90–92]. In the Volmer step, water molecules interact with the catalyst surface to produce H* (Eq. 4). The reaction then diverges into two distinct pathways. The Heyrovsky step involves the reaction of H* with a proton from another water molecule in the electrolyte to form H_2 (Eq. 5). The alternative pathway is the Tafel step, where two H* species combine to form H_2 (Eq. 6). In alkaline environments, the HER proceeds either via the Volmer-Heyrovsky pathway or the Volmer-Tafel pathway (Fig. 3**b**). The intrinsic activity of HER in alkaline electrolytes primarily depends on the ability to cleave the H-OH bond and the binding energy of the hydrogen intermediates. Compared to acidic conditions, the cleavage of the HO-H bond in alkaline media introduces an additional energy barrier for forming protons (H^+) required for the Volmer and Heyrovsky steps. From the perspective of catalyst design, strategies to enhance performance in alkaline HER should aim to reduce the energy barrier for water dissociation. Research has shown that materials with oxophilic properties can play a crucial role in the water activation process, leading to the design and fabrication of catalysts with exceptional activity in HER [93]. In other words, integrating catalysts with oxophilic components effectively reduces the energy barrier for water molecule activation on the catalyst surface, enhancing the kinetics of HER. Oxophilic metals such as Ru, Ni, and Co, due to their suitable oxophilicity, are considered favorable hosts for alkaline HER, as they can modulate the adsorption energy of water molecules, facilitating effective dissociation [94]. Therefore, selecting NF as a carrier material to optimize the overall efficacy of the catalyst represents a promising direction with significant potential.

Volmer step:

$$H_2O + e^- + * \rightarrow H^* + OH^- \quad (4)$$

Heyrovsky step:

$$H_2O + e^- + H^* \rightarrow H_2 + OH^- \quad (5)$$

Tafel step:

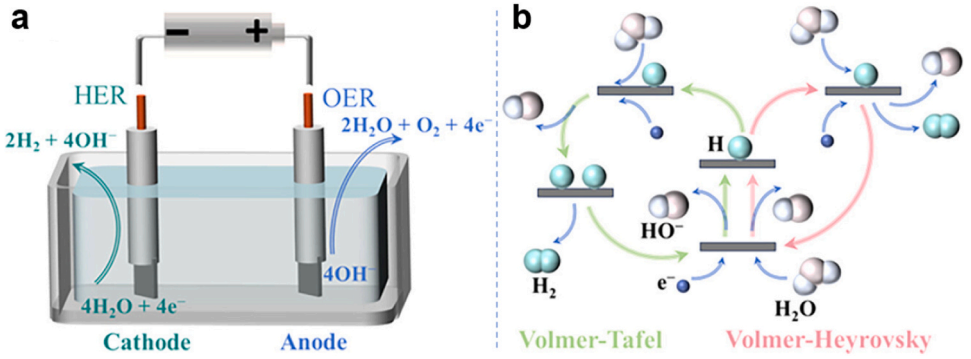

Fig. 3. (a) Schematic of an electrolysis cell for water splitting in alkaline water. (b) Alkaline HER mechanism. (a) and (b) Reproduced with permission [95]. Copyright 2023, American Chemical Society.

$$2H^* \rightarrow H_2 + 2^* \quad (6)$$

2.2. Evaluation metrics of electrochemical catalyst performance

In the realm of electrocatalysis, the assessment of catalyst performance relies heavily on parameters such as overpotential (η), Tafel slope, exchange current density, specific activity, mass activity, electrochemical impedance spectroscopy (EIS), electrochemical active surface area (ECSA), turnover frequency (TOF), Faradaic efficiency, and stability. These metrics profoundly encapsulate the thermodynamic and kinetic characteristics of the reaction. This section aims to delineate the definitions of these pivotal parameters and elucidate their significance in the appraisal of catalyst performance.

2.2.1. Overpotential

Overpotential is a typical parameter for gauging the effectiveness of electrocatalysts, defined as the deviation between the actual working potential and the theoretical equilibrium potential [96]. It predominantly stems from three factors: kinetic hindrances associated with electron transfer, mass transfer limitations within the electrolyte, and interactions at the electrode surface. The overpotential is typically measured utilizing linear sweep voltammetry (LSV) or cyclic voltammetry (CV). The overpotential at a specific current density serves as an indicator of catalyst activity, with lower overpotentials signifying superior electrocatalytic performance. Commonly, overpotentials at current densities of 1 (η_1), 10 (η_{10}), 100 (η_{100}), 500 (η_{500}) and 1000 (η_{1000}) mA cm^{-2} are used to compare the electrocatalytic activities of different cathode materials [97–100]. η_1 is often considered as the initiation point of the reaction, referred to as the onset overpotential. Currently, a current density of 10 mA cm^{-2} is widely used as a benchmark for evaluating the catalytic performance of HER electrocatalysts.

Specifically, overpotential comprises activation, concentration, and ohmic components. Activation overpotential is intimately linked to the optimization of the binding energy on the catalyst and can be mitigated by designing an appropriate catalyst architecture. Concentration overpotential arises chiefly from the local diminution of reactant concentrations near the interface and can be ameliorated by techniques such as employing a rotating disk electrode or agitating the electrolyte. Ohmic overpotential originates from the internal resistance within the electrolytic cell, including the resistance of the electrolyte, conductive connections, and contact points. It can be corrected through ohmic compensation methods applied to the LSV curve.

2.2.2. Tafel slope and exchange current density

The Tafel slope, a pivotal parameter in electrochemical kinetics, elucidates the relationship between overpotential (η) and current density (j) via the Tafel equation (Eq. 7) [101]. The magnitude of this slope is directly correlated with the kinetic rate of the reaction, where a smaller Tafel slope denotes a faster electrochemical reaction rate and enhanced catalytic efficiency. The Tafel slope provides valuable insights for deducing the rate-determining step of the HER. Specifically, the Tafel slopes for the Volmer, Heyrovsky, and Tafel reactions are registered at 118.2, 39.4, and 29.6 mV dec^{-1}, respectively. A Tafel slope within the range of 39.4–118.2 mV dec^{-1} suggests that the rate-determining step is the Volmer-Heyrovsky pathway, while a narrower range of 29.6–39.4 mV dec^{-1} indicates the prevalence of the Volmer-Tafel mechanism [102]. Additionally, the exchange current density (j_0) is ascertained at zero overpotential, representing the intrinsic ability of the catalyst to facilitate electron transfer without an external driving force. A higher exchange current density corresponds to increased reaction efficiency and reduced energy requirements. Ideally, catalysts should exhibit a low Tafel slope and high exchange current density, indicative of rapid electrocatalytic reaction kinetics and superior charge transfer capabilities. Typically, a high j_0 value signifies that the catalyst can effectively initiate reactions under lower driving forces, serving as a critical indicator of its performance.

$$\eta = a + b\log j \quad (7)$$

2.2.3. Specific activity and mass activity

Specific activity quantifies the current density per unit surface area, obtained by normalizing the current density to the catalyst's specific surface area, such as the Brunauer-Emmett-Teller (BET) surface area or the ECSA. This metric enables the exclusion of the number of active sites' influence on performance, thereby reflecting the inherent activity of individual active sites. The ECSA is effectively assessed by correlating it with the double-layer capacitance (C_{dl}), which serves as a significant indicator of specific surface area [103]. To determine the ESSA, CV scans are initially performed multiple times within the non-Faradaic region of the potential window, at scan rates ranging from 10 to 200 mV s^{-1} [104]. Subsequently, the differences in anodic and cathodic current densities at specific overpotentials are calculated and plotted against the scan rates. The resulting plot is then subjected to linear regression to determine C_{dl}, with the value of C_{dl} calculated as half the slope of the fitted line. Regions exhibiting higher current densities, indicative of significant electrochemical activity, are expected to display correspondingly higher C_{dl} values. On the other hand, mass activity normalizes the current generated by redox reactions (OER/HER) to the mass of the catalyst, to assess the activity per unit mass. The specified relationship (Eq. 8) states that the measured current density j (mA cm^{-2}) is directly proportional to the electrode's mass loading m (mg cm^{-2}). The evaluation of mass activity typically transpires among analogous material systems, and its outcomes depend upon the catalyst's active surface area; catalysts with larger surface areas often exhibit elevated

mass activities [53].

$$\text{Mass activity} = j/m \tag{8}$$

2.2.4. Turnover frequency (TOF)

TOF is an index for appraising the catalytic performance of individual active sites, calculated through the TOF equation (Eq. 9) [53]. Herein, j represents the current density, N_A is Avogadro's constant, n denotes the number of electrons transferred in the anodic reaction, F is the Faraday constant, and Γ signifies the number of active sites on the catalyst surface. The TOF is typically plotted as a function of overpotential, reflecting that increased overpotentials enhance the reaction kinetics, subsequently elevating the TOF of the catalyst. A higher TOF indicates greater intrinsic catalytic activity. However, accurate determination of Γ poses a challenge for self-supported electrocatalysts. In transition-metal-based electrocatalysts, quantifying active sites via the integrated area under redox peaks in cyclic voltammograms is a precise approach, with peaks corresponding to the redox process involved in the formation of metal hydroxides.

$$\text{TOF} = jN_A/nF\Gamma \tag{9}$$

2.2.5. Faradaic efficiency (FE)

Faradaic Efficiency (FE) gauges the electron transfer efficiency and selectivity of electrocatalysts during electrochemical reactions, defined as the ratio of the measured hydrogen production to the theoretical hydrogen production [105]. The actual hydrogen yield is typically ascertained via water displacement techniques or gas chromatography, while the theoretical yield can be derived using coulometric titration or chronoamperometry. A higher FE indicates that a greater proportion of the target product is generated during the reaction process, signifying a more ideal reaction outcome. In an ideal scenario, a catalyst should exhibit a FE of 100%. However, during the HER process, the formation of byproducts on the electrode surface frequently precludes the achievement of the FE under optimal conditions.

2.2.6. Electrochemical active surface area (ECSA) and double-layer capacitance (C_{dl})

To elucidate the intrinsic activity of electrocatalysts, ascertaining the quantity of catalytically active sites is imperative. The ECSA is an efficacious metric for gauging the intrinsic activity of catalysts and determining the number of active centers, assessed by normalizing the measured current. The double-layer capacitance (C_{dl}) is typically gauged in the non-Faradaic region via CV and serves as a direct indicator of the ECSA [106,107]. A higher C_{dl} value implies an increased active surface area of the electrocatalyst, facilitating more efficient adsorption of reactants and intermediates. This enhancement in adsorption correlates with accelerated reaction kinetics and improved catalytic efficiency. There exists a direct proportionality between ECSA and C_{dl}, allowing for the computation of ECSA based on Eq. 10, where C_s symbolizes the specific capacitance per unit area of a planar standard electrode, typically ranging between 20 and 60 mF cm^{-2}. It is crucial to acknowledge that the chemical properties and the structural characteristics of the electrode may lead to an overestimation of ECSA, consequently underestimating the catalytic activity. Furthermore, while ECSA provides insights into the quantity of active sites on the electrocatalyst, it does not necessarily imply that all these sites are engaged in the catalysis of the HER process.

$$\text{ECSA}=C_{d1}/C_s \tag{10}$$

2.2.7. Electrochemical impedance spectroscopy (EIS)

Electrochemical Impedance Spectroscopy (EIS) stands as a formidable instrument for dissecting the charge transfer characteristics and reactivity at the electrode/electrolyte interface. The charge transfer resistance (R_{ct}), which mirrors the kinetics of the charge transfer processes at the electrode interface, can be deduced from the diameter of the semicircle in the high-frequency domain obtained through EIS [57]. A small R_{ct} value is indicative of a swift reaction rate, efficacious charge transfer, and minimal overpotential. When comparing R_{ct} values, it is essential to ensure that disparate samples are examined under the same applied potential to guarantee coherence and comparability of the results.

2.2.8. Stability assessment

Stability assessment is conducted through chronoamperometry (CA), chronopotentiometry (CP), and CV to gauge the durability of water-splitting electrocatalysts [47]. In CA assays, a constant potential is typically applied to maintain a current density of 10 mA cm^{-2}, whereas CP assays involve the direct fixation of a current density at 10 mA cm^{-2}. Both tests commonly extend for periods exceeding 24 h. CV assays should be executed for a minimum of 1000 cycles to establish the catalyst's stability credibly. Constant current or constant potential electrolysis involves monitoring changes in potential or current density at a fixed current density or overpotential. CV measurements compare changes in overpotential before and after cycling. The smaller the variation in recorded data over extended operational periods, the greater the stability of the catalyst. Catalysts intended for industrial hydrogen production necessitate extended testing durations. In practical applications, electrocatalysts that demonstrate high efficiency, energy conservation, and the capacity to operate stably for thousands of hours are considered suitable selections. Consequently, research should focus on perpetually enhancing the stability and endurance of electrocatalysts over extended periods to meet the rigorous demands of real-world applications.

3. NF-based electrocatalysts

In the development of electrocatalysts, nanoscale architectural design and compositional optimization are pivotal strategies aimed at augmenting the number and activity of catalytic sites. A plethora of diverse nanostructures, such as nanowires, nanosheets, nanoarrays, microspheres, and nanocubes, have been employed to enhance the exposure of active sites [108–112]. Concurrently, the construction of multi-component systems through compositional engineering has markedly improved the intrinsic activity of these sites, fostering the generation of synergistic effects. Furthermore, the performance of catalysts is significantly influenced by the choice of substrate material. Most experimentally prepared electrocatalysts are in powder form, necessitating the use of conductive substrates such as glassy carbon, carbon paper, or metal foils for electrocatalytic loading. Cai et al. [113] designed and successfully synthesized highly crystalline ternary boride, Mo_2NiB_2, from pure elemental powders. In alkaline solutions, the synthesized Mo_2NiB_2 exhibited low overpotentials in both the OER and the HER, achieving current densities of 10 mA cm^{-2} at overpotentials of just 280 mV and 160 mV, respectively. Mo_2NiB_2 was also employed in a comprehensive water-splitting setup under 1 M KOH, forming a symmetric electrode system. However, LSV curves for Mo_2NiB_2@NF regarding OER and HER reveal notable improvement compared to glassy carbon coatings. Specifically, the overpotential on NF for HER decreased by 38 mV, while for OER, it decreased by 17 mV. These reduction in overall overpotential in the electrolyzer structure is likely due to synergistic effects between the catalyst and the nickel foam substrate, as well as increased catalyst loading. Furthermore, the use of binders impairs the exposure of active sites, electron transfer, and mass transport, and when high current densities are applied, the powdery electrode material may be displaced by the generated gas bubbles. Herein, the

substrate not only provides rapid conduits for charge transfer but also optimizes the utilization efficiency of active sites through the dispersion of the catalyst [63, 114]. Among a wide array of substrate materials, NF is extensively utilized due to its unique advantages; its 3D porous structure effectively prevents the excessive accumulation of product bubbles and promotes rapid renewal of the catalytic surface.

NF is typically fabricated on substrates like polyurethane and other polymers via chemical vapor deposition or electrochemical deposition, followed by a sintering or pyrolysis process to remove the polymer template and its impurities (e.g., S and C), yielding high-purity NF. NF possesses a substantial porosity (70–98%) and a broad pore size distribution (450 μm to 3.2 mm), with the specific range generally influenced by the polymer template, commonly spanning 5–130 ppi (pores per inch) [115–117]. Its 3D structure endows NF with an extensive surface area, making it an exceedingly attractive substrate for electrochemical reactions. Owing to its exceptional electrical conductivity, economical cost, hierarchical porous architecture, commercial availability, and 3D interconnected network, NF is considered an ideal substrate material for HER electrodes [118].

3.1. Metal sulfides/NF

In alkaline media, the development of non-precious metal HER catalysts that match the performance of platinum is of paramount significance for energy conversion technologies [119–121]. Recent investigations by numerous research groups have utilized a variety of technical approaches, such as electrodeposition [122], hydrothermal synthesis [123], acid activation [124], and chemical etching [125], to

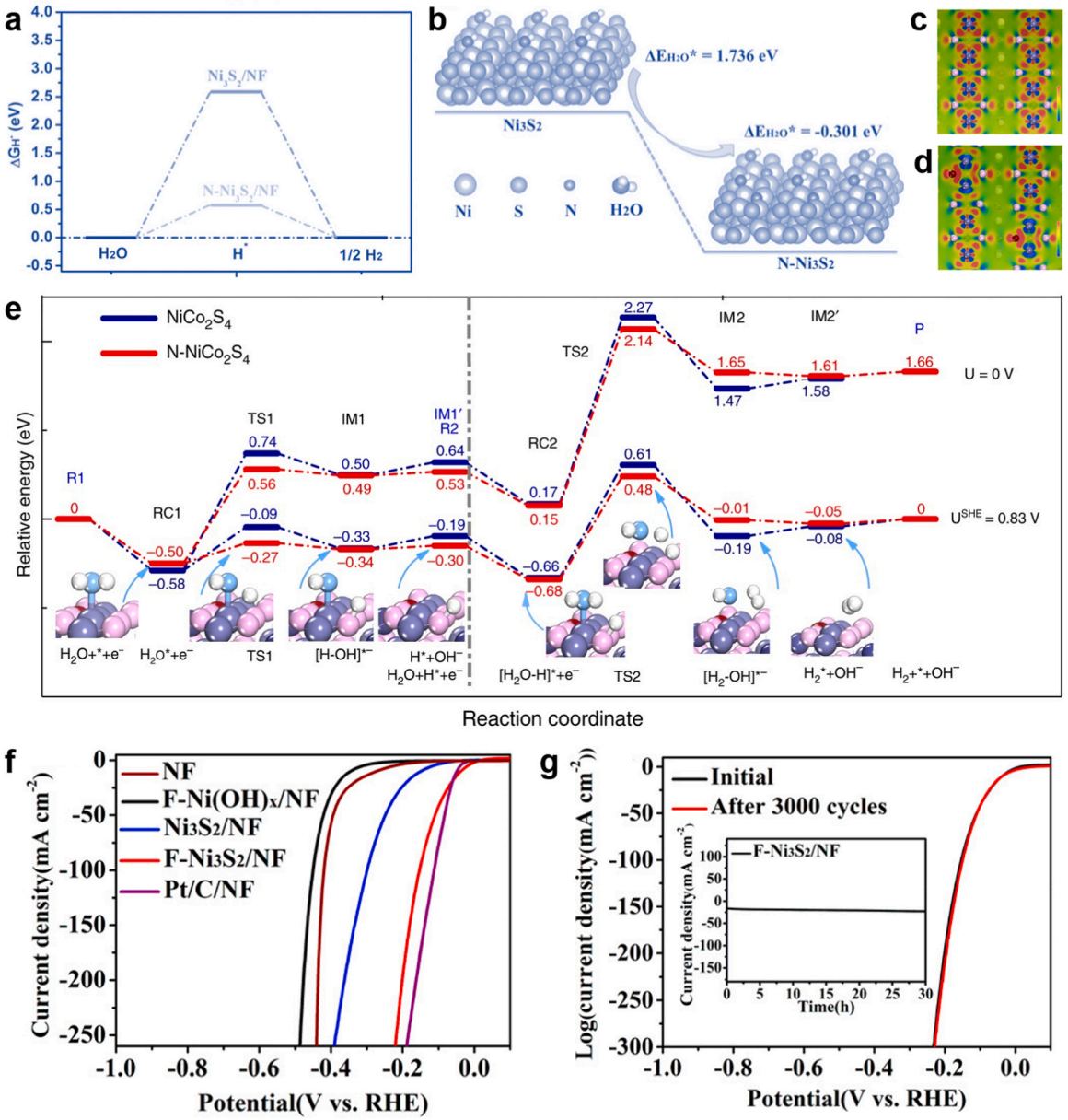

Fig. 4. (a) Calculated HER free-energy change and (b) water adsorption energy for the N-Ni_3S_2 and pristine Ni_3S_2. (a) and (b) Reproduced with permission [144]. Copyright 2017, WILEYWiley-VCH. The top-view electron density difference of (c) $NiCo_2S_4$ (100), and (d) N-$NiCo_2S_4$ (100), ranging from −0.1 to 0.1. (e) Relative energy profiles and the simplified surface structures of the various reaction species along the reaction pathway. (c-e) Reproduced with permission [145]. Copyright 2018, Nature. (f) LSV curves of F-Ni_3S_2/NF, Ni_3S_2/NF, F-Ni(OH)$_x$/NF, NF, and Pt/C/NF toward HER in 1 M KOH. (g) LSV curves of F-Ni_3S_2/NF before and after 3000 CV tests. (Inset: Time-dependent current density curve of F-Ni_3S_2/NF under an overpotential of −50 mV (vs RHE) for 30 h). (f) and (g) Reproduced with permission [146]. Copyright 2019, American Chemical Society.

fabricate a plethora of transition metal sulfides (TMSs) nanostructures on the surface of NF. TMSs, with their abundance, diversity, and cost-effectiveness, have emerged as a focal point of research. TMSs such as MoS_2 [126–128], Ni_3S_2 [129–131], CoS_2 [132–134], and FeS_2 [135–137], known for their high intrinsic electrical conductivity and chemical stability, have become prominent catalysts in the realm of HER. Specifically, the direct growth of electrocatalysts on 3D NF substrates (binder-free) to form a catalytic layer on the electrodes significantly enhances electron conductivity and increases the number of active sites. Liu et al. [138] reported a concise and rapid synthesis strategy for preparing a catalytic layer of Ni_3S_2 on NF (Ni_3S_2/NF) by adding mercaptoethanol solution to NF followed by high-temperature annealing. Here, NF serves not only as a structural scaffold but also as a Ni source, contributing to the formation of Ni_3S_2. The high specific surface area afforded by the porous structure of 3D NF provides ample growth sites for the catalytic material, endowing the resultant Ni_3S_2/NF with remarkable hydrolytic activity and stability. This breakthrough leverages the excellent stability and machinability of NF to realize a synergistic optimization of cost-efficiency and performance in catalyst fabrication.

Anionic doping, employing elements such as F, P, or N, has been validated as a preferred strategy to modulate the electronic structure of Ni_3S_2-based electrocatalysts, not only optimizing the electronic configuration of transition metal compounds (TMCs) but also augmenting the active sites and enhancing electrical conductivity [139–141]. Compared to the incorporation of transition metal cations [142], anionic doping simplifies the identification of active sites [143]. Xie et al. [144] synthesized an innovative material, N-doped Ni_3S_2 (N-Ni_3S_2/NF), directly on NF substrates using a one-step solid-phase method, which exhibited an overpotential of 110 mV at a current density of 10 mA cm^{-2} for HER in 1 M KOH. Furthermore, when incorporated into an overall water-splitting device, this electrode achieved a current density of 10 mA cm^{-2} at an impressively low cell voltage of 1.48 V. Nitrogen doping not only ameliorated the electronic structure and morphology of Ni_3S_2 but also optimized the Gibbs free energy of HER and the adsorption energy of water molecules (Fig. 4**a,b**), facilitating the formation of catalytic H* and H_2O states on the catalyst surface, ultimately boosting the overall HER activity. Nevertheless, its performance in alkaline HER conditions remained suboptimal.

Metal sulfides traditionally encounter challenges in hydrogen evolution catalysis due to the strong H adsorption and the highly electronegative nature of sulfur, which hampers hydrogen desorption. The Wang group [145] introduced a universal strategy to enhance the alkaline HER performance of various transition metal sulfides (such as $NiCo_2S_4$, FeS_2, CoS_2, and NiS_2) through N anionic doping. They highlighted that the higher electronegativity of N (3.05) relative to S (2.58) is pivotal in modulating the electron density at catalytic sites to optimize HER activity (Fig. 4**c-e**). N doping effectively regulates the surface electron density and the *d*-band center of $NiCo_2S_4$. To further elucidate the impact of N on the catalytic process, density functional theory (DFT) simulations demonstrated that the incorporation of N adjusts the electronic properties of $NiCo_2S_4$. This adjustment balances the dissociation of H_2O and the desorption of H*, facilitating these reactions at lower potential surfaces. Additionally, the introduced N sites serve as sacrificial sites to enhance the activity of S sites.

Anion engineering, thus, adjusts the electronic structure of metal sulfides, providing atomic-level insights. Liu et al. [146] postulated that introducing F anions into Ni_3S_2 (F-Ni_3S_2) could enhance the electronic interactions between the transition metal cations and anions, thereby achieving an improved electronic structure and heightened HER activity. Building on this premise, they designed a nanoarray of F-doped Ni_3S_2 on NF substrates (F-Ni_3S_2/NF). At the same overpotential, the TOF of F-Ni_3S_2/NF (2.57 S^{-1}) is significantly higher than that of Ni_3S_2/NF (0.28 S^{-1}). Additionally, the $\triangle G_{H_2O^*}$ on the surface of F-Ni_3S_2 (−1.230 eV) is considerably lower than on the surface of Ni_3S_2 (−0.146 eV). The values of ΔG_H* at the Ni sites (−0.362 eV), S sites (0.441 eV), and F sites (0.375 eV) of F-Ni_3S_2 are closer to the thermoneutral position (zero), indicating superior catalytic activity of F-Ni_3S_2/NF. This F-Ni_3S_2/NF electrode demonstrated superior HER performance in alkaline media, requiring a mere 38 mV overpotential to reach a current density of 10 mA cm^{-2}. It also exhibited a Tafel slope of 78 mV dec^{-1} (Fig. 4**f**), with electrocatalytic stability sustained over 30 h (Fig. 4**g**), rivaling commercial Pt/C catalysts.

In the realm of catalyzing the HER under alkaline conditions, fabrication of heterostructures is deemed a potent strategy to activate interfacial effects and augment electrocatalytic performance. Heterostructures can engender electronic interplay at the interface, thereby substantially enhancing catalytic activity [147–149]. Wu et al. [150] successfully established a hierarchical architecture composed of Ni_2P--$Ni_{12}P_5$@Ni_3S_2/NF hetero-nanorod arrays with pseudo-spiky terminations (Fig. 5**a**), through a sequence of corrosion, sulfidation, and phosphidation processes on a NF substrate, invoking a sequential phase transformation. The contact angles for Ni_2P/NF and Ni_2P-$Ni_{12}P_5$@-Ni_3S_2/NF, post-sequential phase transformation, were measured at 126° and 0° respectively (Fig. 5**b,c**), demonstrating that, compared to direct phase transformation, the sequential strategy more effectively enhances the hydrophilicity of the material's surface. The methodical phase transformation not only ensured robust interfacial coupling between Ni_2P and $Ni_{12}P_5$ but also guaranteed the stability of the Ni_3S_2 film on the 1D heterostructured anodic array, hence optimizing water adsorption/desorption energies, refining hydrogen adsorption affinity, facilitating electron/proton transfer capabilities, and exhibiting commendable stability. Furthermore, it is evident that the presence of the intermediate phase, Ni_3S_2, predominantly dictates the formation of the heterophase Ni_2P-$Ni_{12}P_5$, with a moderate Ni to P ratio (Fig. 5**d**). More importantly, this heterophase Ni_2P-$Ni_{12}P_5$ exhibited significantly enhanced electronic conductivity compared to the directly converted monophase Ni_2P. Consequently, the Ni_2P-$Ni_{12}P_5$@Ni_3S_2/NF required a mere overpotential of 34 mV in 1 M PBS and 32 mV in 1 M KOH solutions to achieve a current density of 10 mA cm^{-2} (Fig. 5**e,f**). *In-situ* Raman spectroscopy elucidated that Ni atoms within the heterophase Ni_2P-$Ni_{12}P_5$ are the veritable active sites for HER (Fig. 5**g**). Furthermore, adopting an autonomously driven synthesis strategy, Feng et al. [151] also fabricated a novel hierarchical Ni_3S_2/VS_4 nanocorner array (NS-horn/NF) on NF. Within the NS-horn/NF, the *in situ* formation of VS_4 not only fostered the creation of a distinctive layered structure but also facilitated a strong coupling interface. This interface promoted the bridging of active S_2^{2-} between Ni_3S_2 and VS_4, effectively enhancing HER kinetics. When deployed in an alkaline electrolysis cell, the NS-horn/NF electrode required a modest cell voltage of just 1.57 V to generate a current density of 10 mA cm^{-2} and maintained this activity for at least 70 h.

Although monometallic transition metal sulfides exhibit limited electrochemically active surface areas when deposited on NF, multimetallic sulfides, owing to their intricate alloying effects, can proffer an expanded electrochemically active surface area and a plethora of active sites (Table 1). Li et al. [88] leveraged an anion exchange method to successfully synthesize a 3D hexagonal-like bimetallic cobalt-manganese sulfide (CMS/NF) on NF. Co and Mn exhibited a pronounced synergistic effect within the composite material, markedly enhancing catalytic activity in alkaline media. Compared to pure Co_9S_8/Ni (24.0 mF cm^{-2}) and MnS/Ni (13.0 mF cm^{-2}), the C_{dl} of CMS/Ni substantially increased to 56.3 mF cm^{-2}. This increase correlated positively with the ECSA, indicating a significant expansion in ECSA and thereby exposing a greater number of accessible catalytic active sites. Compared to the individual Co_9S_8/Ni and MnS/NF, the CMS/NF shows significantly improved electrocatalytic performance for the HER.

3.2. Layered double hydroxides/NF

Layered double hydroxides (LDHs) are a subclass of 2D hydrotalcite-

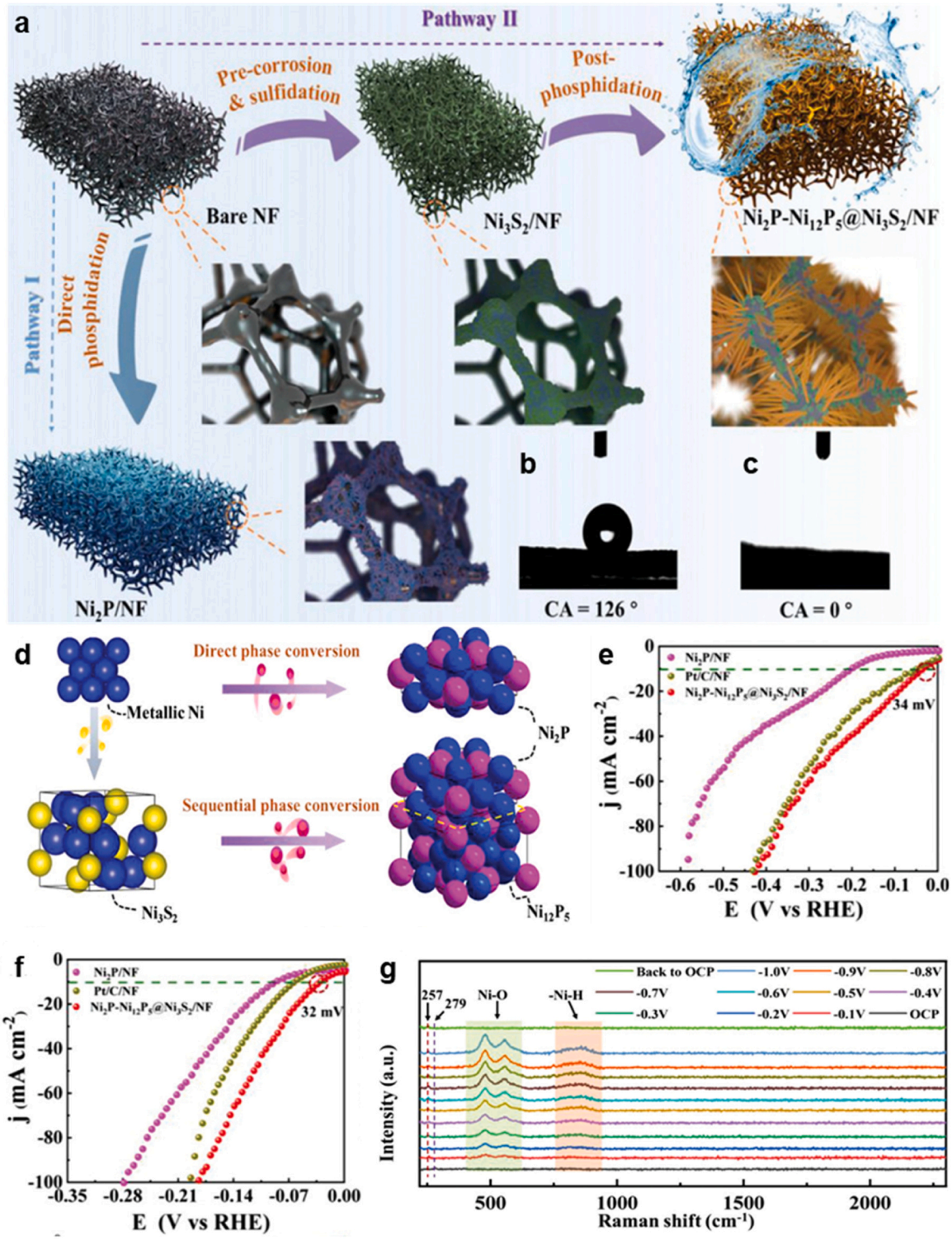

Fig. 5. (a) The schematic illustration of the synthetic procedures for different phase conversion-induced TMPs from NF (Ni_2P-$Ni_{12}P_5$@Ni_3S_2/NF and Ni_2P/NF). Contact angles of (b) Ni_2P/NF and (c) Ni_2P-$Ni_{12}P_5$@Ni_3S_2/NF. (d) Illustration of these two different phase transform pathways. LSV polarization curves of Pt/C/NF, Ni_2P/NF and Ni_2P-$Ni_{12}P_5$@Ni_3S_2/NF for HER in (e) 1 M PBS and (f) 1 M KOH. (g) *In-situ* Raman spectra of Ni_2P-$Ni_{12}P_5$@Ni_3S_2/NF for HER in 1 PBS solution. (a-g) Reproduced with permission [150]. Copyright 2022, Wiley-VCH.

like anionic compounds, encapsulated by the general formula $[M^{2+}_{1-x}M^{3+}_x\cdot(OH)_2]^{x+}(A^{n-})_{x/n}\cdot mH_2O$ [163–165]. Herein, the divalent cations M^{2+} may include Mg^{2+}, Ni^{2+}, Zn^{2+}, Co^{2+}, Ca^{2+}, Fe^{2+}, or Mn^{2+}, while the trivalent cations M^{3+} embrace species such as Al^{3+}, Mn^{3+}, Cr^{3+}, Fe^{3+}, Co^{3+}, Ga^{3+}, or Ni^{3+}. Anions like CO_3^{2-}, NO_3^-, and Cl^- typically reside interstitially between layers [166,167]. Predominantly binary in composition, the introduction of a third metallic cation has expanded the research purview into ternary LDH systems. The versatility in the M^{2+}/M^{3+} ratio and interlayer anionic species endows LDHs with the ability to be tailored to specific requirements, exhibiting a spectrum of physical and chemical properties. The quintessential layered structure formed by MO_6 octahedra lends LDHs exceptional electrocatalytic

Table 1
Comparison of electrocatalytic performance of NF-based sulfide electrocatalysts under alkaline conditions.

Catalysts	Current density (mA cm^{-2})	Overpotential (mV)	Tafel slope for HER (mV dec^{-1})	Ref.
Ni_3S_2/NF	10	131	96	[138]
Fe-Ni_3S_2	100	254	101	[152]
Mo-Ni_3S_2	10	90		[153]
N-Ni_3S_2/NF	10	110		[142]
N-$NiCo_2S_4$ NWs	10	41	37	[145]
F-Ni_3S_2/NF	10	38	78	[146]
Ni_2P-$Ni_{12}P_5$@Ni_3S_2	10	32	146	[150]
NS-horn/NF	10	177	139	[151]
MoS_2/$NiCo_2S_4$/NF	10	90	52	[154]
CMS/NF	100	217	48.2	[88]
Co_9S_8/NF	100	419	81.1	[88]
MnS/NF	100	506	104.1	[88]
NiFeVS_x@NF	10	127	121	[155]
ZCNS-1/2	10	97	42.24	[156]
N-Co_9S_8/Ni_3S_2/NF	10	111	88.6	[157]
NiFeS/NF	500	347	102.93	[158]
$CoMnS_2$@1 T-Fe-VS_2@NF	10	89	61	[159]
NiS@FeNiP/NF	10	52	61.9	[160]
Co_9S_8-Ni_xS_y/Nif	10	163	88	[161]
NiFeS@Ti_3C_2 MXene/NF	20	180	177	[162]

properties in OER [168]. However, the activity of LDHs in HER is inadequate, as evidenced by the overpotentials exceeding 210 mV at a current density of 10 mA cm^{-2}, which significantly heightens the water splitting voltage in alkaline electrolytes [169,170]. The Volmer step predominantly hinders the HER activity, namely, the dissociation step of water under alkaline conditions [169,171,172]. While LDHs abound with oxygen-active sites and possess substantial electronegativity, which favors the adsorption of H_{ads}, the strong interaction between H_{ads} and the highly electronegative oxygen impedes the desorption of H_{ads} for H_2 evolution. The accumulation of H_{ads} leads to a gradual saturation of the LDHs' coordination state, thereby constraining the dissociation of water molecules. To enhance catalytic performance, compositional modulation strategies can be employed to introduce a variety of synergistic, interfacial, and electronic effects. The construction of nanowires, nanosheets, or core-shell structures on LDHs can efficaciously augment their ECSA, facilitate electron transfer, multiply active sites, and thus improve conductivity [173]. Several studies have shown that LDH structures directly grown on the conductive surfaces of NF are favored for their superior electron transport properties, electrolyte permeability, and expansive ECSA.

Bimetallic LDHs and their composite-based electrocatalysts, with their intrinsic self-supporting layered structures and highly tunable compositional attributes, have achieved significant progress [174–176]. Yet, the innate electronic/ion conductivity of LDHs is sub-optimal, and their layered architectures are prone to restacking and collapse, impeding enhancements in catalytic efficiency. Due to insurmountable energy barriers and sluggish water dissociation kinetics, LDH electrocatalysts exhibit a propensity toward OER rather than HER. Consequently, an array of structural and compositional modulation strategies may be employed to circumvent the aforementioned limitations inherent to pristine binary LDHs. NiFe layered double hydroxides demonstrate exemplary OER performance in alkaline media. Coupling NiFe-LDH with entities active in HER can enhance the resultant composite material's HER performance. Moreover, studies indicate that amorphous CoS_x, owing to its isotropic and disordered structure, manifests pronounced catalytic activity for HER in alkaline solutions.

The binary LDHs and their derivative composite electrocatalysts have garnered notable advancements in the realm of electrocatalysis, attributed to their inherent self-supported lamellar structures and the malleability of their chemical compositions, as cited in reference [177–179]. Despite these achievements, the intrinsic limitations in electronic and ionic conductivities, as well as the propensity of lamellar structures to restack and collapse, represent significant bottlenecks in augmenting catalytic efficiencies. Confronted with formidable energy barriers and sluggish hydrolysis kinetics, LDHs are predisposed to favor OER over HER, as indicated in reference [180]. To address this challenge, researchers have devised numerous structural regulations and composite strategies to refine the performance of pristine binary LDHs. Of particular note is the NiFe-LDH (an *n*-type semiconductor), which exhibits outstanding OER activity in alkaline media [181]. Integrating NiFe-LDH with substances that are active in HER can substantially enhance the HER performance of the resulting composite material. For instance, amorphous CoS_x (a *p*-type semiconductor), due to its isotropic and disordered structure, has demonstrated high efficiency in catalyzing HER in alkaline solutions [182,183]. The catalytic superiority of such materials provides new avenues for the development of high-performance electrocatalysts. For example, Yang et al. [184] successfully engineered a hierarchical porous 3D networked bifunctional electrocatalyst, NiFe-LDH@CoS_x/NF, by electrophoretic deposition of amorphous CoS_x onto porous NF-supported 2D NiFe-LDH nanosheets (Fig. 6**a**). When CoS_x is directly deposited onto NF, the ultrathin CoS_x nanosheets are tightly and uniformly coated on the NF surface. In contrast, NiFe-LDH/NF exhibits thicker and larger nanosheet structures with a thickness of approximately 10 nm (Fig. 6**b**). Upon further deposition of CoS_x onto the NiFe-LDH nanosheets, the resultant NiFe-LDH@CoS_x/NF maintains the nanosheet morphology with an increased thickness of about 20 nm (Fig. 6**c**). This interfacial synergy between NiFe-LDH and amorphous CoS_x, with Ni→Co electron transfer resulting in an elevated Ni valence state (forming $Ni^{2+\sigma}$) and a reduced Co valence state (Fig. 6**d**,**e**), significantly promotes electron transport, thereby markedly enhancing its HER activity in 1 M KOH alkaline medium. Beyond heterostructure design, heteroatom doping has also been proven to enhance the HER performance of binary LDHs. Yang et al. [185] induced amorphization of the LDH structure through boron doping (Fig. 6**g**,**h**), effectively activating its capability as a HER catalyst. Compared to NiCo-LDH/NF, in A-NiCo LDH/NF, the Ni and Co elements shifted towards higher binding energies, facilitating electron transfer from Ni or Co atoms to their nearest neighbors. The B atoms were likely incorporated into the crystal precursor in the form of borate. In this scenario, the borate anions (BO_3^{3-}) partially substituted the lattice OH^- in crystalline NiCo LDH. This substitution disrupted the original crystal structure, generating a multitude of O vacancies and unsaturated atomic defects. These defects exposed more catalytic active sites, playing a crucial role in enhancing the performance during the HER. The B-doped amorphous A-NiCo-LDH/NF achieved high current densities at low overpotentials (reaching 100 mA cm^{-2} at an overpotential of 151 mV, 500 mA cm^{-2} at 286 mV, and 1000 mA cm^{-2} at 381 mV, Fig. 6**f**) and maintained high durability after 72 h of operation in an alkaline medium, performing even better than commercial platinum electrocatalysts.

In alkaline media, the catalytic efficacy of LDHs is inherently constrained, primarily due to the kinetic barriers associated with hydrolytic dissociation and the Volmer step in alkaline or neutral environments, posing formidable challenges to their HER performance during water electrolysis [186]. The advent of defect engineering has emerged as an effective strategy to augment the HER performance of LDHs by introducing an array of defect sites, including dislocated edges, atomic steps, terraces, twists, and vacancies. These modifications not only proliferate unsaturated metal centers but also refine the catalyst's surface and electronic states, thereby substantially bolstering the intrinsic activity of the active sites. For instance, Sun and colleagues [187] adopted a metal-organic framework (MOF)-mediated topotactic transformation approach (Fig. 7**a**) to fabricate porous ternary CoFeNi LDHs on a NF

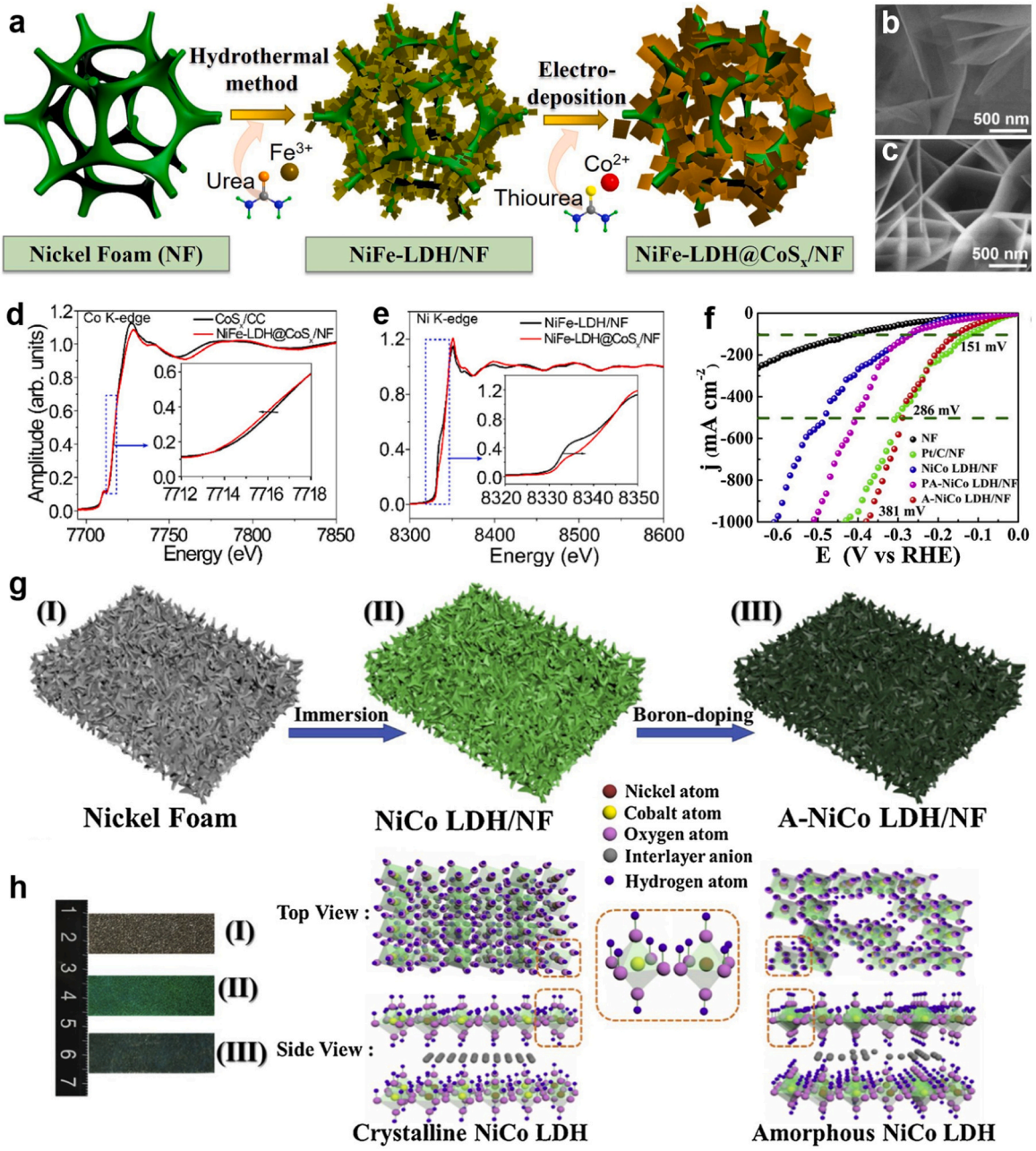

Fig. 6. (a) Schematic illustration of synthetic process of NiFe-LDH@CoS_x/NF. Scanning electron microscopy (SEM) images of (b) NiFe-LDH/NF, and (c) NiFe-LDH@CoS_x/NF. XANES spectra of (d) Co K-edge of CoS_x/CC and NiFe-LDH@CoS_x/NF, (e) Ni K-edge of NiFe-LDH/NF and NiFe-LDH@CoS_x/NF. (a-e) Reproduced with permission [184]. Copyright 2021, Elsevier. (f) LSV polarization curves of bare NF, Pt/C/NF, NiCo LDH/NF, PA-NiCo LDH/NF and A-NiCo LDH/NF for HER in 1 M KOH. (g) The scheme of the preparation process for the A-NiCo LDH nanosheet arrays supported on the NF; (h) corresponding photographs of bare NF (I), NiCo LDH/NF (II) and A-NiCo LDH/NF (III). (f-h) Reproduced with permission [185]. Copyright 2019, Elsevier.

substrate. The resultant hierarchical CoFeNi LDH nanosheets exhibit an irregularly wrinkled polygonal mesoporous structure with atomic-level edge steps and lattice defects (Fig. 7**b-d**). The strategically optimized *h*-$Co_{0.34}Fe_{0.33}Ni_{0.33}$-LDH manifests a high water-splitting current density of 10 mA cm^{-2} at a mere overpotential of 71 mV. The enhanced catalyst necessitates only an external voltage of 1.49 V to sustain a water-splitting current density of 10 mA cm^{-2} (Fig. 7**e**), coupled with exceptional electrolytic stability, far surpassing the benchmark Pt/C||RuO_2 couple and exhibiting superior electrochemical endurance. Mechanistic investigations (Fig. 7**f**), synergizing advanced spectroscopic techniques with DFT, elucidate that Fe doping modulates the *d*-band density of states (DOS) for Co and Ni, simultaneously reducing the hydrolytic dissociation barrier and facilitating adsorption of intermediates, significantly elevating the intrinsic HER activity. Within ternary metallic systems, the synergistic effects and elemental doping not only amplify the catalyst's inherent catalytic activity but also expand the active surface area. For example, Yan et al. [188] synthesized NiFeV ternary LDH nanosheet electrodes ($Ni_{0.75}Fe_{0.125}V_{0.125}$-LDHs/NF) via a hydrothermal method on an NF substrate, demonstrating exceptional HER performance with an overpotential of merely 125 mV in 1 M KOH electrolyte and extremely low Tafel slope of 62.0 mV dec^{-1}. The current density of NiFeV-LDHs/NF with varying compositions showed an increasing trend with the ECSA. Notably, a doubling in ECSA (from 60.3 to 126.2 mF cm^{-2}) resulted in more than an eightfold increase in current density (from 21.5 to 178.5 mA cm^{-2}). This strongly demonstrated that optimizing the ratios of Ni, Fe, and V not only enhanced the number of active

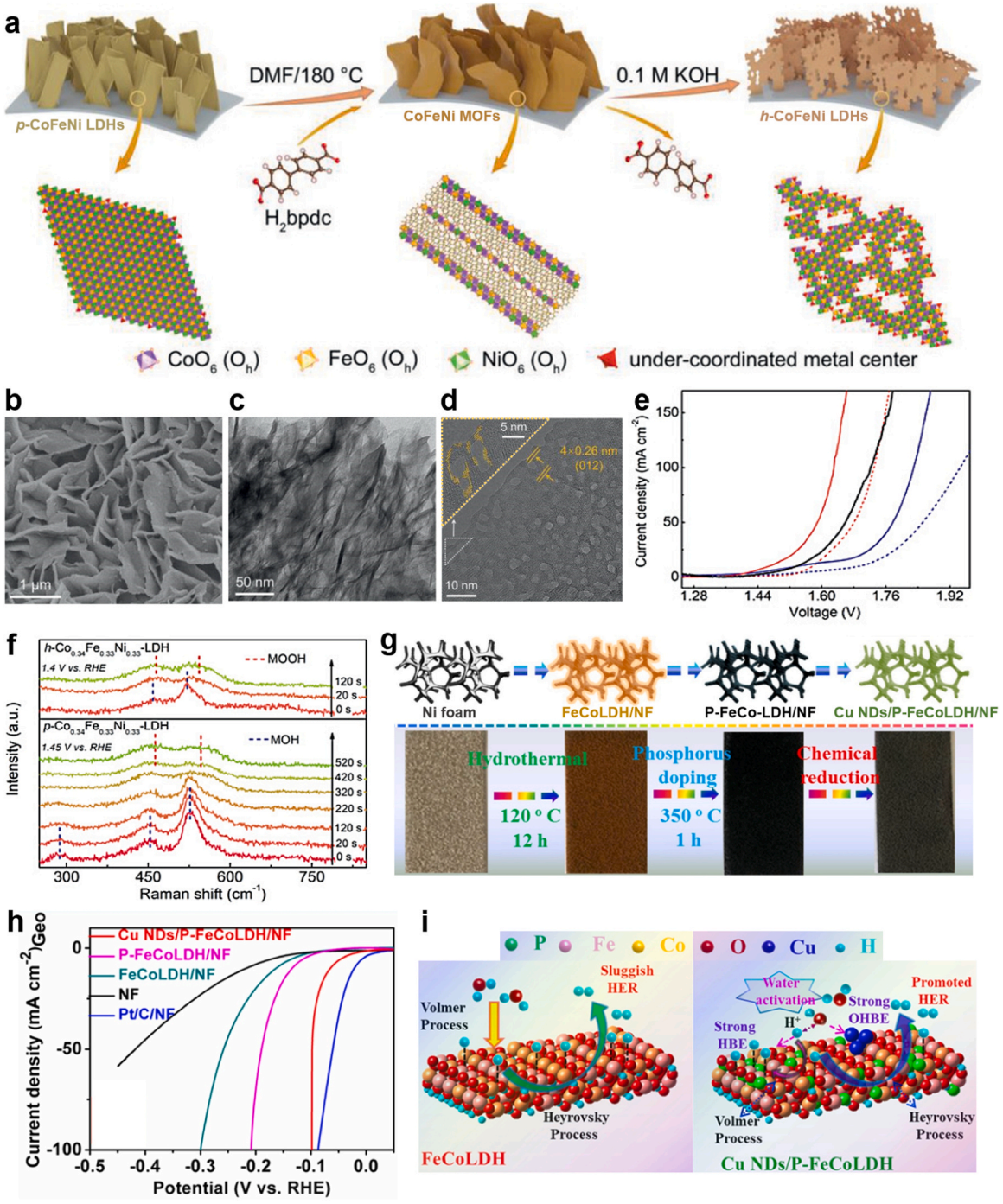

Fig. 7. (a) Schematic illustration of the fabrication process of *h*-CoFeNi LDHs through MOF-mediated topotactic transformation. (b) Top-view SEM, (c) transmission electron microscopy (TEM), and (d) HR-TEM of *h*-$Co_{0.34}Fe_{0.33}Ni_{0.33}$-LDH. (e) Polarization curves of overall water splitting in a two-electrode configuration. (f) Operando Raman spectra of *p*-$Co_{0.34}Fe_{0.33}Ni_{0.33}$-LDH (at 1.45 V) and *h*-$Co_{0.34}Fe_{0.33}Ni_{0.33}$ (at 1.4 V) as a function of reaction time. (a-f) Reproduced with permission [187]. Copyright 2020, Wiley-VCH. (g) Schematic illustration of preparing Cu NDs/P-FeCoLDH/NF electrodes. (h) LSV curves for bare NF, Pt/C, FeCoLDH/NF, P-FeCoLDH/NF, and Cu NDs/P-FeCoLDH/NF electrodes. (i) Schematic illustration of water adsorption and activation process: FeCoLDH and Cu NDs/P-FeCoLDH. (g-i) Reproduced with permission [189]. Copyright 2021, Elsevier.

sites but also significantly improved their intrinsic activity. Table 2 synthesizes recent studies on water electrolysis performance using NF-based LDHs, reflecting the rapid progress in this field.

In alkaline media, doping of compounds with strong H_{ads} or oxygen adsorption energy (OH_{ads}) can promote the dissociation of water molecules, while surface deformation can augment the density of active catalytic sites — such as grain boundaries, edges, and corners — thereby enhancing the HER performance [190–192]. These strategies, which increase the number of active sites or incorporate new complexes with distinctive features, enhance the HER activity of LDHs but do not fundamentally alter the essence of the catalyst. Within the LDHs framework, the interaction between adsorbed H_{ads} and electronegative oxygen is challenging to attenuate, thus necessitating the alteration of the inherent properties of LDHs and the acceleration of water molecule dissociation to improve HER activity. The Feng group [189] has significantly advanced the HER performance of LDHs through dual

Table 2
Comparison of electrocatalytic performance of NF-based double hydroxide electrocatalysts under alkaline conditions.

Catalysts	Current density (mA cm^{-2})	Overpotential (mV)	Tafel slope for HER (mV dec^{-1})	Ref.
NiFe-LDH@CoS_x/NF	10	136	73	[184]
A-NiCo LDH/NF	10	36	57	[185]
h-CoFeNi LDHs	10	71	83	[187]
$Ni_{0.75}Fe_{0.125}V_{0.125}$-DHs/NF	10	125	62	[188]
MoP@NiCo-LDH/NF-20	100	255	145	[196]
Cu NDs/P-FeCoLDH/NF	10	63	41.74	[189]
CoFeLDH/NF@1000 cls	10	144	141	[197]
CoFeZr/NF	10	159	132.7	[198]
NiFe-LDH	10	95	72.2	[197]
Cu_2O/CoCu-LDH	10	96	76.8	[199]
NiCoCu-LDHs	10	87	52	[200]

modification with P-doping and the deposition of metallic nanodots (NDs, Fig. 7**g**), achieving an order of magnitude enhancement over the pristine LDHs (Fig. 7**h**). P doping mitigated the interaction between H_{ads} and the electronegative O by forming P-O bonds in LDHs (Fig. 7**i**) [193–195]. The deposition of Cu NDs destabilized the O-H bonds in water molecules, facilitating the decomposition of H_2O into OH^- and H^+, with the latter rapidly reacting on the LDH surface to produce H_2. Compared to the pristine FeCoLDH, the Cu NDs/P-FeCoLDH exhibited a more favorable water adsorption energy (−0.65 eV) and a lower energy barrier for water dissociation (0.96 eV). The surface bond energy between NDs/P-FeCoLDH and H_{ads} was close to zero, indicating rapid electron/proton transfer steps and swift hydrogen release. The TOF of Cu NDs/P-FeCoLDH, calculated to be approximately $15 \times 10^{-3}\ s^{-1}$, was the highest, indicating superior catalytic activity. This method disrupts the stability of water molecules to expedite the dissociation process. It also optimizes the adsorption energy of hydroxide ions on the catalyst by forming P-O bonds, which weakens the interaction with electronegative oxygen, paving a novel pathway for improving HER performance under alkaline conditions.

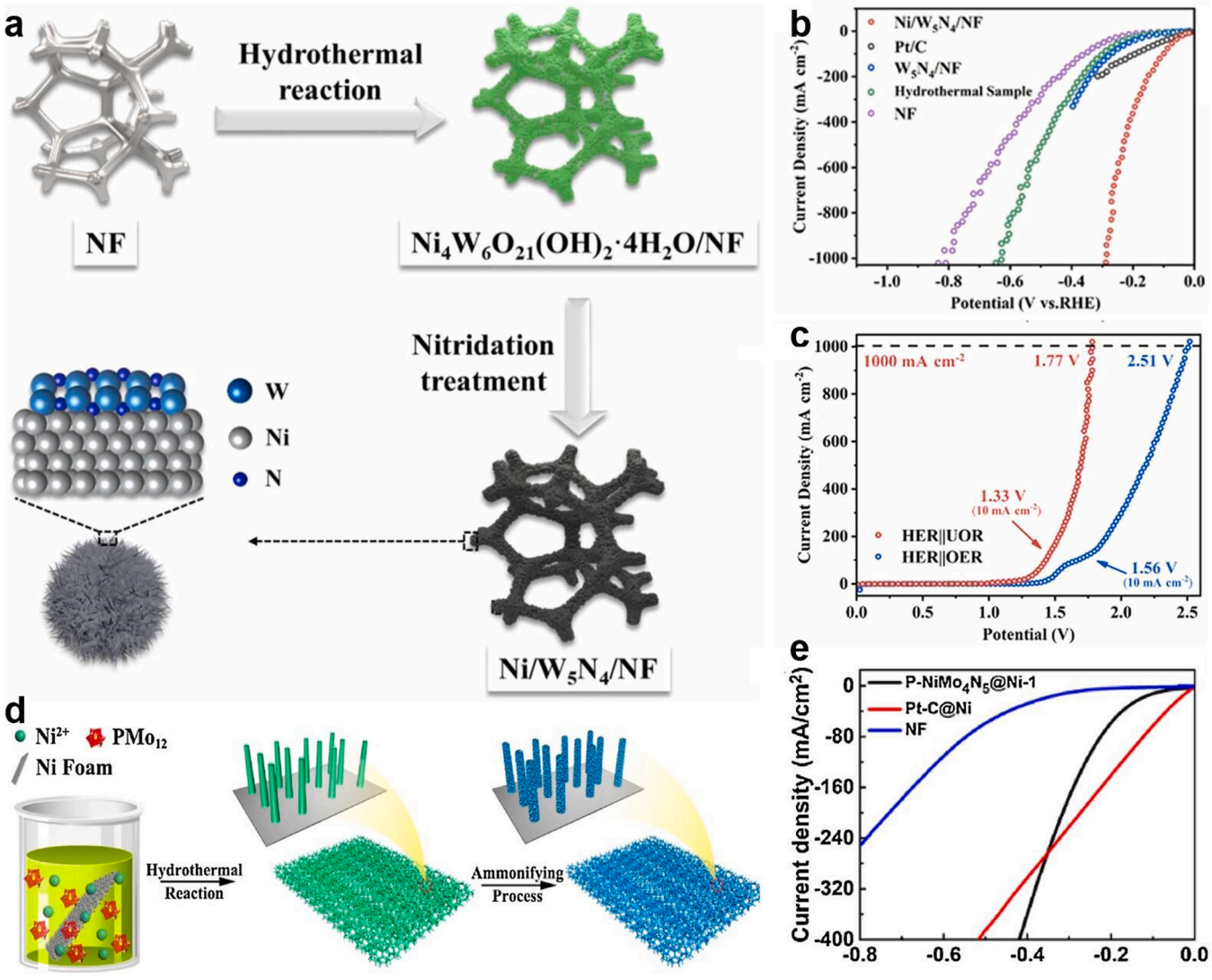

Fig. 8. (a) Schematic flow diagram for the fabrication of the Ni/W_5N_4/NF electrocatalyst. (b) The HER polarization curves of the series of catalysts. (c) The polarization curves of Ni/W_5N_4/NF in HER||UOR and HER||OER coupling systems. (a-c) Reproduced with permission [208]. Copyright 2022, Elsevier. (d) Schematic illustration of the synthetic process of twist braid nanorod arrays P-$NiMo_4N_5$@Ni-1 composite (180°C for 12 h; 500°C for 4 h in NH_3). (e) LSV curves of catalysts for HER in 1 M KOH. (d) and (e) Reproduced with permission [210]. Copyright 2018, Elsevier.

3.3. Metal nitrides/NF

Transition metal nitrides (TMNs), known for their exceptional electrical conductivity, low electrical resistance, and corrosion resistance, have garnered widespread attention in the domain of water electrolysis [201–203]. Notably, within 3D foam architectures, the seamless integration of a porous structure coupled with an expansive specific surface area has substantially enhanced the exposure of active sites, thereby greatly facilitating proton transfer and significantly elevating catalytic efficiency [204]. As an emergent modification strategy, Mott-Schottky heterojunction engineering leverages the formation of an intrinsic electric field to optimize and regulate the electronic spin states at the active interface [205,206], thus accelerating the HER process [207]. For instance, Zhou et al. [208] synthesized Ni/W_5N_4 Mott-Schottky heterostructure nanospheres supported on NF (Ni/W_5N_4/NF, Fig. 8**a**) through a hydrothermal process followed by a nitridation treatment. The Janus electron distribution at the Mott-Schottky interface, where the N atom layers in contact with Ni simultaneously absorb electrons from above and below, resulted in a substantial electron redistribution. This undoubtedly optimized the adsorption/desorption of intermediates, promoted the adsorption and activation of H_2O, and thereby significantly accelerated the entire HER process. Consequently, this unique electron configuration endowed the Ni/W_5N_4/NF catalyst with enhanced electrocatalytic performance for HER. At a current density of 10 mA cm^{-2}, the catalyst exhibited a mere overpotential of 25 mV. A substantial current density of 1000 mA cm^{-2} was achieved at an overpotential of merely 291 mV (Fig. 8**b**). In comparison to a conventional water electrolysis cell (which requires cell voltages of 1.56 and 2.51 V at 10 and 1000 mA cm^{-2}, respectively), the urea-assisted electrolysis using the Ni/W_5N_4/NF catalyst necessitated significantly lower cell voltages of 1.33 and 1.77 V at the corresponding current densities (Fig. 8**c**). Similarly, employing NF as a substrate, Song et al. [209] devised a facile vapor-phase nitridation synthesis method to fabricate layered porous CoN@NC nanosheets supported on NF. This catalyst exhibited a low onset overpotential of 61 mV and a low Tafel slope of 61 mV dec^{-1}, with its highly open 3D layered structure and the robust coupling effect between CoN and NC significantly promoting rapid charge transfer. These advancements not only deepen our understanding of the Mott-Schottky catalytic mechanism but also open novel avenues for the fabrication of highly efficient HER catalysts.

In alkaline media, bimetallic nitrides exhibit a significant enhancement in electrocatalytic performance compared to their monometallic counterparts, attributed to their synergistic improvement in catalytic activity and electrical conductivity [211–214]. Hu et al. [215] reported a mild nitridation strategy for synthesizing Ni-Mo bimetallic nitride nanorods (NMN/NF) on NF. First-principles calculations indicated that H_2O adsorbs more readily on the Mo atoms of Mo_2N, while H preferred the Ni sites of Ni_3N. After H_2O adsorption, the DOS for Mo_2N showed negligible changes and minimal charge transfer (0.04 e), suggesting a moderate interaction with H_2O that facilitated the H_2O dissociation step. In contrast, the DOS near the Fermi level of Ni_3N underwent significant alterations upon H adsorption, with substantial charge transfer (0.35 e), indicating a strong interaction between H and Ni_3N. Ni_3N exhibited a low H_2 desorption barrier (−0.08 eV), which was advantageous for H_2 release [216]. Therefore, the exceptional HER performance of NMN/NF could be attributed to the synergistic effects of the heterostructure Mo_2N/Ni_3N, where the former accelerated H_2O dissociation while the latter promoted H adsorption and H_2 release. The synthesized NMN/NF catalyst achieved a current density of 100 mA cm^{-2} at an ultra-low overpotential of only 66 mV in alkaline media. By *in situ* growth of CuNi bimetallic nitrides ($Cu_xNi_{4-x}N$) on porous NF, Ma et al. [119] facilitated the substitution of Cu(I) ions for Ni ions, leading to the formation of CuNi bimetallic nitrides. The optimized catalyst not only demonstrated outstanding electrocatalytic activity in 1 M KOH solution, requiring a mere overpotential of 110 mV to achieve efficient water splitting at a current density of 100 mA cm^{-2}, but also highlighted the pivotal role of precise synthesis of electrode surfaces and interfaces in elevating electrochemical performance. Additionally, the precise synthesis of electrode surfaces/interfaces plays a crucial role in enhancing electrochemical performance. For instance, Shen et al. [210] employed polyoxometalates as modulators to successfully fabricate arrays of morphologically distinct nanorods on NF (Fig. 8**d**). Notably, the optimized P-$NiMo_4N_5$@Ni-1 nanorod array electrode manifested exceptional HER activity (Fig. 8**e**). The superior catalytic activity was likely due to the modulation of the *d*-band density of positively charged Ni and Mo atoms by N atoms, aligning their electronic structures with those of Group VIII noble metals. The HER activity diminished with decreasing Mo content, attributed to the synergistic effects of the NiMo-based composite material. This material combined the characteristics of the rising branch of the volcano plot (weaker Ni-H bonds) and the descending branch (stronger Mo-H bonds), thereby enhancing the HER performance. It showed bifunctional electrocatalytic activities nearing 50 mA cm^{-2} and 100 mA cm^{-2} at cell voltages of 1.59 V and 1.66 V, respectively, ranking among the elite catalysts for water electrolysis. Table 3 summarizes the recent advances in the performance studies of NF-based nitride electrocatalysts in water electrolysis.

3.4. Metal oxides/NF

Metal oxides have garnered significant attention due to their compositional and structural diversity, tunability, low cost, abundant resources, and environmental benignity [223–225]. However, their application in the HER is constrained by limitations related to the binding energy of intermediates and stability issues [226]. Consequently, researchers have endeavored to develop efficient bifunctional HER catalysts based on metal oxides to meet the pressing demands of practical applications. Recent years have witnessed the deployment of a plethora of strategies, including doping, vacancy engineering, phase structure manipulation, strain engineering, morphological control, crystallinity tuning, precise valence state regulation, compositional optimization, and hybridization with other materials, all of which have substantially enhanced the HER activity of metal oxides. The implementation of these strategies has unveiled the potential of metal oxide-based HER catalysts to supplant precious metal catalysts. Earth-abundant simple transition metal oxides (TMOs), such as NiO [227], Co_3O_4 [228], TiO_2 [229], Ti_2O_3 [230], MoO_3 [231], MoO_2 [232], WO_3 [233], WO_2 [234], MnO_2 [235], and CeO_2 [236], along with their variants, have been thoroughly investigated and are deemed potent candidates for HER electrocatalysis. The exploration of these materials encompasses not only experimental studies aimed at activity enhancement but also theoretical analyses of the catalytic mechanisms, collectively propelling the application progress of metal oxides in HER

Table 3
Comparison of electrocatalytic performance of NF-based nitride electrocatalysts under alkaline conditions.

Catalysts	Current density (mA cm^{-2})	Overpotential (mV)	Tafel slope for HER (mV dec^{-1})	Ref.
CoN@NC-300	10	61	61	[209]
$Cu_xNi_{4-x}N$/NF	10	12	86	[119]
Ni/W_5N_4/ NF	10	25		[208]
P-$NiMo_4N_5$@Ni-1	10	118	125	[210]
Ni_3N@C/NF	100	95	60	[217]
$CoN_{0.73}Co_3$/NF	10	31	82	[218]
CoFe-NA/NF	10	73	96.7	[219]
NiMoN	100	56	45.6	[202]
Ni_3N_{1-x}/NF	10	55	54	[220]
NC/Ni_3Mo_3N/ NF	10	44.6	41.5	[221]
$CoMoN_x$-500 NSAs/NF	10	91	70.3	[222]

[237–239].

In the quest for high-performance oxide electrocatalysts, Li et al. [240] engineered a 3D urchin-like Co_3O_4 sphere array via a straightforward strategy, serving as an efficient bifunctional catalyst in electrochemical water splitting. Utilizing a hydrothermal method followed by subsequent low-temperature annealing, 3D urchin-like Co_3O_4 with a mesoporous structure and reduced charge transfer resistance was directly grown on NF (Fig. 9**a**). This approach offers advantages in streamlining the synthesis process, obviating the need for binders, and cost reduction. Nonetheless, there is room for enhancement in catalytic activity for this catalyst. Zhang et al. [241] swiftly constructed a Co_3O_4 layer rich in oxygen vacancies (O_v) on NF using a solid-phase melting strategy, where the O_v content in Co_3O_4 could be precisely varied between 52% and 74%, thereby modulating its performance in HER within

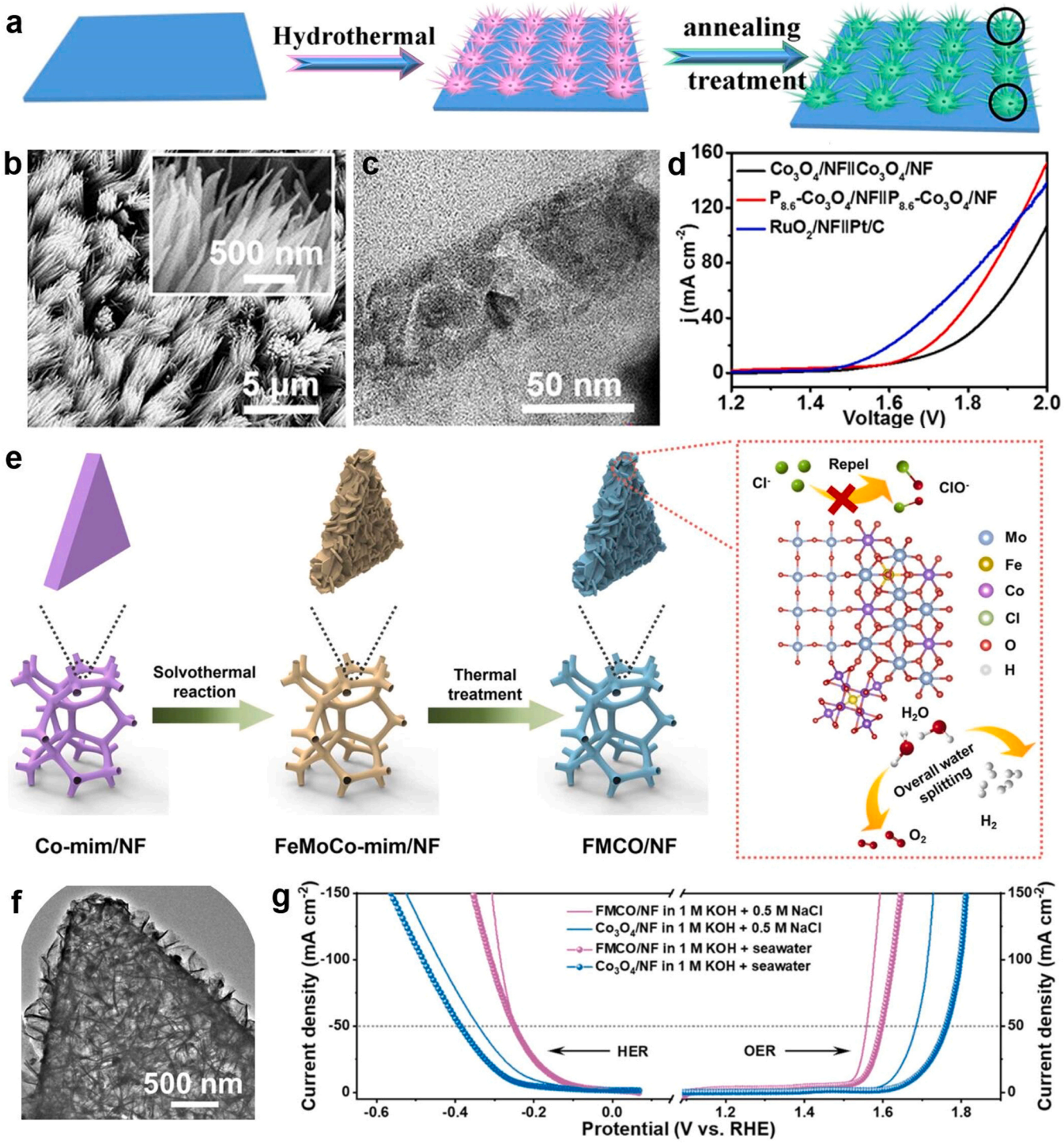

Fig. 9. (a) Schematic illustration of the synthesis of the Co_3O_4@NF. Reproduced with permission [240]. Copyright 2016, Elsevier. (b) SEM and (c) TEM image of $P_{8.6}$-Co_3O_4/NF nanowire. (d) Polarization curves of Co_3O_4/NF||Co_3O_4/NF, $P_{8.6}$-Co_3O_4/NF||$P_{8.6}$-Co_3O_4 /NF, and RuO_2/NF||Pt/C for water splitting in 1 M KOH electrolyte. (b-d) Reproduced with permission [242]. Copyright 2018, American Chemical Society. (e) Schematic illustration of the preparation route of the FMCO/NF catalysts. (f) TEM image of FMCO/NF. (g) OER and HER polarization curves for FMCO/NF and Co_3O_4/NF electrodes in 1 M KOH + 0.5 M NaCl and 1 M KOH + seawater, respectively. (e-g) Reproduced with permission [157]. Copyright 2023, Elsevier.

an alkaline medium. Moreover, the introduction of non-metal heteroatoms such as N, P, and S can further elevate alkaline HER performance through electronic structure modulation. Wang et al. [242] introduced P into Co_3O_4/NF (P-Co_3O_4/NF) by utilizing NaH_2PO_2 during low-temperature annealing, fabricating a P-doped Co_3O_4/NF nanowire array (Fig. 9**b**,**c**). The P-Co_3O_4/NF, serving as a 3D catalyst, exhibited a low overpotential (97 mV at 10 mA cm^{-2}), a modest Tafel slope (86 mV dec^{-1}), and commendable stability in 1 M KOH solution. The assembled $P_{8.6}$-Co_3O_4/NF-based full water-splitting device achieved 10 mA cm^{-2} at a mere 1.63 V (Fig. 9**d**), demonstrating its superior catalytic efficacy.

Mixed metal oxides (MMOs) are emerging as formidable contenders in the domain of efficient electrocatalytic HER, owing to their intrinsically unique properties [243–245]. By optimizing adsorption energies, MMOs transcend the boundaries of inherent catalytic activity, culminating in a marked enhancement in HER efficiency. For instance, Lu et al. [246] synthesized a remarkably active HER catalyst by pyrolyzing a manganese-based metal-organic framework (Mn-MOF) on a NF substrate. The NF provided a scaffold for catalyst growth and facilitated the formation of a Mn-doped nickel oxide/nickel heterostructure (Mn-NiO-Ni/NF) through the interaction between Ni and Mn-MOF. This heterostructure demonstrated superior activity to Pt benchmarks in neutral electrolytes and efficient generation of hydrogen from natural seawater. Moreover, in the promising sustainable hydrogen production method of electrochemical seawater splitting, Liu et al. [157] constructed Fe-doped $Co_2Mo_3O_8/MoO_3/Co_3O_4$ hybrid nanosheets on NF (FMCO/NF, Fig. 9**e**,**f**), which exhibited high resistance to corrosive salts and chloro-oxidation reactions (ClOR) prevalent in seawater (Fig. 9**g**). The core advantage of this material lies in the synergy between the corrosion-resistant Mo-O bond and the high activity of Fe dopants, ensuring FMCO/NF's high activity and durability in both simulated and real seawater media. Following the incorporation of Fe-Mo components, both Co^{3+} and Co^{2+} in FMCO/NF exhibited increased binding energies, indicating an enhancement in the positive charge at the Co sites. This modification accelerated the catalytic kinetics, potentially improving the overall efficiency of the reaction. A symmetric FMCO/NF-based alkaline electrolyzer produced a current density of 10 mA cm^{-2} at a low voltage of just 1.58 V, outperforming the IrO_2/NF||Pt/C/NF and the majority of non-noble metal-based catalysts.

Table 4 summarizes the recent advancements in the performance of oxide-based electrocatalysts on NF substrates for water electrolysis.

3.5. Metal phosphides/NF

Transition metal phosphides (TMPs), distinguished by their exceptional mechanical robustness, electrical conductivity, and chemical stability, have undergone nearly two centuries of development across a diverse array of fields [255–258]. The crystalline architecture of TMPs is constructed from trigonal prismatic primary units, culminating in isotropic crystals of high symmetry, with surfaces enriched in coordination-unsaturated atoms, providing a structural foundation for the significant enhancement of HER catalytic activity [259–261]. Notably, metal TMPs such as Fe, Ni, Co, Cu, and Mo, with their unique catalytic and electronic properties, have assumed a prominent position in the research of HER catalysts [262]. Compared to other compounds such as carbides, nitrides, and sulfides, TMP catalysts exhibit superior electrocatalytic activity due to their moderate affinity for hydrogen and electron-rich metal surfaces [263–265].

In the past decade, Ni/Co-based compounds and composites have garnered attention for their exceptional redox capabilities in OER and HER [68, 266, 267]. Notably, nickel-cobalt phosphides have demonstrated efficient bifunctional catalytic activity within the realm of traditional water electrolysis [268]. A quintessential example is the bifunctional catalyst of Ni-Co bimetallic phosphide (Ni_xCo_yP) on a NF substrate [269] (Fig. 10**a**). The synergistic interplay between Ni and Co optimizes the electronic distribution near the active sites, thereby enhancing the adsorption/desorption kinetics of the catalytic reaction intermediates. Substitution of Co and surface reconstruction significantly enhanced the intrinsic catalytic activity. Furthermore, the high conductivity of the porous NF and its binder-free nature significantly increase the exposure of active species, while the intimate integration with the NF framework greatly promotes electronic transfer efficiency. Consequently, the 0.005-NiCoP@NF catalyst requires a mere 166 mV of overpotential and 1.86 V of cell voltage to achieve a current density of 100 mA cm^{-2} in 1 M KOH solution (Fig. 10**b**) and exhibits outstanding long-term stability. Raman spectroscopy analysis of the 0.005-NiCoP@NF catalyst surface, conducted after 1 h and 40 h stability testing, revealed evolutionary behavior during the HER process. This analysis indicated the formation of a new catalytic system, Ni_xCo_yP/M-OH, as a subsequent reaction phase. This orderly and continuous surface activation process is key to the catalyst's exceptional long-term stability and high performance. The strategic design of nickel-cobalt phosphides to fully exploit active sites presents an attractive approach, Chen et al. [270] utilized a hydrothermal-phosphorization method to tightly bind NiCoP with 3D NF, facilitating the dynamic evolution of NiCoP structure from nanosheets to nanoneedles at varying hydrothermal temperatures (90–150°C). NiCoP-120 that, formed at 120°C, featured a multiscale hierarchical structure (hexagonal nanosheets vertically aligned at the edges, Fig. 10**c**), endowing it with the lowest R_{ct} and the highest ECSA. The NiCoP-120 catalyst requires only 56 mV and 247 mV of overpotential to achieve HER performance at current densities of 10 mA cm^{-2} and 1000 mA cm^{-2}, respectively (Fig. 10**d**), indicative of its superb low-overpotential performance. As both a HER and OER catalyst, NiCoP-120 achieves efficient (1.981 V@1 A cm^{-2}, Fig. 10**e**) and stable (600 h) ampere-level overall water splitting (Fig. 10**f**). The stability of NiCoP-120 was primarily attributed to its multiscale hierarchical structure as evidenced by the extremely low leaching of metal ions into the electrolyte, measured at only 0.045 mg L^{-1}, following the HER. Moreover, the catalyst has also been successfully demonstrated in the integration of renewable energy sources such as solar, wind, thermal, and lithium battery technologies into hydrogen systems, paving the way for the development of catalysts suitable for high-current water electrolysis and externally driven overall water splitting systems. Similarly, the growth of NiFeCo ternary phosphides on NF has also confirmed their commendable HER activity [271].

Although the catalytic activity and reaction kinetics of TMPs have previously constrained their widespread application, the unique electronic states at material interfaces have ushered in new prospects for the development of catalysts with superior activity and stability [272–275]. Wang et al. [276] have successfully fabricated a Ni_2P-$Ni_{12}P_5$ interface through a one-step phosphidation process induced by water on a NF substrate, enabling the heterostructured catalyst to grow directly on NF without the need for complex treatments, thus streamlining the preparation of the working electrode. Since $Ni_{12}P_5$ was the predominant

Table 4
Comparison of electrocatalytic performance of NF-based oxide electrocatalysts under alkaline conditions.

Catalysts	Current density (mA cm^{-2})	Overpotential (mV)	Tafel slope for HER (mV dec^{-1})	Ref.
Co_3O_4@Ni	10	225	53	[240]
M-Co_3O_4	100	203	63	[241]
$P_{8.6}$-Co_3O_4/NF	10	97	86	[242]
FMCO/NF	10	87	147.1	[157]
$Co_2Mo_3O_8$/Co/NF	10	50	49	[247]
$Ni^{III}Co^{II}$Fe-O@NF	10	58	120	[248]
CoNi/$CoFe_2O_4$/NF	10	82	96	[249]
N-Co_2VO_4/VO_2@NF	10	87	88	[250]
$Co_2Mo_3O_8/MoO_2$/NF	10	23	20	[251]
Ni-V_2O_3/NF	10	25	58	[252]
F-Co_2P/NF	10	46	79	[253]
$NiCo_2O_4$@$CoMoO_4$/NF-7	10	121	77	[254]

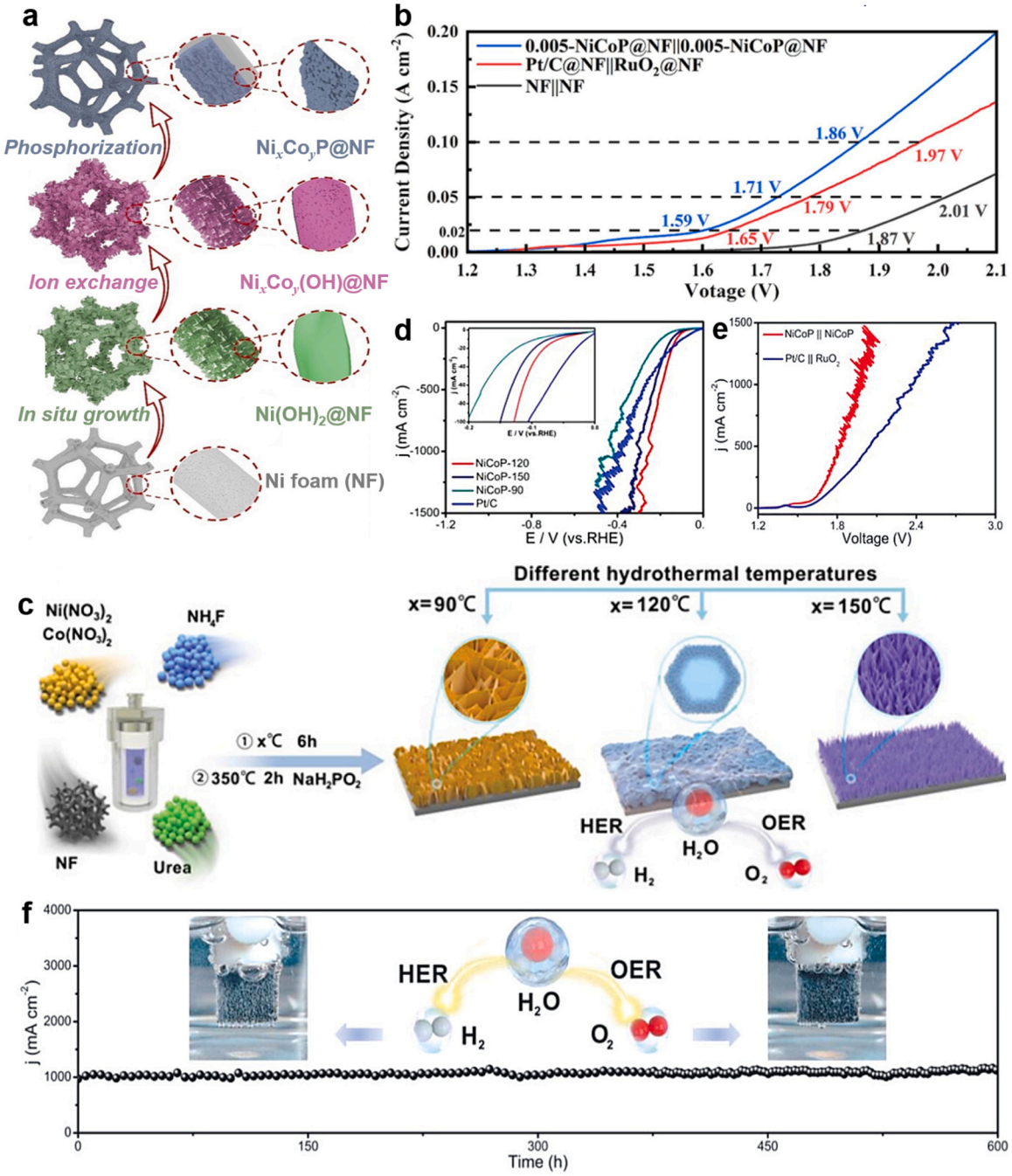

Fig. 10. (a) Synthesis process for X-NiCoP@NF catalysts. (b) Catalytic performance towards overall water electrolysis in 1 M KOH. (a) and (b) Reproduced with permission [269]. Copyright 2023, Elsevier. (c) Schematic illustration of structure design and reaction procedure of NiCoP. (d) HER polarization curves for NiCoP-90, NiCoP-120, NiCoP-150, and commercial Pt/C tested in 1 M KOH. (e) Polarization curves of NiCoP||NiCoP and Pt/C||RuO_2 for overall water splitting in a two-electrode configuration. (f) Long-term tests of water electrolysis with NiCoP||NiCoP system. (c-f) Reproduced with permission [270]. Copyright 2023, Wiley-VCH.

phase, an increase in Ni_2P indicated enhanced interfacial interactions. These rich interfaces conferred exceptional electrocatalytic HER activity to Ni_2P-$Ni_{12}P_5$/NF under alkaline conditions. Significant alterations in the electronic states occurred at the Ni_2P-$Ni_{12}P_5$ interface, where electrons transferred from $Ni_{12}P_5$ to Ni_2P at the interface. Simultaneously, P atoms at the interface of $Ni_{12}P_5$ also gained electrons, indicating a redistribution of charge between Ni and P atoms. This redistribution optimized hydrogen adsorption and thus enhanced HER activity as evidenced by an overpotential of 76 mV at 10 mA cm^{-2}, 147 mV at 100 mA cm^{-2}, and a Tafel slope of 68.0 mV dec^{-1}. Furthermore, Zhang's team [277] utilized a roughened NF as a scaffold and developed a layered, porous Ni_2P-$Ni_{12}P_5$ heterostructured catalyst through hydrothermal synthesis followed by subsequent annealing. This catalyst not only possessed an abundance of active sites but also exhibited high intrinsic activity in promoting the HER across a wide pH range. Table 5 summarizes the recent advancements in the performance of NF-based phosphides in the field of water electrolysis.

3.6. Metal selenides/NF

Transition metal selenides (TMSes), distinguished by their unique layered structure, narrow bandgap, diverse morphologies, and reduced

Table 5
Comparison of electrocatalytic performance of NF-based phosphide electrocatalysts under alkaline conditions.

Catalysts	Current density (mA cm^{-2})	Overpotential (mV)	Tafel slope for HER (mV dec^{-1})	Ref.
0.005-NiCoP@NF	10	81	76	[269]
NiCoP-NWAs/NF	100	197	54	[278]
NiCoP-120	10	56	88.9	[270]
NiFeCo phosphide	10	37	31	[271]
Co_2P/Ni_xP_y@NF	100	155	86	[279]
Ni_2P-$Ni_{12}P_5$/NF	10	76	68	[276]
CoP_3/$NiMoO_4$-NF-2	10	92	79.1	[280]
NF@Co_xP-300	10	32	67.1	[281]
Ni-Fe-Mn-P/NC@NF	10	72	79.8	[282]
Ni-P/Ni/NF	10	129	70	[277]
CoFe-P/NF	10	45	35.4	[283]
Co_2P-Ni_3S_2/NF	100	110	114.2	[284]
Co_2P/Ni_xP_y@NF	100	155	86	[279]

synthesis costs [285], have emerged as outstanding catalysts within the gamut of transition metal chalcogenides, exhibiting superlative catalytic characteristics and robustness, particularly in OER [286,287] and HER [288,289] applications. Indeed, TMSes are favored over their sulfide counterparts due to their superior electrical conductivity attributed to their analogous structures; for instance, $MoSe_2$ is preferred over MoS_2 partly due to the higher metallic character of selenium [290], rendering $MoSe_2$ a potent bifunctional electrocatalyst for both HER and OER.

The electrocatalytic activity of TMSe largely hinges on the exposed edge sites rather than the basal planes [291–293]. Various strategies, including downsizing TMSes to increase the number of active edge sites, fabricating ultrathin TMSe nanosheets, and constructing TMSe nanostructures on conductive substrates such as NF, CC, and CFP, have been developed. For example, Wu et al. [294] successfully synthesized vertically aligned ultrathin $NiSe_2$ nanosheets on NF, exhibiting exceptional and stable performance in overall water splitting. Zhou et al. [295] cultivated $MoS_{2(1-x)}Se_{2x}$ particles enriched with ternary sulfur-selenium molybdenum on porous $NiSe_2$ foam (Fig. 11**a**), leveraging the high electrical conductivity of 3D frameworks, helical structures, and synergistic effects among catalysts to expose a multitude of edge sites (e.g., $MoS_{2(1-x)}Se_{2x}$/$NiSe_2$ (100), $MoS_{2(1-x)}Se_{2x}$/$NiSe_2$ (110), Fig. 11**b,c**), significantly enhancing HER performance beyond that of most reported transition metal sulfides (e.g., MoS_2, $CoSe_2$) [296–298].

In the frontier exploration of 3D NF-supported nanostructured electrocatalysts, the development of selenide-based catalysts has achieved notable success [301–303]. The enhancement in their electrocatalytic performance is attributed not only to the increase of active sites but also to their inherent electrocatalytic ability and improved electrical conductivity [191,304,305]. Strategies such as intermetallic synergistic doping and the construction of hierarchical or heterostructures have demonstrated effectiveness in optimizing the surface and interfacial electronic structure of selenide electrocatalysts, thereby promoting intrinsic catalytic activity and conductivity [306]. For instance, the Tan group [263] engineered a novel 3D bifunctional nickel selenide electrode ($NiSe_2$/Ni_3Se_4/NF) composed of $NiSe_2$ and Ni_3Se_4 rich in phase boundaries, synthesized via an *in-situ* selenization reaction in a tube furnace (Fig. 11**d**). By adjusting the initial Se content, the phase composition, Ni charge state (Ni^{3+}/Ni^{2+} ratio), and electrocatalytic performance of Ni_xSe_y catalysts can be tailored. Catalysts rich in the Ni_3Se_4 phase enhanced the OER, while those with more $NiSe_2$ favored the HER. Electron transfer between these phases improved conductivity and optimized interfacial electronic structures, boosting electrocatalytic activity (Fig. 11**e**). Using $NiSe_2$/Ni_3Se_4/NF-4 and $NiSe_2$/Ni_3Se_4/NF-1 as cathode and anode, respectively, the electrolysis cell operated efficiently at a low voltage of 1.56 V at 10 mA cm^{-2}, showcasing remarkable durability. The construction of heterostructures has been recognized as an effective avenue to elevate the catalytic activity of selenides [307]. Modulating the interlayer spacing is another viable strategy to improve the catalytic performance. Through constructing a $CoSe_2$/$MoSe_2$ heterostructure, Zhang et al. [308] achieved a strong interfacial coupling between them and regulated the interlayer distance, effectively enhancing the electrocatalytic activity. Moreover, Liu et al. [299] successfully synthesized a bimetallic mesoporous nanosheet network selenide ($Ni_{0.89}Co_{0.11}Se_2$ MNSN/NF) on NF (Fig. 11**f**), which exhibited exceptional catalytic activity and stability across a wide pH range (Fig. 11**g,h**). Huang and colleagues [300] constructed a 3D Mo-doped porous $CoSe_2$ nanosheet array on commercial NF (Mo-$CoSe_2$ NS@NF), significantly enhancing charge transfer efficiency and optimizing the binding energy of active intermediates during the rate-determining step, thereby markedly improving the bifunctional electrocatalytic performance (Fig. 11**i**). The latest seminal advancements are summarized in Table 6, showcasing an overview of the performance of NF-based selenide catalysts in water electrolysis.

3.7. Metal alloys/NF

Non-precious metal alloys and their combination with noble metals have emerged as crucial materials in the field of heterogeneous catalysis due to their superior catalytic activity, stability, and selectivity compared to monometallic catalysts [315–317]. The underlying advantage primarily arises from synergistic effects induced by alloying and the optimization of the *d*-band center position [209,258,318]. The physical and chemical properties of the metal constituents undergo alteration during alloying, with the catalytic performance influenced by a confluence of ligand effects, ensemble effects, and strain effects. Depending on the constituent elements, alloys can be categorized into binary, ternary, quaternary, and high-entropy alloys [319]. Despite these advantages, the development of traditional alloy-based electrocatalysts faces challenges. On the one hand, the phase diagrams of bimetallic alloys often display extensive immiscibility gaps, limiting the fine-tuning of compositional ratios and precise control over catalytic activity. On the other hand, the corrosion resistance of most transition metals is relatively weak, which hampers their application in acidic or alkaline electrolytes [320,321].

Ni-based alloys are regarded as HER electrocatalysts with immense developmental potential due to their exceptional electrocatalytic activity and superb electrical conductivity [322–325]. NiCu alloys, in particular, with their high corrosion resistance, outstanding stability, and high HER efficiency, have shown great potential in the field of alkaline HER [326–329]. Sun et al. [330] successfully fabricated uniformly aligned and vertically oriented Ni(Cu)/NF nanotube electrodes via electrodeposition and selective electrochemical alloying techniques (Fig. 12**a**). The NF substrate not only provides a substantial accessible electroactive surface area but also facilitates rapid transfer and dissipation of gas bubbles due to its ultra-large pores (200–500 μm), significantly reducing the “bubble overpotential” and effectively overcoming the limitations of catalytic performance due to restricted active sites on the NiCu alloy surface. This Ni(Cu)/NF electrode possesses an immense electrochemically active surface area and exhibits HER electrocatalytic activity comparable to that of Pt (Fig. 12**b**).

The construction of hierarchical heterostructures has proven to be an effective strategy for enhancing the intrinsic activity of HER by modulating the electronic structure of catalysts and achieving a balance between the adsorption and desorption of intermediates [331–333]. Shi et al. [334] successfully *in-situ* synthesized 1D porous $NiMoO_x$

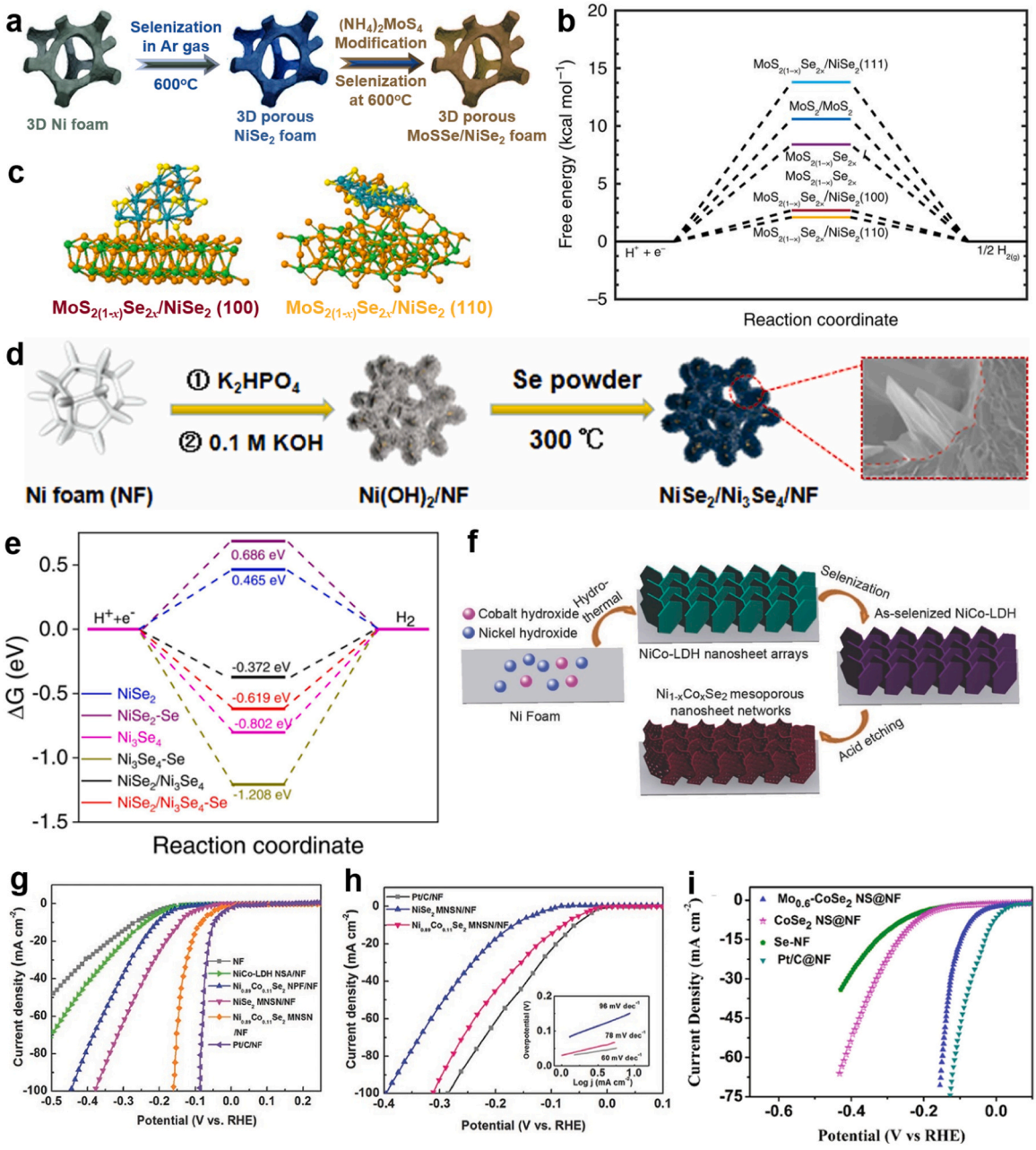

Fig. 11. (a) The procedures for growing ternary $MoS_{2(1-x)}Se_{2x}$ particles on porous $NiSe_2$ foam. (b) Calculated adsorption free energy diagram for hydrogen (H*) adsorption at the equilibrium potential for $MoS_{2(1-x)}Se_{2x}/NiSe_2$ hybrid, binary MoS_2, and ternary $MoS_{2(1-x)}Se_{2x}$ catalysts. (c) Intermediate structures of hydrogen bound $MoS_{2(1-x)}Se_{2x}/NiSe_2$ (100) and $MoS_{2(1-x)}Se_{2x}/NiSe_2$ (110).(a-c) Reproduced with permission [295]. Copyright 2016, Nature. (d) Schematic illustration for the preparation of the $NiSe_2/Ni_3Se_4$/NF samples. (e) The standard free energy diagrams in the HER process on $NiSe_2$, Ni_3Se_4, and $NiSe_2/Ni_3Se_4$ at U = 0. (d) and (e) Reproduced with permission [263]. Copyright 2021, Elsevier. (f) Schematic illustration of the synthesis of 3D $Ni_{1-x}Co_xSe_2$ MNSN on NF. (g) The LSV curves of NF, NiCo-LDH NSA/NF, $Ni_{0.89}Co_{0.11}Se_2$ NPF/NF, $NiSe_2$ MNSN/NF, $Ni_{0.89}Co_{0.11}Se_2$ MNSN/NF, and Pt/C/NF measured in 1 M KOH solution. (h) LSV curves and corresponding Tafel plots of $Ni_{0.89}Co_{0.11}Se_2$ MNSN/NF, $NiSe_2$ MNSN/NF, and Pt/C/NF in 1 M PBS solutions. (f-h) Reproduced with permission [299]. Copyright 2022, Wiley-VCH. (i) LSV curves for Se-NF, $CoSe_2$ NS@NF, $Mo_{0.6}$-$CoSe_2$ NS@NF and Pt/C@NF in 1 M KOH for HER. Reproduced with permission [300]. Copyright 2020, Elsevier.

micro-rods on a 3D NF substrate and uniformly embedded 0D NiMo nanoalloy particles within, culminating in the formation of a MoNi/$NiMoO_x$ hierarchical heterostructure (Fig. 12**c**). This architecture demonstrated exceptional HER performance, manifesting ultra-low overpotentials of merely 139 mV and 289 mV to drive an ampere-level current density of 1.9 A cm^{-2} in 1 M KOH and 1 M PBS solutions, respectively (Fig. 12**d**,**f**). At 1 A cm^{-2}, the MoNi/$NiMoO_x$ catalyst achieved nearly 100% hydrogen FE with a production rate of about 7 ml min^{-1}, showcasing industrial-grade activity and stability (Fig. 12**e**). Remarkably, the MoNi/$NiMoO_x$ also showcased superior HER performance in unacidified and unalkalized seawater (Fig. 12**g**). Especially in a 10×10 cm^2 membrane electrode assembly (MEA) electrolyzer, it achieved a hydrogen production rate of 12.12 L h^{-1} (a twelvefold increase over commercial NF, Fig. 12**h**) and maintained prolonged stability for over 1600 hours (Fig. 12**i**), indicating its significant potential for application in large-scale industrial hydrogen production. The exemplary performance of this structure can be partially attributed to its low water dissociation energy ($\Delta G_{diss} = -1.2$ eV) and

Table 6
Comparison of electrocatalytic performance of NF-based selenide electrocatalysts under alkaline conditions.

Catalysts	Current density (mA cm^{-2})	Overpotential (mV)	Tafel slope for HER mV dec^{-1})	Ref.
Two-tiered NiSe	10	177	58.2	[294]
FNS/0.6	10	156	193	[309]
$Mo_{0.6}$-$CoSe_2$ NS@NF	10	89	69	[300]
$NiSe_2$/Ni_3Se_4/NF-4	10	145	69.7	[263]
$Ni_{0.89}Co_{0.11}Se_2$ MNSN/NF	10	85	52	[299]
O-$Ni_{0.5}W_{0.5}Se_2$/NF	20	109	63.8	[207]
Ni-S-Se/NF	10	98	99.4	[310]
CoO_x-CoSe	10	90	94	[311]
Co-Ni-Se/C/NF	10	90	81	[312]
V,N-Co/Fe-Se/C@NF	10	67	72.1	[313]
$Co_{0.9}Fe_{0.1}$-Se/NF	10	125	85.4	[314]

near-ideal hydrogen adsorption energy ($\Delta G_H^* = -0.01$ eV). Compared to traditional synthesis methods for electrocatalysts, the Zhao group [335] leveraged a rapid Joule heating method to integrate a NiFe alloy onto the MoO_2 surface on NF (Fig. 12**j**), further optimizing the Fe-Ni bond and enhancing electrical conductivity. This innovative approach not only modulated the electronic structure of the alloy but also propelled a significant amelioration in electrochemical performance (Fig. 12**k**). A FeMoNi/NF(+)//FeMoNi/NF(−) coupled membrane electrode electrochemical reactor exhibited a mere 1.45 V at 10 mA cm^{-2} (Fig. 12**l**), marking the lowest energy consumption (6.47 kW h m^{-3}) and suggesting potential for commercial application in seawater. Furthermore, the synergistic effect among the constituent elements can also elevate the intrinsic activity of the active sites. Hsieh et al. [336] synthesized a NiFeMo alloy bournonite on NF, capitalizing on its orderly porous structure and the synergy among the three elements, to establish a new benchmark for overall water splitting. They achieved current densities of 10 and 500 mA cm^{-2} at impressively low cell voltages of 1.47 and 1.75 V, respectively.

High-entropy alloys (HEAs), constituted by five or more metallic elements in equiatomic or near-equiatomic proportions, have been discerned to exhibit a plethora of distinctive and compelling properties owing to the heterogeneity in atomic structure and the flexibility in compositional tuning afforded by their multi-principal element constitution [337–340]. These properties encompass remarkable mechanical strength and ductility, superconductivity, pronounced paramagnetism, thermoelectric characteristics, elevated stability, and superior hydrogen storage capabilities [341]. The structural distinction between conventional alloys and HEAs is that conventional alloys are based on a predominant element with minor dopants, whereas HEAs exhibit lattice distortions and structural modifications [342]. In a recent study, Wang et al. [343] synthesized a hierarchically structured HEA with a composition of $Fe_{0.22}Co_{0.18}Ni_{0.18}Cr_{0.14}Cu_{0.28}$ through a far-from-equilibrium electrochemical process (Fig. 13**a**), which achieved a current density of 10 mA cm^{-2} at a modest overpotential of 84 mV (Fig. 13**b**). The omission of any single metallic constituent from the alloy composition was observed to substantially impair its HER performance (Fig. 13**c**); this effect was particularly pronounced upon the removal of Cr or Cu, which resulted in a significant escalation in overpotential. Thus, comprehending the cooperative interplay of elements within HEAs is of paramount importance for the optimization of their performance. The research collective led by Sivanantham [344] constructed and probed the influence of vanadium incorporation in V_xCuCoNiFeMn ($x = 0$, 0.5, 1.0) HEA series on the enhancement of electrocatalytic activity for the HER (Fig. 13**d**). The findings indicated that the integration of vanadium markedly fostered structural cohesiveness of the alloy. Specifically, the overpotential at 50 mA cm^{-2} (η_{50}) for $V_{1.0}$CuCoNiFeMn ($V_{1.0}$-HEA) in 1 M KOH solution was measured at 250 mV relative to the reversible hydrogen electrode, which is a reduction of approximately 170 mV compared to the vanadium-free benchmark (Fig. 13**e**), significantly augmenting the electrical conductivity and the electrochemically active surface area of $V_{1.0}$-HEA, and thereby accelerating the HER kinetics. Additionally, density functional theory calculations unveiled a diminution in both the water dissociation energy and the hydrogen adsorption energy for $V_{1.0}$-HEA, contributing to an enhanced dynamism in HER performance (Fig. 13**f-h**). Table 7 encapsulates the recent advancements in the performance of NF-based alloy catalysts within the domain of water electrolysis.

To enhance the performance of NF-based non-precious metal electrocatalysts for water splitting, several effective strategies can be employed. These include doping with heteroatoms, boosting electrical conductivity, creating heterostructures, modifying wettability, and applying interfacial and defect engineering. These methods aim to enhance the potential of catalysts such as TMSs, LDHs, TMSes, TMPs, TMNs, TMOs, and alloys on NF substrates. The inherent chemical properties and electronic diversity of compounds like sulfides, phosphides, and selenides largely stem from the electronegativity differences between their elements. Sulfides, stabilizing metal bonds due to sulfur's moderate electronegativity, exhibit good thermodynamic stability and resistance to oxidation. Conversely, the lower electronegativities of phosphorus and selenium make phosphides and selenides more reductive, increasing their sensitivity to oxidative environments and chemical reactivity. LDHs are characterized by their strong affinity for water, which forms structured hydration layers through hydrogen bonds and electrostatic interactions. These layers are crucial for maintaining LDHs' structural integrity and enable their ion exchange and adsorption capabilities, making LDHs valuable for applications in catalysis, environmental remediation, and drug delivery. Nitrides and oxides, formed from metals and non-metallic elements like nitrogen or oxygen, show properties influenced by these elements' electronegativity differences, manifesting in characteristics like high hardness or thermal resistance for nitrides and varying acidity or basicity for oxides. Alloys, composed of mixtures of metals or metals with non-metals in various proportions, are not strictly pure compounds. Their physical and mechanical properties are a blend of their constituent elements, which can be customized through compositional adjustments. Understanding the synthesis characteristics and mechanisms is crucial for designing high-performance catalysts, as summarized in Table 8, which details the pros and cons of prevalent synthesis methods.

Compared to the proton-driven electrocatalytic HER process in acidic media, the need for an additional H_2O dissociation step in alkaline media presents a more challenging scenario for electrocatalytic HER. However, NF is unstable in acidic solutions, making it susceptible to oxidative corrosion. Therefore, while NF acts as an effective electrode substrate in alkaline conditions for electrocatalytic HER, its direct use in acidic media poses a significant challenge, limiting its industrial application. Interestingly, the stability of NF in acidic environments can be enhanced through robust protective measures. For instance, Li et al. [350] improved its acid stability by synthesizing 3D graphene foam on NF using chemical vapor deposition techniques. Zhao et al. [351] employed corrosion-resistant metal phosphides to prevent electrolyte corrosion. Similarly, Wan et al. [352] enhanced both acid and alkaline HER activity of NiMoN@NC-6 by incorporating appropriate N doping, carbon coating, and constructing a 3D self-supporting hierarchical structure. Table 9 summarizes the latest advancements in the performance of NF-based catalysts in acidic media.

4. Conclusions and perspectives

The quest for economical, highly efficient, and exceptionally stable HER electrocatalysts is of paramount significance for the sustainable development of industrial-scale electrolytic hydrogen production [83,

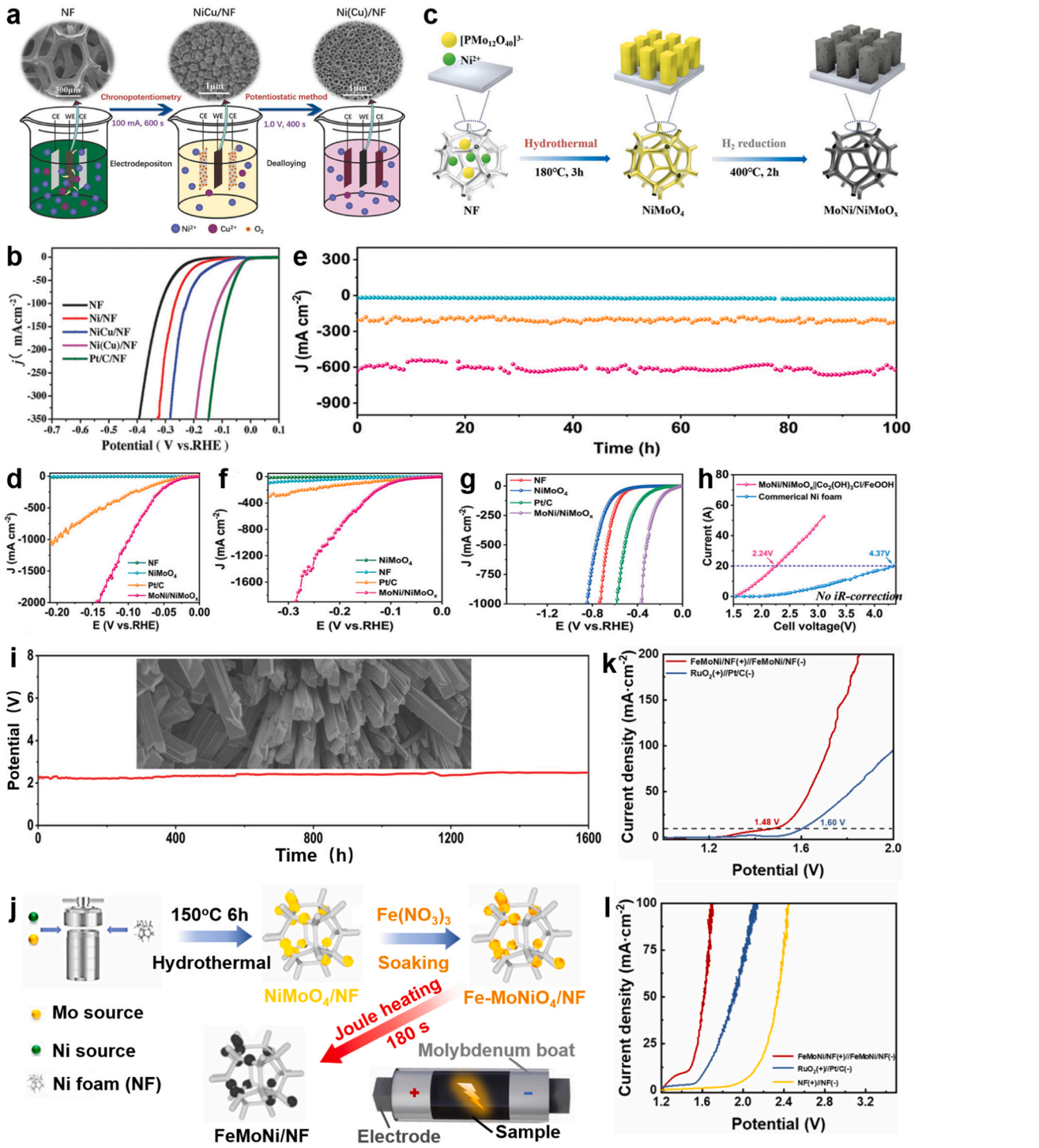

Fig. 12. (a) Schematic illustration of the formation of Ni(Cu)/NF. (b) HER polarization curves for NF, Ni/NF, NiCu/NF, Ni(Cu)/NF, and Pt/C/NF with 95% *iR*-compensations. (a) and (b) Reproduced with permission [330]. Copyright 2018, Wiley-VCH. (c) Schematic illustration of the synthetic process for $MoNi/NiMoO_x$ catalyst. (d) HER polarization curves of different electrocatalysts in 1 M KOH. (e) I-t curves of $MoNi/NiMoO_x$ at different current densities. Electrochemical performance in (f) 1 M PBS solution and (g) seawater. (h) The steady-state current versus potential data for $MoNi/NiMoO_x||Co_2(OH)_3Cl/FeOOH$ and NF||NF toward overall water splitting in a 10 × 10 cm^2 membrane electrode assembly (MEA) electrochemical reactor. (i) Long-term stability test at a fixed current of 20 A in 1 M KOH. (c-i) Reproduced with permission [334]. Copyright 2023, Wiley-VCH. (j) Schematic illustration of the synthesis process for self-supported FeMoNi/NF. (k) LSV curves in 1 M alkaline seawater electrolyte. (l) LSV curves in MEA electrolyzer in 1 M alkaline seawater electrolyte. (j-l) Reproduced with permission [335]. Copyright 2023, Elsevier.

360, 361]. Compared to conventional powder-coated electrodes, the *in-situ* integration of active phases into self-supporting electrodes not only streamlines the electrode fabrication process and reduces interfacial resistance but also enhances catalyst stability and activity due to increased exposure of active sites. This innovative direction has demonstrated substantial potential for application within the field of water splitting [362]. This review concentrates on the cutting-edge research achievements regarding NF-based non-precious metal

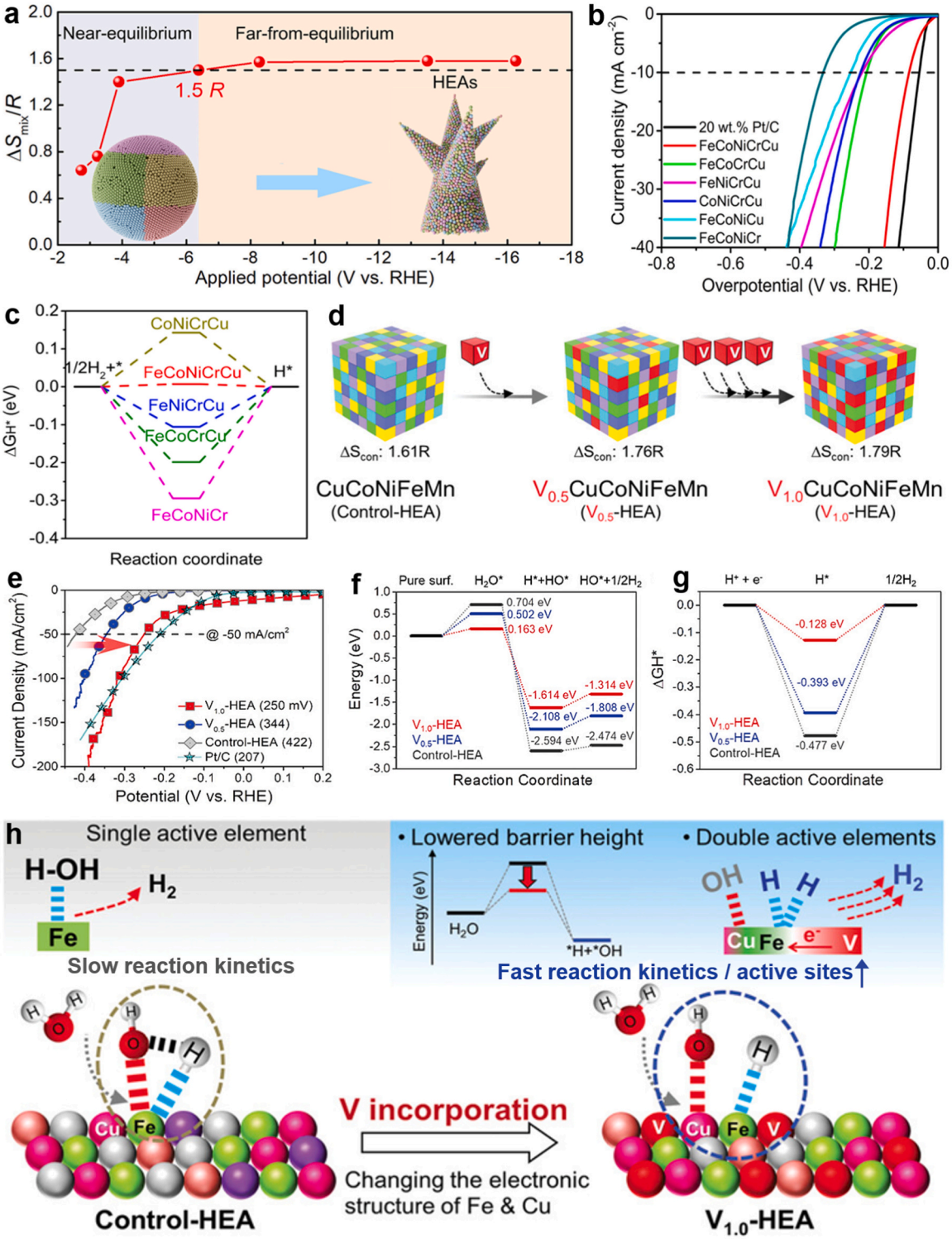

Fig. 13. (a) The dependence of the mixing entropy (ΔS_{mix}) of the as-prepared samples on the applied potential. (b) LSV curves of samples performed in 1 M KOH. (c) Gibbs free energy change (ΔG) of H* species adsorption on the surface of the as-prepared samples. (a-c) Reproduced with permission [343]. Copyright 2023, Elsevier. (d) Schematic representation and configuration entropy values of three HEAs (control-HEA, $V_{0.5}$-HEA, and $V_{1.0}$-HEA). (e) LSV curves measured in 1 M KOH electrolyte. (f) Reaction energy diagram of water dissociation and (g) Gibbs free energy (ΔG_H*) diagram of hydrogen adsorption on the surface of three HEAs. (h) Schematic representation of the effect of V incorporation on the barrier height and active sites at the surface of $V_{1.0}$-HEA. (d-h) Reproduced with permission [344]. Copyright 2023, Wiley-VCH.

electrocatalysts for water splitting, with NF's unique three-dimensional porous structure significantly benefiting as an ideal platform for the growth of nanomaterials. A diverse array of nanostructures, including particles, sheets, films, arrays, rods, layered structures, and composites, have been successfully cultivated directly on NF substrate, exhibiting exceptional HER activity, suggesting their potential to supplant costly and scarce precious metal catalysts. The paper also emphasizes specific strategies for optimizing electrocatalyst performance, such as

Table 7
Comparison of electrocatalytic properties of NF-based alloy electrocatalysts under alkaline conditions.

Catalysts	Current density (mA cm^{-2})	Overpotential (mV)	Tafel slope for HER (mV dec^{-1})	Ref.
Ni(Cu)/NF	10	27	33.3	[330]
ho-LaNi$_5$/NF	10	136	84	[320]
MoNi/NiMoO$_x$	10	9	31	[345]
FeMoNi/NF	10	20	23.2	[335]
NiFeMo IOS@NF	10	33	56	[336]
TMP NiZn-Ni/NF	600	233	47.3	[321]
Ni$_{2-x}$Co$_x$P/N-C NFs	10	130	70	[346]
FeCoNiMo@C/NF	10	55	56.2	[347]
Fe$_{0.22}$Co$_{0.18}$Ni$_{0.18}$Cr$_{0.14}$Cu$_{0.28}$	10	84	62	[343]
V$_{1.0}$-HEA	50	250	148	[344]
NiFeCoCuTi	2000	209	43	[348]
NiCoFeMoMn	1000	150	29	[349]

Table 8
Advantages and disadvantages of Ni-based catalyst synthesis methods.

Methods	Advantages	Disadvantages
Solvothermal/ Hydrothermal growth	Simple process, relatively low temperature, low agglomeration, controlled particle shape	Uneven loading, possibility of side reactions in organic solvents, inability to observe the progress of the reaction
Electrodeposition	Uniform distribution of active substances, short time, high efficiency, precise control	Generally polycrystalline and amorphous, complex processes
High temperature annealing	Ease of use, improved thermal stability	Limited shape adjustability, high costs, and altered the shape at high temperatures
Ion exchange	High efficiency and low cost	Poor general applicability, generation of regeneration waste liquid
Chemical vapor deposition	Excellent film quality, high deposition rate, versatility and controllability	High cost, process complexity, reactant limitations
Corrosion engineering	Low cost, simple synthesis, effective regulation	Easy peeling of corrosion layer, poor material compatibility
Template assisted	Precise control of shape and structure, customizable	High cost, complex process, potential residuals in templates
One-step room temperature	Easy to operate, low cost and environmentally friendly	Limited scope of application, reaction kinetics constraints

heteroatom doping, electrical conductivity enhancement, heterostructure construction, wettability modulation, and surface/defect engineering, to further unlock the catalysts' potential [363]. By implementing of these strategies, we anticipate the development of more economical, efficient, and stable HER catalytic systems, thus advancing the application of clean energy technologies.

3D macroporous metallic NF is widely utilized as a support material for electrocatalysts due to its excellent electrical conductivity. However, under high current density and high-temperature conditions, the mechanical stability of NF may not meet the requirements for long-term usage, particularly during high-temperature pyrolysis processes, where they may become brittle and fragment, constraining the application scope of synthetic methods for self-supported electrocatalysts. NF substrates and Ni-based nanostructured catalysts often display low activity or instability in acidic media due to metal leaching and structural changes. Addressing these issues could involve designing phosphides or selenides of Fe, Co, and Ni on NF, which offer higher corrosion resistance and demonstrate activity in acidic conditions compared to oxides and

Table 9
Comparison of electrocatalytic performance of NF-based electrocatalysts under acidic conditions.

Catalysts	Current density (mA cm^{-2})	Overpotential (mV)	Tafel slope for HER (mV dec^{-1})	Ref.
MoS$_2$/Graphene/ NF	10	141	42.8	[350]
Ni$_3$S$_2$@NiSe/NF	10	103	74.2	[353]
NiMoN@NC-6	10	7	37.1	[354]
MoO$_2$-CeO$_x$/NF	10	41	44.1	[355]
CoMnP/Ni$_2$P/NF	10	84	57	[351]
NiCoP@NC NA/ NF	10	34	51.8	[356]
Ni$_{0.89}$Co$_{0.11}$Se$_2$ MNSN/NF	10	52	39	[357]
Ni-P/Ni/NF	10	83	68	[277]
CoMoNiS-NF-31	10	103	85	[358]
Ni@NCNT/ NiMoN-8	10	31	33	[352]
Cu$_x$Ni$_{4-x}$N/NF	10	52	59	[119]
0.5CDs-NiCoP/NF	10	117	73	[359]

sulfides. Another promising direction is the development of efficient, stable, and acid-insoluble non-precious metal alloys. Despite the focus on electrocatalyst design, there is a need for more research on substrates to develop advanced, efficient materials that enhance catalytic activity and maintain stability in practical applications. Moreover, retaining the advantages of self-supported electrodes in large-scale production and practical applications remains a significant challenge in current research.

Additionally, the chemical and physical characteristics of the substrates directly impact their performance and application fields, with the interfacial interactions between active materials and conductive substrates playing a decisive role in electron transfer efficiency and catalyst durability. However, research in this area is still insufficiently developed. Investigating interactions such as electrostatic attraction, van der Waals forces, and covalent bonding is crucial for optimizing electrocatalyst interface design. These interactions facilitate nearly zero-resistance interfaces, enhancing charge transfer. That is crucial for efficient HER at high current densities. Strong covalent bonds between catalysts and substrates also ensure mechanical stability and prevent catalyst detachment. In addition to interfacial optimization, addressing mass transfer and diffusion is vital. For HER, issues such as the wettability of the electrocatalyst and bubble accumulation on electrodes during prolonged operations significantly impact efficiency. Electrodes with high bubble adhesion obscure active sites and impede electrolyte diffusion, necessitating higher voltages for electrolysis. Designing electrodes with surface structures that promote rapid bubble detachment can enhance catalytic activity. Further, developing uniform nanostructures with superhydrophilic or superhydrophobic properties can improve bubble release and stress regulation. Superhydrophobic surfaces reduce bubble adhesion by creating discontinuous solid/liquid/gas interfaces, while superhydrophilic surfaces increase the interface between the electrolyte and electrode, enhancing permeability and catalytic activity. Additionally, applying magnetic fields and hypergravity during electrolysis can alter the electrolyte environment, inducing convection that reduces bubble accumulation and boosts electrocatalytic efficiency.

Common methods for fabricating self-supporting electrocatalysts, such as hydrothermal/solvothermal growth and heat treatment, often require high temperatures or pressures, which limits their scalability. Conversely, one-step room temperature and electrochemical conversion methods offer simple and mild conditions but may struggle to produce well-defined arrays. There is a pressing need to refine these methods to develop a straightforward, universal strategy for creating structured nanoscale arrays suitable for large-scale production. Additionally, the catalyst loading on the substrate significantly impacts the HER

performance. High loading and active thick layers may lead to detachment of the catalyst layer from the substrate during testing, subsequently dissolving in the electrolyte. Conversely, low loading and thin layers may reduce catalytic activity. Ensuring the optimal catalyst loading is crucial for efficient water splitting. Future research should focus on these issues to advance the application and development of self-supporting electrocatalysts for sustainable energy devices.

In pursuit of enhancing the efficacy of electrocatalysts, the precision selection of appropriate active sites to reduce overpotential is of paramount importance. Optimal active sites should demonstrate moderate adsorption capabilities for reaction intermediates, facilitating effective binding while ensuring the smooth release of the products. Reference to the volcano plot represents a pragmatic strategy [364]; metals located at the apex of the curve typically possess ideal adsorptive properties, reflecting their intrinsic advantage as active sites. Following the identification of such sites, strategies including augmenting the intrinsic activity of the sites, increasing their exposure, and enhancing the wettability of the catalyst surface can comprehensively elevate the overall activity of the catalyst.

To significantly enhance the intrinsic activity at active sites, it is essential to investigate the fundamental reaction mechanisms. Theoretical calculations and *in-situ* spectroscopic studies are powerful tools for elucidating the electrode catalytic mechanisms and structural transformations. Techniques such as Raman spectroscopy, X-ray photoelectron spectroscopy (XPS), X-ray diffraction (XRD), and Fourier-transform infrared spectroscopy (FTIR) have been employed to probe surface species during the HER, aiding in the identification of true catalytic active sites and mechanisms. Concurrently, TEM can provide in-depth insights into the morphology, microstructure, and chemical properties of catalysts at the nanoscale. *In-situ* TEM allows for real-time studies of the dynamic processes of catalytic reactions under gas and liquid environments. Furthermore, more refined characterizations at the atomic level should be employed. For instance, characterization using both non-*in situ* and *in situ* synchrotron radiation can investigate electronic structures, oxidation states, and coordination environments. Rapid development of additional high-resolution techniques is essential for studying reaction processes and the evolution of surfaces/interfaces/bulk materials. DFT calculations, integrated with transition state theory, can identify reaction pathways during the process, and molecular dynamics simulations can track the trajectories and transport of H_2O molecules, OH, and H intermediates over time. By calculating the free energy changes and barriers of reaction intermediates along these pathways, one can estimate reaction rates for each fundamental reaction step and identify the rate-determining step. Finally, solving microkinetic equations allows for elucidating the mechanism of the alkaline HER, evaluating the activity and selectivity of the catalysts, and verifying the reliability of the proposed reaction mechanisms. In conjunction with the catalytic mechanism, adjusting the structural and electronic *d*-band center of the metal active sites strategically aligns them closer to the apex of the volcano plot, further unleashing the catalytic potential of the electrocatalyst [343].

Concerning stability, although most reported NF-based electrodes operate for tens of hours at a current density of 10 mA cm^{-2}, they fall short of the industrial electrolysis requirement of an overpotential below 300 mV and stability for thousands of hours at 500 or even 1000 mA cm^{-2}. To develop robust self-supporting electrodes, catalysts have been designed and synthesized with optimal intermediate adsorption energies and porous structures, facilitating the release of H_2 bubbles from the surface and enhancing mass transfer. However, it is imperative to evaluate the fabricated electrocatalysts under simulated industrial conditions. Industrial electrocatalysis of water often requires a high concentration of electrolytes, elevated temperature, and high pressure. Ion migration rates, electrolyte conductivity, and the structural stability of electrocatalytic materials under industrial conditions significantly differ from those observed in laboratory-scale experiments. Given the substantial differences between laboratory-scale experiments and industrial conditions, it is crucial to apply the electrocatalysts in actual electrolysis cells to transition them to industrial applications. This transition not only tests the practical viability of the catalysts but also ensures that they can perform effectively and sustainably under the demanding conditions of industrial operations. This step not only tests the practical viability of the catalyst but also ensures its effectiveness and sustainability under harsh industrial conditions. Thus, to improve the stability of the catalyst, it is crucial to consider several key factors. These include the composition of the catalyst, the type of support it utilizes, the interfacial interaction between the catalyst and the conductive support, as well as the wettability between the electrode and the electrolyte. These factors collectively influence the durability of the electrocatalyst [41].

In summary, overcoming existing constraints requires ongoing and in-depth research and development efforts. These include optimizing synthesis and characterization techniques for electrocatalysts on NF supports, advancing understanding of the water-splitting mechanism, and dedicating efforts to develop more robust and stable catalysts. These endeavors aim to ensure outstanding performance under practical application conditions.

CRediT authorship contribution statement

Jiajia Li: Formal analysis, Data curation. **Jin Jia:** Writing – review & editing, Writing – original draft, Funding acquisition, Formal analysis, Data curation, Conceptualization. **Yuanyuan Zhu:** Writing – review & editing, Writing – original draft, Project administration, Funding acquisition, Formal analysis. **Shanhai Ge:** Writing – review & editing, Supervision, Conceptualization. **Chengzhi Xiao:** Writing – original draft, Data curation. **Tongzhou Hong:** Writing – original draft, Data curation. **Haowen Jia:** Formal analysis, Data curation. **Conghu Liu:** Writing – review & editing, Supervision, Project administration, Funding acquisition, Formal analysis. **Guang Zhu:** Writing – review & editing, Writing – original draft, Supervision, Project administration, Funding acquisition, Formal analysis, Conceptualization.

Declaration of Competing Interest

The authors declare that they have no known competing financial interests or personal relationships that could have appeared to influence the work reported in this paper.

Data Availability

No data was used for the research described in the article.

Acknowledgements

This work was financially supported by the fund of the State Key Laboratory of Catalysis in DICP (Grant No. N-23-08), Doctor Research Startup Foundation of Suzhou University (Grant Nos. 2022BSK005 and 2023BSK015), Provincial of the Anhui Scientific Research Innovation Team of Photoelectric Information Materials and New Energy Devices (Grant No. 2016SCXPTTD), Support Program for Excellent Young Talents in Universities of Anhui Province (Grant No. 2022AH030134), Anhui Province Higher Education Innovation Team: Key Technologies and Equipment Innovation Team for Clean Energy (Grant No. 2023AH010055), and Joint Cultivation Postgraduate Research and Innovation Fund Project of Suzhou University (Grant No. 2023KYCX13).

References

[1] C. B, Solving the energy crisis, Nature 609 (2022) S1.
[2] M. Farghali, A.I. Osman, I.M.A. Mohamed, Z. Chen, L. Chen, I. Ihara, P.-S. Yap, D. W. Rooney, Strategies to save energy in the context of the energy crisis: a review, Environ. Chem. Lett. 21 (2023) 2003–2039.

[3] E.D. Coyle, R.A. Simmons, Understanding the Global Energy Crisis, Purdue University Press, 2014.
[4] M. Cai, L. Xu, J. Guo, X. Yang, X. He, P. Hu, Recent advances in metal-free electrocatalysts for hydrogen evolution reaction, J. Mater. Chem. A 12 (2023) 592–612.
[5] B. Wang, F. Yang, L. Feng, Recent advances in Co-based electrocatalysts for hydrogen evolution reaction, Small 19 (2023) 2302866.
[6] R. Zhang, A. Xie, L. Cheng, Z. Bai, Y. Tang, P. Wan, Hydrogen production by traditional and novel alkaline water electrolysis on nickel or iron based electrocatalysts, Chem. Commun. 59 (2023) 8205–8221.
[7] I. Sullivan, A. Goryachev, I.A. Digdaya, X. Li, H.A. Atwater, D.A. Vermaas, C. Xiang, Coupling electrochemical CO_2 conversion with CO_2 capture, Nat. Catal. 4 (2021) 952–958.
[8] C. Chen, Y. Zhang, Q. Li, Y. Wang, J. Ma, Guanidine-embedded poly(ionic liquid) as a versatile precursor for self-templated synthesis of nitrogen-doped carbons: tailoring the microstructure for enhanced CO_2 capture, Fuel 329 (2022) 125357.
[9] Z.Y. Yu, Y. Duan, X.Y. Feng, X. Yu, M.R. Gao, S.H. Yu, Clean and affordable hydrogen fuel from alkaline water splitting: Past, recent progress, and future prospects, Adv. Mater. 33 (2021) 2007100.
[10] L. Kruitwagen, K.T. Story, J. Friedrich, L. Byers, S. Skillman, C. Hepburn, A global inventory of photovoltaic solar energy generating units, Nature 598 (2021) 604–610.
[11] I. Gunnarsdottir, B. Davidsdottir, E. Worrell, S. Sigurgeirsdottir, Sustainable energy development: history of the concept and emerging themes, Renew. Sust. Energ. Rev. 141 (2021) 110770.
[12] Y. Liu, Q. Wang, J. Zhang, J. Ding, Y. Cheng, T. Wang, J. Li, F. Hu, H.B. Yang, B. Liu, Recent advances in carbon-supported noble-metal electrocatalysts for hydrogen evolution reaction: syntheses, structures, and properties, Adv. Energy Mater. 12 (2022) 2200928.
[13] F. Sun, Q. Tang, D.-e Jiang, Theoretical advances in understanding and designing the active sites for hydrogen evolution reaction, ACS Catal. 12 (2022) 8404–8433.
[14] W. Zhou, J. Jia, J. Lu, L. Yang, D. Hou, G. Li, S. Chen, Recent developments of carbon-based electrocatalysts for hydrogen evolution reaction, Nano Energy 28 (2016) 29–43.
[15] G. Gao, X. Chen, L. Han, G. Zhu, J. Jia, A. Cabot, Z. Sun, Advances in MOFs and their derivatives for non-noble metal electrocatalysts in water splitting, Coord. Chem. Rev. 503 (2024) 215639.
[16] V.R. Stamenkovic, D. Strmcnik, P.P. Lopes, N.M. Markovic, Energy and fuels from electrochemical interfaces, Nat. Mater. 16 (2016) 57–69.
[17] S.T. Wismann, J.S. Engbæk, S.B. Vendelbo, F.B. Bendixen, W.L. Eriksen, K. Aasberg-Petersen, C. Frandsen, I. Chorkendorff, P.M. Mortensen, Electrified methane reforming: a compact approach to greener industrial hydrogen production, Science 364 (2019) 756–759.
[18] X. Zhang, M. Zhang, Y. Deng, M. Xu, L. Artiglia, W. Wen, R. Gao, B. Chen, S. Yao, X. Zhang, M. Peng, J. Yan, A. Li, Z. Jiang, X. Gao, S. Cao, C. Yang, A.J. Kropf, J. Shi, J. Xie, M. Bi, J.A. van Bokhoven, Y.-W. Li, X. Wen, M. Flytzani-Stephanopoulos, C. Shi, W. Zhou, D. Ma, A stable low-temperature H_2-production catalyst by crowding Pt on α-MoC, Nature 589 (2021) 396–401.
[19] H. Nishiyama, T. Yamada, M. Nakabayashi, Y. Maehara, M. Yamaguchi, Y. Kuromiya, Y. Nagatsuma, H. Tokudome, S. Akiyama, T. Watanabe, R. Narushima, S. Okunaka, N. Shibata, T. Takata, T. Hisatomi, K. Domen, Photocatalytic solar hydrogen production from water on a 100-m^2 scale, Nature 598 (2021) 304–307.
[20] M. Chatenet, B.G. Pollet, D.R. Dekel, F. Dionigi, J. Deseure, P. Millet, R.D. Braatz, M.Z. Bazant, M. Eikerling, I. Staffell, P. Balcombe, Y. Shao-Horn, H. Schäfer, Water electrolysis: from textbook knowledge to the latest scientific strategies and industrial developments, Chem. Soc. Rev. 51 (2022) 4583–4762.
[21] R. Daiyan, I. MacGill, R. Amal, Opportunities and challenges for renewable power-to-X, ACS Energy Lett. 5 (2020) 3843–3847.
[22] O. Schmidt, A. Gambhir, I. Staffell, A. Hawkes, J. Nelson, S. Few, Future cost and performance of water electrolysis: an expert elicitation study, Int. J. Hydrog. Energy 42 (2017) 30470–30492.
[23] R. Du, W. Jin, R. Hübner, L. Zhou, Y. Hu, A. Eychmüller, Engineering multimetallic aerogels for pH-universal HER and ORR electrocatalysis, Adv. Energy Mater. 10 (2020) 1903857.
[24] J. Jia, W. Zhou, Z. Wei, T. Xiong, G. Li, L. Zhao, X. Zhang, H. Liu, J. Zhou, S. Chen, Molybdenum carbide on hierarchical porous carbon synthesized from Cu-MoO_2 as efficient electrocatalysts for electrochemical hydrogen generation, Nano Energy 41 (2017) 749–757.
[25] X. Li, J. Yu, J. Jia, A. Wang, L. Zhao, T. Xiong, H. Liu, W. Zhou, Confined distribution of platinum clusters on MoO_2 hexagonal nanosheets with oxygen vacancies as a high-efficiency electrocatalyst for hydrogen evolution reaction, Nano Energy 62 (2019) 127–135.
[26] Y. Zhang, J. Wu, B. Guo, H. Huo, S. Niu, S. Li, P. Xu, Recent advances of transition-metal metaphosphates for efficient electrocatalytic water splitting, Carbon Energy 5 (2023) e375.
[27] H. Dong, H. Zhu, Q. Li, M. Zhou, X. Ren, T. Ma, J. Liu, Z. Zeng, X. Luo, S. Li, C. Cheng, Atomically structured metal-organic frameworks: a powerful chemical path for noble metal-based electrocatalysts, Adv. Funct. Mater. 33 (2023) 2300294.
[28] Z. Cui, W. Jiao, Z. Huang, G. Chen, B. Zhang, Y. Han, W. Huang, Design and synthesis of noble metal-based alloy electrocatalysts and their application in hydrogen evolution reaction, Small 19 (2023) 2301465.
[29] Z. Su, T. Chen, Porous noble metal electrocatalysts: synthesis, performance, and development, Small 17 (2021) 2005354.
[30] H. Yuan, X. Wan, J. Ye, T. Ma, F. Ma, J. Gao, W. Gao, D. Wen, Molecular engineering of noble metal aerogels boosting electrocatalytic oxygen reduction, Adv. Funct. Mater. 33 (2023) 2302561.
[31] Y. Hu, J. Liu, C. Lee, M. Li, B. Han, T. Wu, H. Pan, D. Geng, Q. Yan, Integration of metal-organic frameworks and metals: synergy for electrocatalysis, Small 19 (2023) 2300916.
[32] M. Humayun, M. Israr, A. Khan, M. Bououdina, State-of-the-art single-atom catalysts in electrocatalysis: from fundamentals to applications, Nano Energy 113 (2023) 108570.
[33] B. Jiang, Y. Guo, F. Sun, S. Wang, Y. Kang, X. Xu, J. Zhao, J. You, M. Eguchi, Y. Yamauchi, H. Li, Nanoarchitectonics of metallene materials for electrocatalysis, ACS Nano 17 (2023) 13017–13043.
[34] S. Kogularasu, Y.Y. Lee, B. Sriram, S.F. Wang, M. George, G.P. Chang-Chien, J. K. Sheu, Unlocking catalytic potential: exploring the impact of thermal treatment on enhanced electrocatalysis of nanomaterials, Angew. Chem. Int. Ed. 63 (2023) e202311806.
[35] L. Luo, L. Xu, Q. Wang, Q. Shi, H. Zhou, Z. Li, M. Shao, X. Duan, Recent advances in external fields-enhanced electrocatalysis, Adv. Energy Mater. 13 (2023) 2301276.
[36] H. Xu, L. Chen, J. Shi, Advanced electrocatalytic systems for enhanced atom/electron utilization, Energy Environ. Sci. 16 (2023) 1334–1363.
[37] X. Yang, W. Song, T. Zhang, Z. Huang, J. Zhang, J. Ding, W. Hu, Review of emerging atomically precise composite site-based electrocatalysts, Adv. Energy Mater. 13 (2023) 2301737.
[38] L. Zhang, N. Jin, Y. Yang, X.-Y. Miao, H. Wang, J. Luo, L. Han, Advances on axial coordination design of single-atom catalysts for energy electrocatalysis: a review, Nano-Micro Lett. 15 (2023) 228.
[39] Y. Zhang, H. Liu, S. Zhao, C. Xie, Z. Huang, S. Wang, Insights into the dynamic evolution of defects in electrocatalysts, Adv. Mater. 35 (2023) 2209680.
[40] Y. Zhao, S. Wei, L. Xia, K. Pan, B. Zhang, H. Huang, Z. Dong, H.-H. Wu, J. Lin, H. Pang, Sintered Ni metal as a matrix of robust self-supporting electrode for ultra-stable hydrogen evolution, Chem. Eng. J. 430 (2022) 133040.
[41] H. Sun, Z. Yan, F. Liu, W. Xu, F. Cheng, J. Chen, Self-supported transition-metal-based electrocatalysts for hydrogen and oxygen evolution, Adv. Mater. 32 (2019) 1806326.
[42] S. Li, E. Li, X. An, X. Hao, Z. Jiang, G. Guan, Transition metal-based catalysts for electrochemical water splitting at high current density: current status and perspectives, Nanoscale 13 (2021) 12788–12817.
[43] Z. Li, X. Zhang, C. Ou, Y. Zhang, W. Wang, S. Dong, X. Dong, Transition metal-based self-supported anode for electrocatalytic water splitting at a large current density, Coord. Chem. Rev. 495 (2023) 215381.
[44] M. Wang, Z. Wang, X. Gong, Z. Guo, The intensification technologies to water electrolysis for hydrogen production – a review, Renew. Sust. Energ. Rev. 29 (2014) 573–588.
[45] Y. Zeng, M. Zhao, Z. Huang, W. Zhu, J. Zheng, Q. Jiang, Z. Wang, H. Liang, Surface reconstruction of water splitting electrocatalysts, Adv. Energy Mater. 12 (2022) 2201713.
[46] S. Chandrasekaran, M. Khandelwal, F. Dayong, L. Sui, J.S. Chung, R.D.K. Misra, P. Yin, E.J. Kim, W. Kim, A. Vanchiappan, Y. Liu, S.H. Hur, H. Zhang, C. Bowen, Developments and perspectives on robust nano- and microstructured binder-free electrodes for bifunctional water electrolysis and beyond, Adv. Energy Mater. 12 (2022) 2200409.
[47] H. Yang, M. Driess, P.W. Menezes, Self-supported electrocatalysts for practical water electrolysis, Adv. Energy Mater. 11 (2021) 2102074.
[48] B.R. Anne, J. Kundu, M.K. Kabiraz, J. Kim, D. Cho, S.I. Choi, A review on mxene as promising support materials for oxygen evolution reaction catalysts, Adv. Funct. Mater. 33 (2023) 2306100.
[49] H. Jiang, Y. Yu, X. Duan, P. Chen, S. Wang, X. Qiu, L. Ye, X. Tu, Heterostructured MoO_3 anchored defect-rich NiFe-LDH/NF as a robust self-supporting electrocatalyst for overall water splitting, Small (2023) 2307797.
[50] P. Moreno-García, M. de Jesús Gálvez-Vázquez, T. Prenzel, J. Winter, L. Gálvez-Vázquez, P. Broekmann, S.R. Waldvogel, Self-standing metal foam catalysts for cathodic electro-organic synthesis, Adv. Mater. (2023) 2307461.
[51] F. Li, M. Du, X. Xiao, Q. Xu, Self-supporting metal-organic framework-based nanoarrays for electrocatalysis, ACS Nano 16 (2022) 19913–19939.
[52] X. Sun, S. Wang, Y. Hou, X.F. Lu, J. Zhang, X. Wang, Self-supporting metal-organic framework-based hydrogen and oxygen electrocatalysts, J. Mater. Chem. A 11 (2023) 13089–13106.
[53] R. Yao, Y. Li, X. Zhang, Y. Zhao, Y. Wang, X. Lang, Q. Jiang, H. Tan, Y. Li, Self-supported nanoporous CuNiAl alloy as highly efficient electrocatalyst for nitrobenzene hydrogenation to aniline, Chem. Eng. J. 471 (2023) 144487.
[54] A. Kong, M. Liu, H. Zhang, Z. Cao, J. Zhang, W. Li, Y. Han, Y. Fu, Highly selective electrocatalytic hydrogenation of benzoic acid over Pt/C catalyst supported on carbon fiber, Chem. Eng. J. 445 (2022) 136719.
[55] D. Kong, H. Wang, Z. Lu, Y. Cui, $CoSe_2$ nanoparticles grown on carbon fiber paper: an efficient and stable electrocatalyst for hydrogen evolution reaction, J. Am. Chem. Soc. 136 (2014) 4897–4900.
[56] X. Wang, W. Li, D. Xiong, D.Y. Petrovykh, L. Liu, Bifunctional nickel phosphide nanocatalysts supported on carbon fiber paper for highly efficient and stable overall water splitting, Adv. Funct. Mater. 26 (2016) 4067–4077.
[57] M. You, X. Du, X. Hou, Z. Wang, Y. Zhou, H. Ji, L. Zhang, Z. Zhang, S. Yi, D. Chen, In-situ growth of ruthenium-based nanostructure on carbon cloth for superior electrocatalytic activity towards HER and OER, Appl. Catal. B-Environ. 317 (2022) 121729.

[58] X.-Z. Fan, Q.-Q. Pang, S.-S. Yi, X. Du, S. Zhang, Z.-Y. Liu, X.-Z. Yue, Intrinsic-structural-modulated carbon cloth as efficient electrocatalyst for water oxidation, Appl. Catal. B-Environ. 292 (2021) 120152.

[59] Q. Dang, Y. Sun, X. Wang, W. Zhu, Y. Chen, F. Liao, H. Huang, M. Shao, Carbon dots-Pt modified polyaniline nanosheet grown on carbon cloth as stable and high-efficient electrocatalyst for hydrogen evolution in pH-universal electrolyte, Appl. Catal. B-Environ. 257 (2019) 117905.

[60] W. Sun, L. Zhou, G. Liu, Y. Zheng, H. Zou, J. Song, Enhanced electro-fenton degradation of sulfamethazine using Co-based selenite modified graphite cathode via in-situ generation of $^{\bullet}$OH, Chem. Eng. J. 463 (2023) 142419.

[61] G. Zhang, Z. Yang, W. Zhang, Y. Wang, Facile synthesis of graphene nanoplate-supported porous Pt-Cu alloys with high electrocatalytic properties for methanol oxidation, J. Mater. Chem. A 4 (2016) 3316–3323.

[62] R. Venkata Jagadeesh, V. Lakshminarayanan, Enhanced electrocatalytic activity of Pd and Pd-polyaniline nanoparticles on electrochemically exfoliated graphite sheets, Appl. Catal. B-Environ. 251 (2019) 25–36.

[63] M. Tang, Y. Liu, H. Cao, Q. Zheng, X. Wei, K.H. Lam, D. Lin, Cu_2S/Ni_3S_2 ultrathin nanosheets on Ni foam as a highly efficient electrocatalyst for oxygen evolution reaction, Int. J. Hydrog. Energy 47 (2022) 3013–3021.

[64] J. Zhou, L. Yu, Q. Zhou, C. Huang, Y. Zhang, B. Yu, Y. Yu, Ultrafast fabrication of porous transition metal foams for efficient electrocatalytic water splitting, Appl. Catal. B-Environ. 288 (2021) 120002.

[65] R. Du, X. Jin, R. Hübner, X. Fan, Y. Hu, A. Eychmüller, Engineering self-supported noble metal foams toward electrocatalysis and beyond, Adv. Energy Mater. 10 (2020) 1901945.

[66] J. Wang, R. Li, R. Li, T. Xie, S. Liu, Y. Wang, Metal-organic framework derived Co_3S_4 nanosheets grown on Ti mesh: an efficient electrocatalyst for electrochemical sensing of hydrazine, N. J. Chem. 47 (2023) 11071–11077.

[67] Q. Liu, H. Wu, H. Gu, Z. Jiang, W. Zhang, H. Li, Z. Wang, P. Liu, D. Li, M. Zhu, Electrochemical synthesis of copper mesh-supported thermo-catalysts, Small (2023) 2307859.

[68] Y. Li, H. Zhang, M. Jiang, Y. Kuang, X. Sun, X. Duan, Ternary NiCoP nanosheet arrays: an excellent bifunctional catalyst for alkaline overall water splitting, Nano Res. 9 (2016) 2251–2259.

[69] Y. Tuo, W. Liu, Q. Lu, X. Wang, J. Luo, S. Wang, Y. Zhou, M. Wang, X. Sun, X. Feng, M. Wu, D. Chen, J. Zhang, SO_4^{2-} mediated CO_2 activation on metal electrode for efficient CO_2 electroreduction, Chem. Eng. J. 464 (2023) 142510.

[70] J. Hao, L. Huang, S. Han, J. Lian, MnS-MoS_2 nanosheets supported on Mo plates as electrocatalyst for the hydrogen evolution reaction, ACS Appl. Nano Mater. 7 (2024) 638–648.

[71] H. Xiao, S. Wang, C. Wang, Y. Li, H. Zhang, Z. Wang, Y. Zhou, C. An, J. Zhang, Lamellar structured $CoSe_2$ nanosheets directly arrayed on Ti plate as an efficient electrochemical catalyst for hydrogen evolution, Electrochim. Acta 217 (2016) 156–162.

[72] R. Zaffaroni, R.J. Detz, J.I. van der Vlugt, J.N.H. Reek, A functional hydrogenase mimic chemisorbed onto fluorine-doped tin oxide electrodes: a strategy towards water splitting devices, ChemSusChem 11 (2018) 209–218.

[73] G. Rahman, S.Y. Chae, O.-s Joo, Efficient hydrogen evolution performance of phase-pure NiS electrocatalysts grown on fluorine-doped tin oxide-coated glass by facile chemical bath deposition, Int. J. Hydrog. Energy 43 (2018) 13022–13031.

[74] N. Dhabarde, A. Ferrer, P.M. Tembo, K.S. Raja, V.R. Subramanian, Chalcogenide-based complex transition metal electrocatalyst for hydrogen peroxide production, J. Electroanal. Chem. 170 (2023) 016506.

[75] W. Zhang, D. Li, L. Zhang, X. She, D. Yang, NiFe-based nanostructures on nickel foam as highly efficiently electrocatalysts for oxygen and hydrogen evolution reactions, J. Energy Chem. 39 (2019) 39–53.

[76] S.H. Yu, W. Chen, H. Wang, H. Pan, D.H.C. Chua, Highly stable tungsten disulfide supported on a self-standing nickel phosphide foam as a hybrid electrocatalyst for efficient electrolytic hydrogen evolution, Nano Energy 55 (2019) 193–202.

[77] L. He, Z. Cai, D. Zheng, L. Ouyang, X. He, J. Chen, Y. Li, X. Guo, Q. Liu, L. Li, W. Chu, S. Zhu, X. Sun, B. Tang, Three-dimensional porous NiCoP foam enabled high-performance overall seawater splitting at high current density, J. Mater. Chem. A 12 (2024) 2680–2684.

[78] M.S. Ratsoma, B.L.O. Poho, K. Makgopa, K. Raju, K.D. Modibane, C.J. Jafta, K. O. Oyedotun, Application of nickel foam in electrochemical systems: a review, J. Energy Chem. 52 (2023) 2264–2291.

[79] F. Rocha, R. Delmelle, C. Georgiadis, J. Proost, Effect of pore size and electrolyte flow rate on the bubble removal efficiency of 3D pure Ni foam electrodes during alkaline water electrolysis, J. Environ. Chem. Eng. 10 (2022) 107648.

[80] M.Y. Zu, P.F. Liu, C. Wang, Y. Wang, L.R. Zheng, B. Zhang, H. Zhao, H.G. Yang, Bimetallic carbide as a stable hydrogen evolution catalyst in harsh acidic water, ACS Energy Lett. 3 (2018) 78–84.

[81] G. Xiong, Y. Chen, Z. Zhou, F. Liu, X. Liu, L. Yang, Q. Liu, Y. Sang, H. Liu, X. Zhang, J. Jia, W. Zhou, Rapid synthesis of various electrocatalysts on Ni foam using a universal and facile induction heating method for efficient water splitting, Adv. Funct. Mater. 31 (2021) 2009580.

[82] H. Sun, B. Yao, Y. Han, L. Yang, Y. Zhao, S. Wang, C. Zhong, J. Chen, C.-P. Li, M. Du, Multi-interface engineering of self-supported nickel/yttrium oxide electrode enables kinetically accelerated and ultra-stable alkaline hydrogen evolution at industrial-level current density, Adv. Energy Mater. 14 (2024) 2303563.

[83] Y. Cheng, H. Chen, L. Zhang, X. Xu, H. Cheng, C. Yan, T. Qian, Evolution of grain boundaries promoted hydrogen production for industrial-grade current density, Adv. Mater. 36 (2024) 2313156.

[84] W. Bi, L. Zhang, Z. Sun, X. Li, T. Jin, X. Wu, Q. Zhang, Y. Luo, C. Wu, Y. Xie, Insight into electrocatalysts as Co-catalysts in efficient photocatalytic hydrogen evolution, ACS Catal. 6 (2016) 4253–4257.

[85] G. Zhao, Y. Jiang, S.-X. Dou, W. Sun, H. Pan, Interface engineering of heterostructured electrocatalysts towards efficient alkaline hydrogen electrocatalysis, Sci. Bull. 66 (2021) 85–96.

[86] L. Sun, V. Reddu, X. Wang, Multi-atom cluster catalysts for efficient electrocatalysis, Chem. Soc. Rev. 51 (2022) 8923–8956.

[87] Z. Kou, Y. Yu, X. Liu, X. Gao, L. Zheng, H. Zou, Y. Pang, Z. Wang, Z. Pan, J. He, S. J. Pennycook, J. Wang, Potential-dependent phase transition and Mo-enriched surface reconstruction of γ-CoOOH in a heterostructured Co-Mo_2C precatalyst enable water oxidation, ACS Catal. 10 (2020) 4411–4419.

[88] H. Liu, Q. He, H. Jiang, Y. Lin, Y. Zhang, M. Habib, S. Chen, L. Song, Electronic structure reconfiguration toward pyrite NiS_2 via engineered heteroatom defect boosting overall water splitting, ACS Nano 11 (2017) 11574–11583.

[89] D. Yao, L. Gu, B. Zuo, S. Weng, S. Deng, W. Hao, A strategy for preparing high-efficiency and economical catalytic electrodes toward overall water splitting, Nanoscale 13 (2021) 10624–10648.

[90] S. Anantharaj, S. Noda, V.R. Jothi, S. Yi, M. Driess, P.W. Menezes, Strategies and perspectives to catch the missing pieces in energy-efficient hydrogen evolution reaction in alkaline media, Angew. Chem. Int. Ed. 60 (2021) 18981–19006.

[91] L. Fu, Y. Li, N. Yao, F. Yang, G. Cheng, W. Luo, IrMo nanocatalysts for efficient alkaline hydrogen electrocatalysis, ACS Catal. 10 (2020) 7322–7327.

[92] C. Hu, L. Zhang, Z.J. Zhao, A. Li, X. Chang, J. Gong, Synergism of geometric construction and electronic regulation: 3D Se-$(NiCo)S_x/(OH)_x$ nanosheets for highly efficient overall water splitting, Adv. Mater. 30 (2018) 1705538.

[93] W. Ma, X. Zhang, W. Li, M. Jiao, L. Zhang, R. Ma, Z. Zhou, Advanced Pt-based electrocatalysts for the hydrogen evolution reaction in alkaline medium, Nanoscale 15 (2023) 11759–11776.

[94] G.O. Kayode, M.M. Montemore, Factors controlling oxophilicity and carbophilicity of transition metals and main group metals, J. Mater. Chem. A 9 (2021) 22325–22333.

[95] G. Gao, G. Zhu, X. Chen, Z. Sun, A. Cabot, Optimizing Pt-based alloy electrocatalysts for improved hydrogen evolution performance in alkaline electrolytes: a comprehensive review, ACS Nano 17 (2023) 20804–20824.

[96] H. Wang, W. Fu, X. Yang, Z. Huang, J. Li, H. Zhang, Y. Wang, Recent advancements in heterostructured interface engineering for hydrogen evolution reaction electrocatalysis, J. Mater. Chem. A 8 (2020) 6926–6956.

[97] L. Yu, I.K. Mishra, Y. Xie, H. Zhou, J. Sun, J. Zhou, Y. Ni, D. Luo, F. Yu, Y. Yu, S. Chen, Z. Ren, Ternary $Ni_{2(1-x)}Mo_{2x}P$ nanowire arrays toward efficient and stable hydrogen evolution electrocatalysis under large-current-density, Nano Energy 53 (2018) 492–500.

[98] P. Chen, J. Ye, H. Wang, L. Ouyang, M. Zhu, Recent progress of transition metal carbides/nitrides for electrocatalytic water splitting, J. Alloy. Compd. 883 (2021) 160833.

[99] J. Liang, Z. Cai, Z. Li, Y. Yao, Y. Luo, S. Sun, D. Zheng, Q. Liu, X. Sun, B. Tang, Efficient bubble/precipitate traffic enables stable seawater reduction electrocatalysis at industrial-level current densities, Nat. Commun. 15 (2024) 2950.

[100] S. Kaushik, D. Wu, Z. Zhang, X. Xiao, C. Zhen, W. Wang, N.-Y. Huang, M. Gu, Q. Xu, Universal synthesis of single-atom catalysts by direct thermal decomposition of molten salts for boosting acidic water splitting, Adv. Mater. (2024) 2401163.

[101] Y. Yao, Z. Zhang, L. Jiao, Development strategies in transition metal borides for electrochemical water splitting, Energy Environ. Mater. 5 (2022) 470–485.

[102] Y. Jiang, J. Huang, B. Mao, T. An, J. Wang, M. Cao, Inside solid-liquid interfaces: understanding the influence of the electrical double layer on alkaline hydrogen evolution reaction, Appl. Catal. B-Environ. 293 (2021) 120220.

[103] S. Anantharaj, S. Noda, Appropriate use of electrochemical impedance spectroscopy in water splitting electrocatalysis, ChemElectroChem 7 (2020) 2297–2308.

[104] P.M. Bodhankar, P.B. Sarawade, G. Singh, A. Vinu, D.S. Dhawale, Recent advances in highly active nanostructured NiFe LDH catalyst for electrochemical water splitting, J. Mater. Chem. A 9 (2021) 3180–3208.

[105] D.H. Kweon, M.S. Okyay, S.-J. Kim, J.-P. Jeon, H.-J. Noh, N. Park, J. Mahmood, J.-B. Baek, Ruthenium anchored on carbon nanotube electrocatalyst for hydrogen production with enhanced Faradaic efficiency, Nat. Commun. 11 (2020) 1278.

[106] M. Lao, K. Rui, G. Zhao, P. Cui, X. Zheng, S.X. Dou, W. Sun, Platinum/nickel bicarbonate heterostructures towards accelerated hydrogen evolution under alkaline conditions, Angew. Chem. Int. Ed. 58 (2019) 5432–5437.

[107] F. Zhou, Y. Zhou, G.-G. Liu, C.-T. Wang, J. Wang, Recent advances in nanostructured electrocatalysts for hydrogen evolution reaction, Rare Met. 40 (2021) 3375–3405.

[108] K. Hemmati, A. Kumar, A.R. Jadhav, O. Moradlou, A.Z. Moshfegh, H. Lee, Nanorod array-based hierarchical NiO microspheres as a bifunctional electrocatalyst for a selective and corrosion-resistance seawater photo/electrolysis system, ACS Catal. 13 (2023) 5516–5528.

[109] W. Liu, C. Ni, M. Gao, X. Zhao, W. Zhang, R. Li, K. Zhou, Metal-organic-framework-based nanoarrays for oxygen evolution electrocatalysis, ACS Nano 17 (2023) 24564–24592.

[110] D. Takimoto, S. Toma, Y. Suda, T. Shirokura, Y. Tokura, K. Fukuda, M. Matsumoto, H. Imai, W. Sugimoto, Platinum nanosheets synthesized via topotactic reduction of single-layer platinum oxide nanosheets for electrocatalysis, Nat. Commun. 14 (2023) 19.

[111] Q. Yao, S.-Y. Lv, Z. Yu, Y.-C. Chang, C.-W. Pao, Z. Hu, L.-M. Yang, X. Huang, Q. Shao, J. Lu, Face-centered cubic ruthenium nanocrystals with promising

thermal stability and electrocatalytic performance, ACS Catal. 13 (2023) 11023–11032.
[112] W. Zhang, Y. Qi, Y. Zhao, W. Ge, L. Dong, J. Shen, H. Jiang, C. Li, Rh-dispersed Cu nanowire catalyst for boosting electrocatalytic hydrogenation of 5-hydroxymethylfurfural, Sci. Bull. 68 (2023) 2190–2199.
[113] A. Saad, Y. Gao, K.A. Owusu, W. Liu, Y. Wu, A. Ramiere, H. Guo, P. Tsiakaras, X. Cai, Ternary Mo_2NiB_2 as a superior bifunctional electrocatalyst for overall water splitting, Small 18 (2022) 2104303.
[114] P. Liao, J. Kang, Y. Zhong, R. Xiang, S. Wang, S. Li, X. Liu, G. Li, Recent advances of two-dimensional metal-organic frameworks in alkaline electrolysis water for hydrogen production, Sci. China Chem. 66 (2023) 1924–1939.
[115] N.K. Chaudhari, H. Jin, B. Kim, K. Lee, Nanostructured materials on 3D nickel foam as electrocatalysts for water splitting, Nanoscale 9 (2017) 12231–12247.
[116] Z. Tu, X. Liu, D. Xiong, J. Wang, S. Gong, C. Xu, D. Wu, Z. Chen, Ultrafast room-temperature activation of nickel foams as highly efficient electrocatalysts, Chem. Eng. J. 475 (2023) 146253.
[117] B. Gao, X. Yang, X. Fan, Z. Gui, W. Zhang, Y. Jia, S. Wang, Y. Zhang, Q. Gao, Y. Tang, Activating commercial nickel foam to a highly efficient electrocatalyst for oxygen evolution reaction through a three-step surface reconstruction, ACS Appl. Mater. Interfaces 15 (2023) 57239–57251.
[118] T. Zhang, J. Sun, J. Guan, Self-supported transition metal chalcogenides for oxygen evolution, Nano Res. 16 (2023) 8684–8711.
[119] Y. Ma, Z. He, Z. Wu, B. Zhang, Y. Zhang, S. Ding, C. Xiao, Galvanic-replacement mediated synthesis of copper-nickel nitrides as electrocatalyst for hydrogen evolution reaction, J. Mater. Chem. A 5 (2017) 24850–24858.
[120] Y. Jiao, Y. Zheng, M. Jaroniec, S.Z. Qiao, Design of electrocatalysts for oxygen- and hydrogen-involving energy conversion reactions, Chem. Soc. Rev. 44 (2015) 2060–2086.
[121] J. Li, J. Zhang, J. Zhang, K. Pan, H. Xu, H. Chen, G. Liu, N. Wu, C. Yuan, X. Liu, Tailoring supports for enhancing the electrocatalytic hydrogen evolution performance of platinum species: a review, J. Mater. Chem. A 11 (2023) 19812–19844.
[122] A. Sajeev, K. Krishnamoorthy, P. Pazhamalai, K. Bhunia, A. Sathyaseelan, S.-J. Kim, Methanol-assisted energy-saving green hydrogen production using electrodeposited 3D-metallic tin as an electrocatalyst, J. Mater. Chem. A 11 (2023) 22419–22429.
[123] J. Wang, J. Feng, Y. Li, F. Lai, G.C. Wang, T. Liu, J. Huang, G. He, Multilayered molybdate microflowers fabricated by one-pot reaction for efficient water splitting, Adv. Sci. 10 (2023) 2206952.
[124] X. Liu, J. Wang, Z. Fang, S. Gong, D. Xiong, W. Chen, D. Wu, Z. Chen, Ultrafast activation of Ni foam by electro-corrosion and its use for upcycling PBT plastic waste, Appl. Catal. B-Environ. 334 (2023) 122870.
[125] F.M. Li, L. Huang, S. Zaman, W. Guo, H. Liu, X. Guo, B.Y. Xia, Corrosion chemistry of electrocatalysts, Adv. Mater. 34 (2022) 2200840.
[126] Y. Luo, X. Li, X. Cai, X. Zou, F. Kang, H.-M. Cheng, B. Liu, Two-dimensional MoS_2 confined $Co(OH)_2$ electrocatalysts for hydrogen evolution in alkaline electrolytes, ACS Nano 12 (2018) 4565–4573.
[127] L. Zhao, J. Jia, Z. Yang, J. Yu, A. Wang, Y. Sang, W. Zhou, H. Liu, One-step synthesis of CdS nanoparticles/MoS_2 nanosheets heterostructure on porous molybdenum sheet for enhanced photocatalytic H_2 evolution, Appl. Catal. B-Environ. 210 (2017) 290–296.
[128] L. Zhao, T. Dong, J. Du, H. Liu, H. Yuan, Y. Wang, J. Jia, H. Liu, W. Zhou, Synthesis of CdS/MoS_2 nanooctahedrons heterostructure with a tight interface for enhanced photocatalytic H_2 evolution and biomass upgrading, Sol. RRL 5 (2021) 2000415.
[129] Y. Wu, G.D. Li, Y. Liu, L. Yang, X. Lian, T. Asefa, X. Zou, Overall water splitting catalyzed efficiently by an ultrathin nanosheet-built, hollow Ni_3S_2-based electrocatalyst, Adv. Funct. Mater. 26 (2016) 4839–4847.
[130] T. Kou, T. Smart, B. Yao, I. Chen, D. Thota, Y. Ping, Y. Li, Theoretical and experimental insight into the effect of nitrogen doping on hydrogen evolution activity of Ni_3S_2 in alkaline medium, Adv. Energy Mater. 8 (2018) 1703538.
[131] L.-L. Feng, G. Yu, Y. Wu, G.-D. Li, H. Li, Y. Sun, T. Asefa, W. Chen, X. Zou, High-index faceted Ni_3S_2 nanosheet arrays as highly active and ultrastable electrocatalysts for water splitting, J. Am. Chem. Soc. 137 (2015) 14023–14026.
[132] M.S. Faber, R. Dziedzic, M.A. Lukowski, N.S. Kaiser, Q. Ding, S. Jin, High-performance electrocatalysis using metallic cobalt pyrite (CoS_2) micro- and nanostructures, J. Am. Chem. Soc. 136 (2014) 10053–10061.
[133] J. Zhang, W. Xiao, P. Xi, S. Xi, Y. Du, D. Gao, J. Ding, Activating and optimizing activity of CoS_2 for hydrogen evolution reaction through the synergic effect of N dopants and S vacancies, ACS Energy Lett. 2 (2017) 1022–1028.
[134] W. Xie, K. Liu, G. Shi, X. Fu, X. Chen, Z. Fan, M. Liu, M. Yuan, M. Wang, CoS_2 nanowires supported graphdiyne for highly efficient hydrogen evolution reaction, J. Energy Chem. 60 (2021) 272–278.
[135] A.M. Huerta-Flores, L.M. Torres-Martínez, E. Moctezuma, A.P. Singh, B. Wickman, Green synthesis of earth-abundant metal sulfides (FeS_2, CuS, and NiS_2) and their use as visible-light active photocatalysts for H_2 generation and dye removal, J. Mater. Sci. Mater. Electron. 29 (2018) 11613–11626.
[136] J. Wu, Q. Zhang, K. Shen, R. Zhao, W. Zhong, C. Yang, H. Xiang, X. Li, N. Yang, Modulating interband energy separation of boron-doped Fe_7S_8/FeS_2 electrocatalysts to boost alkaline hydrogen evolution reaction, Adv. Funct. Mater. 32 (2022) 2107802.
[137] Y. Yang, J. Liu, F. Liu, Z. Wang, D. Wu, FeS_2-anchored transition metal single atoms for highly efficient overall water splitting: a DFT computational screening study, J. Mater. Chem. A 9 (2021) 2438–2447.
[138] G. Ren, Q. Hao, J. Mao, L. Liang, H. Liu, C. Liu, J. Zhang, Ultrafast fabrication of nickel sulfide film on Ni foam for efficient overall water splitting, Nanoscale 10 (2018) 17347–17353.
[139] J. Hu, C. Zhang, X. Meng, H. Lin, C. Hu, X. Long, S. Yang, Hydrogen evolution electrocatalysis with binary-nonmetal transition metal compounds, J. Mater. Chem. A 5 (2017) 5995–6012.
[140] R. Boppella, J. Tan, J. Yun, S.V. Manorama, J. Moon, Anion-mediated transition metal electrocatalysts for efficient water electrolysis: recent advances and future perspectives, Coord. Chem. Rev. 427 (2021) 213552.
[141] P. Xu, Z. Bao, Y. Zhao, L. Zheng, Z. Lv, X. Shi, H.-E. Wang, X. Fang, H. Zheng, Anionic regulation and heteroatom doping of Ni-based electrocatalysts to boost biomass valorization coupled with hydrogen production, Adv. Energy Mater. 14 (2024) 2303557.
[142] J. Yu, F.-X. Ma, Y. Du, P.-P. Wang, C.-Y. Xu, L. Zhen, *In situ* growth of sn-doped Ni_3S_2 nanosheets on Ni foam as high-performance electrocatalyst for hydrogen evolution reaction, ChemElectroChem 4 (2017) 594–600.
[143] X. Zhong, J. Tang, J. Wang, M. Shao, J. Chai, S. Wang, M. Yang, Y. Yang, N. Wang, S. Wang, B. Xu, H. Pan, 3D heterostructured pure and N-Doped Ni_3S_2/VS_2 nanosheets for high efficient overall water splitting, Electrochim. Acta 269 (2018) 55–61.
[144] P. Chen, T. Zhou, M. Zhang, Y. Tong, C. Zhong, N. Zhang, L. Zhang, C. Wu, Y. Xie, 3D nitrogen-anion-decorated nickel sulfides for highly efficient overall water splitting, Adv. Mater. 29 (2017) 1701584.
[145] Y. Wu, X. Liu, D. Han, X. Song, L. Shi, Y. Song, S. Niu, Y. Xie, J. Cai, S. Wu, J. Kang, J. Zhou, Z. Chen, X. Zheng, X. Xiao, G. Wang, Electron density modulation of $NiCo_2S_4$ nanowires by nitrogen incorporation for highly efficient hydrogen evolution catalysis, Nat. Commun. 9 (2018) 1425.
[146] W. He, L. Han, Q. Hao, X. Zheng, Y. Li, J. Zhang, C. Liu, H. Liu, H.L. Xin, Fluorine-anion-modulated electron structure of nickel sulfide nanosheet arrays for alkaline hydrogen evolution, ACS Energy Lett. 4 (2019) 2905–2912.
[147] J. Hou, B. Zhang, Z. Li, S. Cao, Y. Sun, Y. Wu, Z. Gao, L. Sun, Vertically aligned oxygenated-CoS_2-MoS_2 heteronanosheet architecture from polyoxometalate for efficient and stable overall water splitting, ACS Catal. 8 (2018) 4612–4621.
[148] Y. Guo, X. Zhou, J. Tang, S. Tanaka, Y.V. Kaneti, J. Na, B. Jiang, Y. Yamauchi, Y. Bando, Y. Sugahara, Multiscale structural optimization: highly efficient hollow iron-doped metal sulfide heterostructures as bifunctional electrocatalysts for water splitting, Nano Energy 75 (2020) 104913.
[149] Q. Lu, H. Wu, X. Zheng, Y. Cao, J. Li, Y. Wang, H. Wang, C. Zhi, Y. Deng, X. Han, W. Hu, Controllable constructing janus homologous heterostructures of transition metal alloys/sulfides for efficient oxygen electrocatalysis, Adv. Energy Mater. 12 (2022) 2202215.
[150] H. Yang, P. Guo, R. Wang, Z. Chen, H. Xu, H. Pan, D. Sun, F. Fang, R. Wu, Sequential phase conversion-induced phosphides heteronanorod arrays for superior hydrogen evolution performance to Pt in wide pH media, Adv. Mater. 34 (2022) 2107548.
[151] D. Yang, L. Cao, L. Feng, J. Huang, K. Kajiyoshi, Y. Feng, Q. Liu, W. Li, L. Feng, G. Hai, Formation of hierarchical Ni_3S_2 nanohorn arrays driven by in-situ generation of VS_4 nanocrystals for boosting alkaline water splitting, Appl. Catal. B-Environ. 257 (2019) 117911.
[152] D. Li, W. Wan, Z. Wang, H. Wu, S. Wu, T. Jiang, G. Cai, C. Jiang, F. Ren, Self-derivation and surface reconstruction of Fe-Doped Ni_3S_2 electrode realizing high-efficient and stable overall water and urea electrolysis, Adv. Energy Mater. 12 (2022) 2201913.
[153] H. Xu, Y. Liao, Z. Gao, Y. Qing, Y. Wu, L. Xia, A branch-like Mo-doped Ni_3S_2 nanoforest as a high-efficiency and durable catalyst for overall urea electrolysis, J. Mater. Chem. A 9 (2021) 3418–3426.
[154] X. Xu, W. Zhong, L. Zhang, G. Liu, W. Xu, Y. Zhang, Y. Du, NiCo-LDHs derived $NiCo_2S_4$ nanostructure coated by MoS_2 nanosheets as high-efficiency bifunctional electrocatalysts for overall water splitting, Surf. Coat. Technol. 397 (2020) 126065.
[155] Y. He, J. Shen, Q. Li, X. Zheng, Z. Wang, L. Cui, J. Xu, J. Liu, In-situ growth of VS_4 nanorods on Ni-Fe sulfides nanoplate array towards achieving a highly efficient and bifunctional electrocatalyst for total water splitting, Chem. Eng. J. 474 (2023) 145461.
[156] X. Du, Y. Ding, X. Zhang, MOF-derived Zn-Co-Ni sulfides with hollow nanosword arrays for high-efficiency overall water and urea electrolysis, Green. Energy Environ. 8 (2023) 798–811.
[157] H. Xie, Y. Feng, X. He, Y. Zhu, Z. Li, H. Liu, S. Zeng, Q. Qian, G. Zhang, Construction of nitrogen-doped biphasic transition-metal sulfide nanosheet electrode for energy-efficient hydrogen production via urea electrolysis, Small 19 (2023) 2207425.
[158] J. Chen, L. Zhang, J. Li, X. He, Y. Zheng, S. Sun, X. Fang, D. Zheng, Y. Luo, Y. Wang, J. Zhang, L. Xie, Z. Cai, Y. Sun, A.A. Alshehri, Q. Kong, C. Tang, X. Sun, High-efficiency overall alkaline seawater splitting: using a nickel-iron sulfide nanosheet array as a bifunctional electrocatalyst, J. Mater. Chem. A 11 (2023) 1116–1122.
[159] P.P. Dhakal, U.N. Pan, D.R. Paudel, M.R. Kandel, N.H. Kim, J.H. Lee, Cobalt-manganese sulfide hybridized Fe-doped 1T-vanadium disulfide 3D-hierarchical core-shell nanorods for extreme low potential overall water-splitting, Mater. Today Nano 20 (2022) 100272.
[160] J.T. Ren, L. Chen, W.W. Tian, X.L. Song, Q.H. Kong, H.Y. Wang, Z.Y. Yuan, Rational synthesis of core-shell-structured nickel sulfide-based nanostructures for efficient seawater electrolysis, Small 19 (2023) 2300194.
[161] D. Ansovini, C.J. Jun Lee, C.S. Chua, L.T. Ong, H.R. Tan, W.R. Webb, R. Raja, Y.-F. Lim, A highly active hydrogen evolution electrocatalyst based on a cobalt-nickel sulfide composite electrode, J. Mater. Chem. A 4 (2016) 9744–9749.

[162] D. Chanda, K. Kannan, J. Gautam, M.M. Meshesha, S.G. Jang, V.A. Dinh, B. L. Yang, Effect of the interfacial electronic coupling of nickel-iron sulfide nanosheets with layer Ti_3C_2 MXenes as efficient bifunctional electrocatalysts for anion-exchange membrane water electrolysis, Appl. Catal. B-Environ. 321 (2023) 122039.
[163] R. Gao, J. Zhu, D. Yan, Transition metal-based layered double hydroxides for photo(electro)chemical water splitting: a mini review, Nanoscale 13 (2021) 13593–13603.
[164] J.M. Gonçalves, P.R. Martins, K. Araki, L. Angnes, Recent progress in water splitting and hybrid supercapacitors based on nickel-vanadium layered double hydroxides, J. Energy Chem. 57 (2021) 496–515.
[165] G.M. Tomboc, J. Kim, Y. Wang, Y. Son, J. Li, J.Y. Kim, K. Lee, Hybrid layered double hydroxides as multifunctional nanomaterials for overall water splitting and supercapacitor applications, J. Mater. Chem. A 9 (2021) 4528–4557.
[166] Q. Chen, Y. Yu, J. Li, H. Nan, S. Luo, C. Jia, P. Deng, S. Zhong, X. Tian, Recent progress in layered double hydroxide-based electrocatalyst for hydrogen evolution reaction, ChemElectroChem 9 (2022) e202101387.
[167] L. Wu, L. Yu, X. Xiao, F. Zhang, S. Song, S. Chen, Z. Ren, Recent advances in self-supported layered double hydroxides for oxygen evolution reaction, Research 2020 (2020) 3976278.
[168] X. Han, C. Yu, J. Yang, C. Zhao, H. Huang, Z. Liu, P.M. Ajayan, J. Qiu, Mass and charge transfer coenhanced oxygen evolution behaviors in CoFe-layered double hydroxide assembled on graphene, Adv. Mater. Interfaces 3 (2016) 1500782.
[169] Y. Deng, L. Tang, C. Feng, G. Zeng, Z. Chen, J. Wang, H. Feng, B. Peng, Y. Liu, Y. Zhou, Insight into the dual-channel charge-charrier transfer path for nonmetal plasmonic tungsten oxide based composites with boosted photocatalytic activity under full-spectrum light, Appl. Catal. B-Environ. 235 (2018) 225–237.
[170] J. Luo, J.-H. Im, M.T. Mayer, M. Schreier, M.K. Nazeeruddin, N.-G. Park, S. D. Tilley, H.J. Fan, M. Grätzel, Water photolysis at 12.3% efficiency via perovskite photovoltaics and Earth-abundant catalysts, Science 345 (2014) 1593–1596.
[171] H.-p Feng, L. Tang, G.-m Zeng, J. Tang, Y.-c Deng, M. Yan, Y.-n Liu, Y.-y Zhou, X.-y Ren, S. Chen, Carbon-based core-shell nanostructured materials for electrochemical energy storage, J. Mater. Chem. A 6 (2018) 7310–7337.
[172] H.-p Feng, L. Tang, G.-m Zeng, Y. Zhou, Y.-c Deng, X. Ren, B. Song, C. Liang, M.-y Wei, J.-f Yu, Core-shell nanomaterials: applications in energy storage and conversion, Adv. Colloid Interface Sci. 267 (2019) 26–46.
[173] F. Song, X. Hu, Exfoliation of layered double hydroxides for enhanced oxygen evolution catalysis, Nat. Commun. 5 (2014) 4477.
[174] W. Ye, X. Fang, X. Chen, D. Yan, A three-dimensional nickel-chromium layered double hydroxide micro/nanosheet array as an efficient and stable bifunctional electrocatalyst for overall water splitting, Nanoscale 10 (2018) 19484–19491.
[175] X. Han, Z. Lin, X. He, L. Cui, D. Lu, The construction of defective FeCo-LDHs by in-situ polyaniline curved strategy as a desirable bifunctional electrocatalyst for OER and HER, Int. J. Hydrog. Energy 45 (2020) 26989–26999.
[176] J. Jiang, X.-L. Zhou, H.-G. Lv, H.-Q. Yu, Y. Yu, Bimetallic-based electrocatalysts for oxygen evolution reaction, Adv. Funct. Mater. 33 (2023) 2212160.
[177] J. Cheng, D. Wang, 2D materials modulating layered double hydroxides for electrocatalytic water splitting, Chin. J. Catal. 43 (2022) 1380–1398.
[178] W. Zhang, Y. Li, L. Zhou, Q. Zheng, F. Xie, K.H. Lam, D. Lin, Ultrathin amorphous CoFeP nanosheets derived from CoFe LDHs by partial phosphating as excellent bifunctional catalysts for overall water splitting, Electrochim. Acta 323 (2019) 134595.
[179] H. Lei, Q. Wan, S. Tan, Z. Wang, W. Mai, Pt-quantum-dot-modified sulfur-doped NiFe layered double hydroxide for high-current-density alkaline water splitting at industrial temperature, Adv. Mater. 35 (2023) 2208209.
[180] L. Yang, Z. Liu, S. Zhu, L. Feng, W. Xing, Ni-based layered double hydroxide catalysts for oxygen evolution reaction, Mater. Today Phys. 16 (2021) 100292.
[181] K.R. Park, J. Jeon, H. Choi, J. Lee, D.-H. Lim, N. Oh, H. Han, C. Ahn, B. Kim, S. Mhin, NiFe layered double hydroxide electrocatalysts for an efficient oxygen evolution reaction, ACS Appl. Energy Mater. 5 (2022) 8592–8600.
[182] N. Kornienko, J. Resasco, N. Becknell, C.-M. Jiang, Y.-S. Liu, K. Nie, X. Sun, J. Guo, S.R. Leone, P. Yang, Operando spectroscopic analysis of an amorphous cobalt sulfide hydrogen evolution electrocatalyst, J. Am. Chem. Soc. 137 (2015) 7448–7455.
[183] W. He, R. Ifraemov, A. Raslin, I. Hod, Room-temperature electrochemical conversion of metal-organic frameworks into porous amorphous metal sulfides with tailored composition and hydrogen evolution activity, Adv. Funct. Mater. 28 (2018) 1707244.
[184] Y. Yang, Y. Xie, Z. Yu, S. Guo, M. Yuan, H. Yao, Z. Liang, Y.R. Lu, T.-S. Chan, C. Li, H. Dong, S. Ma, Self-supported NiFe-LDH@CoS_x nanosheet arrays grown on nickel foam as efficient bifunctional electrocatalysts for overall water splitting, Chem. Eng. J. 419 (2021) 129512.
[185] H. Yang, Z. Chen, P. Guo, B. Fei, R. Wu, B-doping-induced amorphization of LDH for large-current-density hydrogen evolution reaction, Appl. Catal. B-Environ. 261 (2020) 118240.
[186] D.P. Sahoo, K.K. Das, S. Mansingh, S. Sultana, K. Parida, Recent progress in first row transition metal layered double hydroxide (LDH) based electrocatalysts towards water splitting: a review with insights on synthesis, Coord. Chem. Rev. 469 (2022) 214666.
[187] H. Sun, L. Chen, Y. Lian, W. Yang, L. Lin, Y. Chen, J. Xu, D. Wang, X. Yang, M. H. Rümmerli, J. Guo, J. Zhong, Z. Deng, Y. Jiao, Y. Peng, S. Qiao, Topotactically transformed polygonal mesopores on ternary layered double hydroxides exposing under-coordinated metal centers for accelerated water dissociation, Adv. Mater. 32 (2020) 2006784.
[188] K.N. Dinh, P. Zheng, Z. Dai, Y. Zhang, R. Dangol, Y. Zheng, B. Li, Y. Zong, Q. Yan, Ultrathin porous NiFeV ternary layer hydroxide nanosheets as a highly efficient bifunctional electrocatalyst for overall water splitting, Small 14 (2017) 1703257.
[189] H. Feng, J. Yu, L. Tang, J. Wang, H. Dong, T. Ni, J. Tang, W. Tang, X. Zhu, C. Liang, Improved hydrogen evolution activity of layered double hydroxide by optimizing the electronic structure, Appl. Catal. B-Environ. 297 (2021) 120478.
[190] Z. Liu, T. He, Q. Jiang, W. Wang, J. Tang, A review of heteroatomic doped two-dimensional materials as electrocatalysts for hydrogen evolution reaction, Int. J. Hydrog. Energy 47 (2022) 29698–29729.
[191] Z. Li, M. Huang, J. Li, H. Zhu, Large-scale, controllable synthesis of ultrathin platinum diselenide ribbons for efficient electrocatalytic hydrogen evolution, Adv. Funct. Mater. 33 (2023) 2300376.
[192] N. Shi, R. Ma, L. Lin, W. Xie, P. Liu, P. Li, H. Fan, Y. Tang, Y. Wang, S. Lin, X. Huang, *In-situ* derived defective Ru particles anchored on Ru-Ni layered double hydroxides for enhanced alkaline hydrogen evolution, Small (2024) 2311076.
[193] C.-T. Dinh, A. Jain, F.P.G. de Arquer, P. De Luna, J. Li, N. Wang, X. Zheng, J. Cai, B.Z. Gregory, O. Voznyy, B. Zhang, M. Liu, D. Sinton, E.J. Crumlin, E.H. Sargent, Multi-site electrocatalysts for hydrogen evolution in neutral media by destabilization of water molecules, Nat. Energy 4 (2018) 107–114.
[194] H. Feng, L. Tang, J. Tang, G. Zeng, H. Dong, Y. Deng, L. Wang, Y. Liu, X. Ren, Y. Zhou, Cu-Doped Fe@Fe_2O_3 core-shell nanoparticle shifted oxygen reduction pathway for high-efficiency arsenic removal in smelting wastewater, Environ. Sci. Nano 5 (2018) 1595–1607.
[195] L.K. Putri, B.-J. Ng, R.Y.Z. Yeo, W.-J. Ong, A.R. Mohamed, S.-P. Chai, Engineering nickel phosphides for electrocatalytic hydrogen evolution: a doping perspective, Chem. Eng. J. 461 (2023) 141845.
[196] T. Wang, H. Wu, C. Feng, L. Zhang, J. Zhang, MoP@NiCo-LDH on nickel foam as bifunctional electrocatalyst for high efficiency water and urea-water electrolysis, J. Mater. Chem. A 8 (2020) 18106–18116.
[197] J. Cheng, Y. Xu, X. Yang, X. Yang, W. Sun, A. Hu, J. Liu, Pulse-activation engineering induced lattice transformation of layered double hydroxides for efficient alkaline hydrogen evolution, Int. J. Hydrog. Energy 47 (2022) 39328–39337.
[198] W. Liu, K. Jiang, Y. Hu, Q. Li, Y. Deng, J. Bao, Y. Lei, Zr-doped CoFe-layered double hydroxides for highly efficient seawater electrolysis, J. Colloid Interface Sci. 604 (2021) 767–775.
[199] H. He, J. Xiao, Z. Liu, B. Yang, D. Wang, X. Peng, L. Zeng, Z. Li, L. Lei, M. Qiu, Y. Hou, Boosting the hydrogen evolution of layered double hydroxide by optimizing the electronic structure and accelerating the water dissociation kinetics, Chem. Eng. J. 453 (2023) 139751.
[200] A. Raja, N. Son, Y.-I. Kim, M. Kang, Hybrid ternary NiCoCu layered double hydroxide electrocatalyst for alkaline hydrogen and oxygen evolution reaction, J. Colloid Interface Sci. 647 (2023) 104–114.
[201] Y. Abghoui, E. Skúlason, Hydrogen evolution reaction catalyzed by transition-metal nitrides, J. Phys. Chem. C. 121 (2017) 24036–24045.
[202] L. Yu, Q. Zhu, S. Song, B. McElhenny, D. Wang, C. Wu, Z. Qin, J. Bao, Y. Yu, S. Chen, Z. Ren, Non-noble metal-nitride based electrocatalysts for high-performance alkaline seawater electrolysis, Nat. Commun. 10 (2019) 5106.
[203] L. Yu, S. Song, B. McElhenny, F. Ding, D. Luo, Y. Yu, S. Chen, Z. Ren, A universal synthesis strategy to make metal nitride electrocatalysts for hydrogen evolution reaction, J. Mater. Chem. A 7 (2019) 19728–19732.
[204] J. Theerthagiri, S.J. Lee, A.P. Murthy, J. Madhavan, M.Y. Choi, Fundamental aspects and recent advances in transition metal nitrides as electrocatalysts for hydrogen evolution reaction: a review, Curr. Opin. Solid. State Mater. Sci. 24 (2020) 100805.
[205] H. Yang, B. Wang, S. Kou, G. Lu, Z. Liu, Mott-Schottky heterojunction of Co/Co_2P with built-in electric fields for bifunctional oxygen electrocatalysis and zinc-air battery, Chem. Eng. J. 425 (2021) 131589.
[206] Q. Zhang, F. Luo, X. Long, X. Yu, K. Qu, Z. Yang, N.P. doped, carbon nanotubes confined WN-Ni Mott-Schottky heterogeneous electrocatalyst for water splitting and rechargeable zinc-air batteries, Appl. Catal. B-Environ. 298 (2021) 120511.
[207] M. Singh, T.T. Nguyen, J. Balamurugan, N.H. Kim, J.H. Lee, Rational manipulation of 3D hierarchical oxygenated nickel tungsten selenide nanosheet as the efficient bifunctional electrocatalyst for overall water splitting, Chem. Eng. J. 430 (2022) 132888.
[208] Y. Zhou, B. Chu, Z. Sun, L. Dong, F. Wang, B. Li, M. Fan, Z. Chen, Surface reconstruction and charge distribution enabling Ni/W_5N_4 Mott-Schottky heterojunction bifunctional electrocatalyst for efficient urea-assisted water electrolysis at a large current density, Appl. Catal. B-Environ. 323 (2023) 122168.
[209] J. Song, D. Yu, X. Wu, D. Xie, Y. Sun, P. Vishniakov, F. Hu, L. Li, C. Li, M. Yu. Maximov, K.M. El-Khatib, S. Peng, Interfacial coupling porous cobalt nitride nanosheets array with N-doped carbon as robust trifunctional electrocatalysts for water splitting and Zn-air battery, Chem. Eng. J. 437 (2022) 135281.
[210] F.-C. Shen, S.-N. Sun, Z.-F. Xin, S.-L. Li, L.-Z. Dong, Q. Huang, Y.-R. Wang, J. Liu, Y.-Q. Lan, Hierarchically phosphorus doped bimetallic nitrides arrays with unique interfaces for efficient water splitting, Appl. Catal. B-Environ. 243 (2019) 470–480.
[211] N. Han, P. Liu, J. Jiang, L. Ai, Z. Shao, S. Liu, Recent advances in nanostructured metal nitrides for water splitting, J. Mater. Chem. A 6 (2018) 19912–19933.
[212] S. Sanati, A. Morsali, H. García, First-row transition metal-based materials derived from bimetallic metal-organic frameworks as highly efficient electrocatalysts for electrochemical water splitting, Energy Environ. Sci. 15 (2022) 3119–3151.
[213] H.-M. Zhang, J.-J. Wang, Y. Meng, F. Lu, M. Ji, C. Zhu, J. Xu, J. Sun, Review on intrinsic electrocatalytic activity of transition metal nitrides on HER, Energy Mater. Adv. 2022 (2022) 0006.

[214] S.H. Park, T.H. Jo, M.H. Lee, K. Kawashima, C.B. Mullins, H.-K. Lim, D.H. Youn, Highly active and stable nickel-molybdenum nitride (Ni_2Mo_3N) electrocatalyst for hydrogen evolution, J. Mater. Chem. A 9 (2021) 4945–4951.
[215] Y. Wei, L. Yi, S. Zhang, C. Ni, X. Cai, W. Sun, W. Hu, Ni-Mo nitride synthesized via mild plasma for efficient alkaline hydrogen evolution electrocatalysis, J. Mater. Chem. A 12 (2024) 8534–8542.
[216] S. Niu, Y. Fang, J. Zhou, J. Cai, Y. Zang, Y. Wu, J. Ye, Y. Xie, Y. Liu, X. Zheng, W. Qu, X. Liu, G. Wang, Y. Qian, Manipulating the water dissociation kinetics of Ni_3N nanosheets via *in situ* interfacial engineering, J. Mater. Chem. A 7 (2019) 10924–10929.
[217] B. Wang, M. Lu, D. Chen, Q. Zhang, W. Wang, Y. Kang, Z. Fang, G. Pang, S. Feng, Ni_xFe_yN@C microsheet arrays on Ni foam as an efficient and durable electrocatalyst for electrolytic splitting of alkaline seawater, J. Mater. Chem. A 9 (2021) 13562–13569.
[218] L. Zhu, C. Li, H. Li, H. Li, Z. Wu, Y. Huang, X. Zhu, Y. Sun, Adjustable antiperovskite cobalt-based nitrides as efficient electrocatalysts for overall water splitting, J. Mater. Chem. A 10 (2022) 15520–15527.
[219] M. Chen, D. Liu, B. Zi, Y. Chen, D. Liu, X. Du, F. Li, P. Zhou, Y. Ke, J. Li, K.H. Lo, C. T. Kwok, W.F. Ip, S. Chen, S. Wang, Q. Liu, H. Pan, Remarkable synergistic effect in cobalt-iron nitride/alloy nanosheets for robust electrochemical water splitting, J. Energy Chem. 65 (2022) 405–414.
[220] B. Liu, B. He, H.-Q. Peng, Y. Zhao, J. Cheng, J. Xia, J. Shen, T.-W. Ng, X. Meng, C.-S. Lee, W. Zhang, Unconventional nickel nitride enriched with nitrogen vacancies as a high-efficiency electrocatalyst for hydrogen evolution, Adv. Sci. 5 (2018) 1800406.
[221] Y. Chen, J. Yu, J. Jia, F. Liu, Y. Zhang, G. Xiong, R. Zhang, R. Yang, D. Sun, H. Liu, W. Zhou, Metallic Ni_3Mo_3N porous microrods with abundant catalytic sites as efficient electrocatalyst for large current density and superstability of hydrogen evolution reaction and water splitting, Appl. Catal. B-Environ. 272 (2020) 118956.
[222] Y. Lu, Z. Li, Y. Xu, L. Tang, S. Xu, D. Li, J. Zhu, D. Jiang, Bimetallic Co-Mo nitride nanosheet arrays as high-performance bifunctional electrocatalysts for overall water splitting, Chem. Eng. J. 411 (2021) 128433.
[223] F. Song, L. Bai, A. Moysiadou, S. Lee, C. Hu, L. Liardet, X. Hu, Transition metal oxides as electrocatalysts for the oxygen evolution reaction in alkaline solutions: an application-inspired renaissance, J. Am. Chem. Soc. 140 (2018) 7748–7759.
[224] Y. Zhu, Q. Lin, Y. Zhong, H.A. Tahini, Z. Shao, H. Wang, Metal oxide-based materials as an emerging family of hydrogen evolution electrocatalysts, Energy Environ. Sci. 13 (2020) 3361–3392.
[225] X. Zhang, M. Jin, Q. Lian, O. Peng, S. Niu, Z. Ai, A. Amini, S. Song, C. Cheng, Ion modification of transition cobalt oxide by soaking strategy for enhanced water splitting, Chem. Eng. J. 423 (2021) 130218.
[226] Y.-B. Cho, A. Yu, C. Lee, M.H. Kim, Y. Lee, Fundamental study of facile and stable hydrogen evolution reaction at electrospun Ir and Ru mixed oxide nanofibers, ACS Appl. Mater. Interfaces 10 (2017) 541–549.
[227] Y. Yan, J. Lin, T. Xu, B. Liu, K. Huang, L. Qiao, S. Liu, J. Cao, S.C. Jun, Y. Yamauchi, J. Qi, Atomic-level platinum filling into Ni-vacancies of dual-deficient NiO for boosting electrocatalytic hydrogen evolution, Adv. Energy Mater. 12 (2022) 2200434.
[228] J. Li, J. Li, J. Ren, H. Hong, D. Liu, L. Liu, D. Wang, Electric-field-treated Ni/Co_3O_4 film as high-performance bifunctional electrocatalysts for efficient overall water splitting, Nano-Micro Lett. 14 (2022) 148.
[229] C. Zhang, H. Song, Z. Wang, Q. Ye, D. Zhang, Y. Zhao, J. Ma, Y. Cheng, Titanium dioxide and N-doped carbon hybrid nanofiber modulated Ru nanoclusters for high-efficient hydrogen evolution reaction electrocatalyst, Small (2024) 2311667.
[230] Y. Li, Z.G. Yu, L. Wang, Y. Weng, C.S. Tang, X. Yin, K. Han, H. Wu, X. Yu, L. M. Wong, D. Wan, X.R. Wang, J. Chai, Y.-W. Zhang, S. Wang, J. Wang, A.T. S. Wee, M.B.H. Breese, S.J. Pennycook, T. Venkatesan, S. Dong, J.M. Xue, J. Chen, Electronic-reconstruction-enhanced hydrogen evolution catalysis in oxide polymorphs, Nat. Commun. 10 (2019) 3149.
[231] J. Bai, J. Shang, J. Mei, X. Wang, C. Zhang, H. Kandambige, D.-C. Qi, T. Liao, Z. Sun, Hydrogen spillover intensified by Pt sites on single-crystalline MoO_3 interconnected branches for hydrogen evolution, ACS Energy Lett. 8 (2023) 3868–3875.
[232] J. Sun, S. Qin, Z. Zhao, Z. Zhang, X. Meng, Rapid carbothermal shocking fabrication of iron-incorporated molybdenum oxide with heterogeneous spin states for enhanced overall water/seawater splitting, Mater. Horiz. 11 (2024) 1199–1211.
[233] H. Chen, J. Yu, L. Liu, R.-T. Gao, Z. Gao, Y. Yang, Z. Chen, S. Zhan, X. Liu, X. Zhang, H. Dong, L. Wu, L. Wang, Modulating Pt-N/O bonds on Co-doped WO_3 for acid electrocatalytic hydrogen evolution with over 2000 h operation, Adv. Energy Mater. 14 (2024) 2303635.
[234] Z. Chen, W. Gong, J. Wang, S. Hou, G. Yang, C. Zhu, X. Fan, Y. Li, R. Gao, Y. Cui, Metallic W/WO_2 solid-acid catalyst boosts hydrogen evolution reaction in alkaline electrolyte, Nat. Commun. 14 (2023) 5363.
[235] S. Rojas, Durable MnO_2 electrocatalysts by stronger Mn-O bonds, Nat. Catal. 7 (2024) 227–228.
[236] P. Zhou, G. Hai, G. Zhao, R. Li, X. Huang, Y. Lu, G. Wang, CeO_2 as an "electron pump" to boost the performance of Co_4N in electrocatalytic hydrogen evolution, oxygen evolution and biomass oxidation valorization, Appl. Catal. B-Environ. 325 (2023) 122364.
[237] M.S. Alom, C.C.W. Kananke-Gamage, F. Ramezanipour, Perovskite oxides as electrocatalysts for hydrogen evolution reaction, ACS Omega 7 (2022) 7444–7451.
[238] J. Ma, H. Wei, Y. Liu, X. Ren, Y. Li, F. Wang, X. Han, E. Xu, X. Cao, G. Wang, F. Ren, S. Wei, Application of Co_3O_4-based materials in electrocatalytic hydrogen evolution reaction: a review, Int. J. Hydrog. Energy 45 (2020) 21205–21220.
[239] D.S.A. Pratama, A. Haryanto, C.W. Lee, Heterostructured mixed metal oxide electrocatalyst for the hydrogen evolution reaction, Front. Chem. 11 (2023), https://doi.org/10.3389/fchem.2023.1141361.
[240] R. Li, D. Zhou, J. Luo, W. Xu, J. Li, S. Li, P. Cheng, D. Yuan, The urchin-like sphere arrays Co_3O_4 as a bifunctional catalyst for hydrogen evolution reaction and oxygen evolution reaction, J. Power Sources 341 (2017) 250–256.
[241] H. Zhang, J. Zhang, Y. Li, H. Jiang, H. Jiang, C. Li, Continuous oxygen vacancy engineering of the Co_3O_4 layer for an enhanced alkaline electrocatalytic hydrogen evolution reaction, J. Mater. Chem. A 7 (2019) 13506–13510.
[242] Z. Wang, H. Liu, R. Ge, X. Ren, J. Ren, D. Yang, L. Zhang, X. Sun, Phosphorus-doped Co_3O_4 nanowire array: a highly efficient bifunctional electrocatalyst for overall water splitting, ACS Catal. 8 (2018) 2236–2241.
[243] R.A. Krivina, Y. Ou, Q. Xu, L.P. Twight, T.N. Stovall, S.W. Boettcher, Oxygen electrocatalysis on mixed-metal oxides/oxyhydroxides: from fundamentals to membrane electrolyzer technology, Acc. Chem. Res. 2 (2021) 548–558.
[244] D. Gao, R. Liu, J. Biskupek, U. Kaiser, Y.-F. Song, C. Streb, Modular design of noble-metal-free mixed metal oxide electrocatalysts for complete water splitting, Angew. Chem. Int. Ed. 58 (2019) 4644–4648.
[245] S. Samira, X.-K. Gu, E. Nikolla, Design strategies for efficient nonstoichiometric mixed metal oxide electrocatalysts: correlating measurable oxide properties to electrocatalytic performance, ACS Catal. 9 (2019) 10575–10586.
[246] X. Lu, J. Pan, E. Lovell, T.H. Tan, Y.H. Ng, R. Amal, A sea-change: manganese doped nickel/nickel oxide electrocatalysts for hydrogen generation from seawater, Energy Environ. Sci. 11 (2018) 1898–1910.
[247] Y. Ou, W. Tian, L. Liu, Y. Zhang, P. Xiao, Bimetallic $Co_2Mo_3O_8$ suboxides coupled with conductive cobalt nanowires for efficient and durable hydrogen evolution in alkaline electrolyte, J. Mater. Chem. A 6 (2018) 5217–5228.
[248] Z. Wang, P. Guo, S. Cao, H. Chen, S. Zhou, H. Liu, H. Wang, J. Zhang, S. Liu, S. Wei, D. Sun, X. Lu, Contemporaneous inverse manipulation of the valence configuration to preferred Co^{2+} and Ni^{3+} for enhanced overall water electrocatalysis, Appl. Catal. B-Environ. 284 (2021) 119725.
[249] S. Li, S. Sirisomboonchai, A. Yoshida, X. An, X. Hao, A. Abudula, G. Guan, Bifunctional CoNi/$CoFe_2O_4$/Ni foam electrodes for efficient overall water splitting at a high current density, J. Mater. Chem. A 6 (2018) 19221–19230.
[250] Z. Luo, Q. Peng, Z. Huang, L. Wang, Y. Yang, J. Dong, T.T. Isimjan, X. Yang, Fine-tune *d*-band center of cobalt vanadium oxide nanosheets by N-doping as a robust overall water splitting electrocatalyst, J. Colloid Interface Sci. 629 (2023) 111–120.
[251] J. Sun, S. Qin, Z. Zhang, C. Li, X. Xu, Z. Li, X. Meng, Joule heating synthesis of well lattice-matched $Co_2Mo_3O_8$/MoO_2 heterointerfaces with greatly improved hydrogen evolution reaction in alkaline seawater electrolysis with 12.4% STH efficiency, Appl. Catal. B-Environ. 338 (2023) 123015.
[252] X.Y. Zhang, H. Yuan, F. Mao, C.F. Wen, L.R. Zheng, P.F. Liu, H.G. Yang, Boosting alkaline hydrogen evolution electrocatalysis over metallic nickel sites through synergistic coupling with vanadium sesquioxide, ChemSusChem 12 (2019) 5063–5069.
[253] X. Chen, M. Wei, J. Zhou, Fluorine-doping-assisted vacancy engineering for efficient electrocatalyst toward hydrogen production, J. Mater. Chem. A 9 (2021) 22626–22634.
[254] Y. Gong, Z. Yang, Y. Lin, J. Wang, H. Pan, Z. Xu, Hierarchical heterostructure $NiCo_2O_4$@$CoMoO_4$/NF as an efficient bifunctional electrocatalyst for overall water splitting, J. Mater. Chem. A 6 (2018) 16950–16958.
[255] Y. Wang, B. Kong, D. Zhao, H. Wang, C. Selomulya, Strategies for developing transition metal phosphides as heterogeneous electrocatalysts for water splitting, Nano Today 15 (2017) 26–55.
[256] J. Su, J. Zhou, L. Wang, C. Liu, Y. Chen, Synthesis and application of transition metal phosphides as electrocatalyst for water splitting, Sci. Bull. 62 (2017) 633–644.
[257] H. Zhang, A.W. Maijenburg, X. Li, S.L. Schweizer, R.B. Wehrspohn, Bifunctional heterostructured transition metal phosphides for efficient electrochemical water splitting, Adv. Funct. Mater. 30 (2020) 2003261.
[258] Y. He, X. Zhu, C. Zhang, Z. Liu, B. Cao, L. Sheng, Y. Yang, Q. Feng, N. Wang, J. Z. Ou, Y. Xu, Self-circulating adsorption-desorption structure of non-noble high-entropy alloy electrocatalyst facilitates efficient water splitting, ACS Sustain. Chem. Eng. 11 (2023) 5055–5064.
[259] M. Du, D. Li, S. Liu, J. Yan, Transition metal phosphides: a wonder catalyst for electrocatalytic hydrogen production, Chin. Chem. Lett. 34 (2023) 108156.
[260] H. Yin, F. Rong, Y. Xie, A review of typical transition metal phosphides electrocatalysts for hydrogen evolution reaction, Int. J. Hydrog. Energy 52 (2024) 350–375.
[261] Z. Ge, B. Fu, J. Zhao, X. Li, B. Ma, Y. Chen, A review of the electrocatalysts on hydrogen evolution reaction with an emphasis on Fe, Co and Ni-based phosphides, J. Mater. Sci. 55 (2020) 14081–14104.
[262] D. Liu, G. Xu, H. Yang, H. Wang, B.Y. Xia, Rational design of transition metal phosphide-based electrocatalysts for hydrogen evolution, Adv. Funct. Mater. 33 (2023) 2208358.
[263] L. Tan, J. Yu, H. Wang, H. Gao, X. Liu, L. Wang, X. She, T. Zhan, Controllable synthesis and phase-dependent catalytic performance of dual-phase nickel selenides on Ni foam for overall water splitting, Appl. Catal. B-Environ. 303 (2022) 120915.
[264] T. Xiong, J. Li, J. Chandra Roy, M. Koroma, Z. Zhu, H. Yang, L. Zhang, T. Ouyang, M.S. Balogun, M. Al-Mamun, Hetero-interfacial nickel nitride/vanadium

oxynitride porous nanosheets as trifunctional electrodes for HER, OER and sodium ion batteries, J. Energy Chem. 81 (2023) 71–81.
[265] L. Men, Y. Zhang, X. Li, Q. Pan, J. Li, Z. Su, Highly active bimetallic phosphide electrocatalysts for hydrogen evolution, N. J. Chem. 47 (2023) 11459–11464.
[266] Y. Bai, H. Zhang, Y. Feng, L. Fang, Y. Wang, Sandwich-like CoP/C nanocomposites as efficient and stable oxygen evolution catalysts, J. Mater. Chem. A 4 (2016) 9072–9079.
[267] X. Peng, X. Jin, B. Gao, Z. Liu, P.K. Chu, Strategies to improve cobalt-based electrocatalysts for electrochemical water splitting, J. Catal. 398 (2021) 54–66.
[268] C. Wang, J. Jiang, T. Ding, G. Chen, W. Xu, Q. Yang, Monodisperse ternary NiCoP Nanostructures as a bifunctional electrocatalyst for both hydrogen and oxygen evolution reactions with excellent performance, Adv. Mater. Interfaces 3 (2015).
[269] H. Liu, J. Li, Y. Zhang, R. Ge, J. Yang, Y. Li, J. Zhang, M. Zhu, S. Li, B. Liu, L. Dai, W. Li, Boosted water electrolysis capability of Ni_xCo_yP via charge redistribution and surface activation, Chem. Eng. J. 473 (2023) 145397.
[270] D. Chen, H. Bai, J. Zhu, C. Wu, H. Zhao, D. Wu, J. Jiao, P. Ji, S. Mu, Multiscale hierarchical structured NiCoP enabling ampere-level water splitting for multi-scenarios green energy-to-hydrogen systems, Adv. Energy Mater. 13 (2023) 2300499.
[271] J. Lee, H. Jung, Y.S. Park, N. Kwon, S. Woo, N.C.S. Selvam, G.S. Han, H.S. Jung, P. J. Yoo, S.M. Choi, J.W. Han, B. Lim, Chemical transformation approach for high-performance ternary NiFeCo metal compound-based water splitting electrodes, Appl. Catal. B-Environ. 294 (2021) 120246.
[272] Y. Shi, B. Zhang, Recent advances in transition metal phosphide nanomaterials: synthesis and applications in hydrogen evolution reaction, Chem. Soc. Rev. 45 (2016) 1529–1541.
[273] H. Du, R.-M. Kong, X. Guo, F. Qu, J. Li, Recent progress in transition metal phosphides with enhanced electrocatalysis for hydrogen evolution, Nanoscale 10 (2018) 21617–21624.
[274] Y. Li, R. Li, D. Wang, H. Xu, F. Meng, D. Dong, J. Jiang, J. Zhang, M. An, P. Yang, A review: target-oriented transition metal phosphide design and synthesis for water splitting, Int. J. Hydrog. Energy 46 (2021) 5131–5149.
[275] Y. Chu, D. Wang, X. Shan, C. Liu, W. Wang, N. Mitsuzaki, Z. Chen, Activity engineering to transition metal phosphides as bifunctional electrocatalysts for efficient water-splitting, Int. J. Hydrog. Energy 47 (2022) 38983–39000.
[276] Z. Wang, S. Wang, L. Ma, Y. Guo, J. Sun, N. Zhang, R. Jiang, Water-induced formation of Ni_2P-$Ni_{12}P_5$ interfaces with superior electrocatalytic activity toward hydrogen evolution reaction, Small 17 (2021) 2006770.
[277] J. Zhang, Z. Zhang, Y. Ji, J. Yang, K. Fan, X. Ma, C. Wang, R. Shu, Y. Chen, Surface engineering induced hierarchical porous $Ni_{12}P_5$-Ni_2P polymorphs catalyst for efficient wide pH hydrogen production, Appl. Catal. B-Environ. 282 (2021) 119609.
[278] J. Li, G. Wei, Y. Zhu, Y. Xi, X. Pan, Y. Ji, I.V. Zatovsky, W. Han, Hierarchical NiCoP nanocone arrays supported on Ni foam as an efficient and stable bifunctional electrocatalyst for overall water splitting, J. Mater. Chem. A 5 (2017) 14828–14837.
[279] H. Liu, Y. Zhang, R. Ge, J.M. Cairney, R. Zheng, A. Khan, S. Li, B. Liu, L. Dai, W. Li, Tailoring the electronic structure of Ni_5P_4/Ni_2P catalyst by Co_2P for efficient overall water electrolysis, Appl. Energy 349 (2023) 121582.
[280] Y.-Q. Wang, L. Zhao, X.-L. Sui, D.-M. Gu, Z.-B. Wang, Hierarchical CoP_3/$NiMoO_4$ heterostructures on Ni foam as an efficient bifunctional electrocatalyst for overall water splitting, Ceram. Int. 45 (2019) 17128–17136.
[281] X. Chen, L. Sheng, S. Li, Y. Cui, T. Lin, X. Que, Z. Du, Z. Zhang, J. Peng, H. Ma, J. Li, J. Qiu, M. Zhai, Facile syntheses and in-situ study on electrocatalytic properties of superaerophobic CoP-nanoarray in hydrogen evolution reaction, Chem. Eng. J. 426 (2021) 131029.
[282] R.B. Ghising, U.N. Pan, D.R. Paudel, M.R. Kandel, N.H. Kim, J.H. Lee, A hybrid trimetallic-organic framework-derived N, C co-doped Ni-Fe-Mn-P ultrathin nanosheet electrocatalyst for proficient overall water-splitting, J. Mater. Chem. A 10 (2022) 16457–16467.
[283] D. Duan, D. Guo, J. Gao, S. Liu, Y. Wang, Electrodeposition of cobalt-iron bimetal phosphide on Ni foam as a bifunctional electrocatalyst for efficient overall water splitting, J. Colloid Interface Sci. 622 (2022) 250–260.
[284] H. Li, X. Gao, G. Li, Construction of Co_2P-Ni_3S_2/NF heterogeneous structural hollow nanowires as bifunctional electrocatalysts for efficient overall water splitting, Small 19 (2023) 2304081.
[285] Y. Deng, S. Xiao, Y. Zheng, X. Rong, M. Bai, Y. Tang, T. Ma, C. Cheng, C. Zhao, Emerging electrocatalytic activities in transition metal selenides: synthesis, electronic modulation, and structure-performance correlations, Chem. Eng. J. 451 (2023) 138514.
[286] R. Gao, H. Zhang, D. Yan, Iron diselenide nanoplatelets: stable and efficient water-electrolysis catalysts, Nano Energy 31 (2017) 90–95.
[287] Y. Liu, H. Cheng, M. Lyu, S. Fan, Q. Liu, W. Zhang, Y. Zhi, C. Wang, C. Xiao, S. Wei, B. Ye, Y. Xie, Low overpotential in vacancy-rich ultrathin $CoSe_2$ nanosheets for water oxidation, J. Am. Chem. Soc. 136 (2014) 15670–15675.
[288] D. Kong, H. Wang, J.J. Cha, M. Pasta, K.J. Koski, J. Yao, Y. Cui, Synthesis of MoS_2 and $MoSe_2$ films with vertically aligned layers, Nano Lett. 13 (2013) 1341–1347.
[289] Z. Lei, S. Xu, P. Wu, Ultra-thin and porous $MoSe_2$ nanosheets: facile preparation and enhanced electrocatalytic activity towards the hydrogen evolution reaction, Phys. Chem. Chem. Phys. 18 (2016) 70–74.
[290] C. Xu, S. Peng, C. Tan, H. Ang, H. Tan, H. Zhang, Q. Yan, Ultrathin S-doped $MoSe_2$ nanosheets for efficient hydrogen evolution, J. Mater. Chem. A 2 (2014) 5597–5601.
[291] H.I. Karunadasa, E. Montalvo, Y. Sun, M. Majda, J.R. Long, C.J. Chang, A molecular MoS_2 edge site mimic for catalytic hydrogen generation, Science 335 (2012) 698–702.
[292] X. Zhao, Y. Zhao, B. Huang, W. Cai, J. Sui, Z. Yang, H.-E. Wang, $MoSe_2$ nanoplatelets with enriched active edge sites for superior sodium-ion storage and enhanced alkaline hydrogen evolution activity, Chem. Eng. J. 382 (2020) 123047.
[293] I. Hussain, S. Sahoo, C. Lamiel, T.T. Nguyen, M. Ahmed, C. Xi, S. Iqbal, A. Ali, N. Abbas, M.S. Javed, K. Zhang, Research progress and future aspects: metal selenides as effective electrodes, Energy Storage Mater. 47 (2022) 13–43.
[294] H. Wu, X. Lu, G. Zheng, G.W. Ho, Topotactic engineering of ultrathin 2D nonlayered nickel selenides for full water electrolysis, Adv. Energy Mater. 8 (2018) 1702704.
[295] H. Zhou, F. Yu, Y. Huang, J. Sun, Z. Zhu, R.J. Nielsen, R. He, J. Bao, W.A. Goddard Iii, S. Chen, Z. Ren, Efficient hydrogen evolution by ternary molybdenum sulfoselenide particles on self-standing porous nickel diselenide foam, Nat. Commun. 7 (2016) 12765.
[296] J. Jia, W. Zhou, G. Li, L. Yang, Z. Wei, L. Cao, Y. Wu, K. Zhou, S. Chen, Regulated synthesis of Mo sheets and their derivative MoX sheets (X: P, S, or C) as efficient electrocatalysts for hydrogen evolution reactions, ACS Appl. Mater. Interfaces 9 (2017) 8041–8046.
[297] S. Deng, M. Luo, C. Ai, Y. Zhang, B. Liu, L. Huang, Z. Jiang, Q. Zhang, L. Gu, S. Lin, X. Wang, L. Yu, J. Wen, J. Wang, G. Pan, X. Xia, J. Tu, Synergistic doping and intercalation: realizing deep phase modulation on MoS_2 arrays for high-efficiency hydrogen evolution reaction, Angew. Chem. Int. Ed. 58 (2019) 16289–16296.
[298] Y. Cao, Roadmap and direction toward high-performance MoS_2 hydrogen evolution catalysts, ACS Nano 15 (2021) 11014–11039.
[299] B. Liu, Y.F. Zhao, H.Q. Peng, Z.Y. Zhang, C.K. Sit, M.F. Yuen, T.R. Zhang, C.S. Lee, W.J. Zhang, Nickel-cobalt diselenide 3D mesoporous nanosheet networks supported on Ni foam: an all-ph highly efficient integrated electrocatalyst for hydrogen evolution, Adv. Mater. 29 (2017) 1606521.
[300] J. Huang, S. Wang, J. Nie, C. Huang, X. Zhang, B. Wang, J. Tang, C. Du, Z. Liu, J. Chen, Active site and intermediate modulation of 3D $CoSe_2$ nanosheet array on Ni foam by Mo doping for high-efficiency overall water splitting in alkaline media, Chem. Eng. J. 417 (2021) 128055.
[301] A. Sivanantham, S. Shanmugam, Nickel selenide supported on nickel foam as an efficient and durable non-precious electrocatalyst for the alkaline water electrolysis, Appl. Catal. B-Environ. 203 (2017) 485–493.
[302] K. Akbar, J.H. Jeon, M. Kim, J. Jeong, Y. Yi, S.-H. Chun, Bifunctional electrodeposited 3D $NiCoSe_2$/nickle foam electrocatalysts for its applications in enhanced oxygen evolution reaction and for hydrazine oxidation, ACS Sustain. Chem. Eng. 6 (2018) 7735–7742.
[303] Y. Huang, L.-W. Jiang, X.-L. Liu, T. Tan, H. Liu, J.-J. Wang, Precisely engineering the electronic structure of active sites boosts the activity of iron-nickel selenide on nickel foam for highly efficient and stable overall water splitting, Appl. Catal. B-Environ. 299 (2021) 120678.
[304] L. Tian, K. Wang, H. Wo, X. Pang, X. Zhai, W. Zhuang, T. Li, Y. Chen, Bundle-shaped cobalt-nickel selenides as advanced electrocatalysts for water oxidation, Int. J. Hydrog. Energy 44 (2019) 2868–2876.
[305] Y. Li, Y. Zhang, X. Tong, X. Wang, L. Zhang, X. Xia, J. Tu, Recent progress on the phase modulation of molybdenum disulphide/diselenide and their applications in electrocatalysis, J. Mater. Chem. A 9 (2021) 1418–1428.
[306] X. Peng, Y. Yan, X. Jin, C. Huang, W. Jin, B. Gao, P.K. Chu, Recent advance and prospectives of electrocatalysts based on transition metal selenides for efficient water splitting, Nano Energy 78 (2020) 105234.
[307] M.F. Iqbal, W. Gao, Z. Mao, E. Hu, X. Gao, J. Zhang, Z. Chen, Strategies to enhance the electrocatalytic behavior of metal selenides for hydrogen evolution reaction: a review, Int. J. Hydrog. Energy 48 (2023) 36722–36749.
[308] L. Zhang, S. Shen, J. Zhang, Z. Lin, Z. Wang, Q. Zhang, W. Zhong, L. Zhu, G. Wu, Interlayer spacing regulation of molybdenum selenide promotes electrocatalytic hydrogen evolution in alkaline media, Small Methods 6 (2022) 2200900.
[309] Z. Luo, L. Tong, Z. Lin, R.S. Amin, J. Ren, K.M. El-Khatib, C. Wang, Ferrum-doped nickel selenide@tri-nickel diselenide heterostructure electrocatalysts with efficient and stable water splitting for hydrogen and oxygen production, Adv. Compos. Hybrid. Mater. 6 (2023) 159.
[310] N. Chen, Y.-X. Du, G. Zhang, W.-T. Lu, F.-F. Cao, Amorphous nickel sulfoselenide for efficient electrochemical urea-assisted hydrogen production in alkaline media, Nano Energy 81 (2021) 105605.
[311] X. Xu, P. Du, Z. Chen, M. Huang, An electrodeposited cobalt-selenide-based film as an efficient bifunctional electrocatalyst for full water splitting, J. Mater. Chem. A 4 (2016) 10933–10939.
[312] F. Ming, H. Liang, H. Shi, X. Xu, G. Mei, Z. Wang, MOF-derived Co-doped nickel selenide/C electrocatalysts supported on Ni foam for overall water splitting, J. Mater. Chem. A 4 (2016) 15148–15155.
[313] R.B. Ghising, U.N. Pan, M.R. Kandel, P.P. Dhakal, S. Prabhakaran, D.H. Kim, N. H. Kim, J.H. Lee, Bimetallic-organic frameworks derived heterointerface arrangements of V, N co-doped Co/Fe-selenide nanosheets electrocatalyst for efficient overall water-splitting, Mater. Today Nano 24 (2023) 100390.
[314] H. Ren, L. Yu, L. Yang, Z.-H. Huang, F. Kang, R. Lv, Efficient electrocatalytic overall water splitting and structural evolution of cobalt iron selenide by one-step electrodeposition, J. Energy Chem. 60 (2021) 194–201.
[315] R.T. Hannagan, G. Giannakakis, M. Flytzani-Stephanopoulos, E.C.H. Sykes, Single-atom alloy catalysis, Chem. Rev. 120 (2020) 12044–12088.
[316] N. Kumar Katiyar, K. Biswas, J.-W. Yeh, S. Sharma, C. Sekhar Tiwary, A perspective on the catalysis using the high entropy alloys, Nano Energy 88 (2021) 106261.
[317] Y. Nakaya, S. Furukawa, Catalysis of alloys: classification, principles, and design for a variety of materials and reactions, Chem. Rev. 123 (2023) 5859–5947.

[318] Y. Qiao, M. Peng, J. Lan, K. Jiang, D. Chen, Y. Tan, Active-site engineering in dealloyed nanoporous catalysts for electrocatalytic water splitting, J. Mater. Chem. A 11 (2023) 495–511.
[319] M. Du, X. Li, H. Pang, Q. Xu, Alloy electrocatalysts, EnergyChem 5 (2023) 100083.
[320] Y. Wu, Y. Liu, K. Liu, L. Wang, L. Zhang, D. Wang, Z. Chai, W. Shi, Hierarchical and self-supporting honeycomb $LaNi_5$ alloy on nickel foam for overall water splitting in alkaline media, Green. Energy Environ. 7 (2022) 799–806.
[321] Q. Zhou, Q. Hao, Y. Li, J. Yu, C. Xu, H. Liu, S. Yan, Free-standing trimodal porous NiZn intermetallic and Ni heterojunction as highly efficient hydrogen evolution electrocatalyst in the alkaline electrolyte, Nano Energy 89 (2021) 106402.
[322] M. Gong, D.-Y. Wang, C.-C. Chen, B.-J. Hwang, H. Dai, A mini review on nickel-based electrocatalysts for alkaline hydrogen evolution reaction, Nano Res. 9 (2016) 28–46.
[323] L. Ji, C. Lv, Z. Chen, Z. Huang, C. Zhang, Nickel-based (photo)electrocatalysts for hydrogen production, Adv. Mater. 30 (2018) 1705653.
[324] J. Li, S. Wang, J. Chang, L. Feng, A review of Ni based powder catalyst for urea oxidation in assisting water splitting reaction, Adv. Powder Mater. 1 (2022) 100030.
[325] R.A. Mir, D.W. Kirk, S.J. Thorpe, Recent progress and advances in nickel (Ni) based amorphous metal alloys towards alkaline water splitting: a review, J. Alloy. Compd. 976 (2024) 173211.
[326] Y.-C. Qin, F.-Q. Wang, X.-M. Wang, M.-W. Wang, W.-L. Zhang, W.-K. An, X.-P. Wang, Y.-L. Ren, X. Zheng, D.-C. Lv, A. Ahmad, Noble metal-based high-entropy alloys as advanced electrocatalysts for energy conversion, Rare Met 40 (2021) 2354–2368.
[327] N.B. Ysea, V. Benavente Llorente, A. Loiácono, L. Lagucik Marquez, L. Diaz, G. I. Lacconi, E.A. Franceschini, Critical insights from alloys and composites of Ni-based electrocatalysts for HER on NaCl electrolyte, J. Alloy. Compd. 915 (2022) 165352.
[328] J. Wang, S. Xin, Y. Xiao, Z. Zhang, Z. Li, W. Zhang, C. Li, R. Bao, J. Peng, J. Yi, S. Chou, Manipulating the water dissociation electrocatalytic sites of bimetallic nickel-based alloys for highly efficient alkaline hydrogen evolution, Angew. Chem. Int. Ed. 61 (2022) e202202518.
[329] A. Kumar, S.K. Purkayastha, A.K. Guha, M.R. Das, S. Deka, Designing nanoarchitecture of NiCu dealloyed nanoparticles on hierarchical Co nanosheets for alkaline overall water splitting at low cell voltage, ACS Catal. 13 (2023) 10615–10626.
[330] Q. Sun, Y. Dong, Z. Wang, S. Yin, C. Zhao, Synergistic nanotubular copper-doped nickel catalysts for hydrogen evolution reactions, Small 14 (2018) 1704137.
[331] K. Tu, D. Tranca, F. Rodríguez-Hernández, K. Jiang, S. Huang, Q. Zheng, M.-X. Chen, C. Lu, Y. Su, Z. Chen, H. Mao, C. Yang, J. Jiang, H.-W. Liang, X. Zhuang, A novel heterostructure based on RuMo nanoalloys and N-doped carbon as an efficient electrocatalyst for the hydrogen evolution reaction, Adv. Mater. 32 (2020) 2005433.
[332] X. Wang, X. Xu, Y. Nie, R. Wang, J. Zou, Electronic-state modulation of metallic Co-assisted Co_7Fe_3 alloy heterostructure for highly efficient and stable overall water splitting, Adv. Sci. 10 (2023) 2301961.
[333] T. Ren, X. Huang, J. Chen, G. Wang, Y. Liu, F. Bao, W. Guo, Surface-sulphurated nickel-molybdenum alloy film as enhanced electrocatalysts for alkaline overall water splitting, Int. J. Hydrog. Energy 57 (2024) 983–989.
[334] X. Shi, X. Zheng, H. Wang, H. Zhang, M. Qin, B. Lin, M. Qi, S. Mao, H. Ning, R. Yang, L. Xi, Y. Wang, Hierarchical crystalline/amorphous heterostructure $MoNi/NiMoO_x$ for electrochemical hydrogen evolution with industry-level activity and stability, Adv. Funct. Mater. 33 (2023) 2307109.
[335] Z. Zhao, J. Sun, X. Li, Z. Zhang, X. Meng, Joule heating synthesis of NiFe alloy/MoO_2 and in-situ transformed (Ni,Fe)OOH/MoO_2 heterostructure as effective complementary electrocatalysts for overall splitting in alkaline seawater, Appl. Catal. B-Environ. 340 (2024) 123277.
[336] C.-T. Hsieh, C.-L. Huang, Y.-A. Chen, S.-Y. Lu, NiFeMo alloy inverse-opals on Ni foam as outstanding bifunctional catalysts for electrolytic water splitting of ultra-low cell voltages at high current densities, Appl. Catal. B-Environ. 267 (2020) 118376.
[337] T.A.A. Batchelor, J.K. Pedersen, S.H. Winther, I.E. Castelli, K.W. Jacobsen, J. Rossmeisl, High-entropy alloys as a discovery platform for electrocatalysis, Joule 3 (2019) 834–845.
[338] H. Li, J. Lai, Z. Li, L. Wang, Multi-sites electrocatalysis in high-entropy alloys, Adv. Funct. Mater. 31 (2021) 2106715.
[339] Y. Li, Z. Yao, W. Gao, W. Shang, T. Deng, J. Wu, Nanoscale design for high entropy alloy electrocatalysts, Small (2023) 2310006.
[340] P. Das, Y. Dong, X. Wu, Y. Zhu, Z.-S. Wu, Perspective on high entropy MXenes for energy storage and catalysis, Sci. Bull. 68 (2023) 1735–1739.
[341] J.-T. Ren, L. Chen, H.-Y. Wang, Z.-Y. Yuan, High-entropy alloys in electrocatalysis: from fundamentals to applications, Chem. Soc. Rev. 52 (2023) 8319–8373.
[342] X. Han, G. Wu, S. Zhao, J. Guo, M. Yan, X. Hong, D. Wang, Nanoscale high-entropy alloy for electrocatalysis, Matter 6 (2023) 1717–1751.
[343] Y. Wang, H. Yang, Z. Zhang, X. Meng, T. Cheng, G. Qin, S. Li, Far-from-equilibrium electrosynthesis ramifies high-entropy alloy for alkaline hydrogen evolution, J. Mater. Sci. Technol. 166 (2023) 234–240.
[344] A. Sivanantham, H. Lee, S.W. Hwang, H.U. Lee, S.B. Cho, B. Ahn, I.S. Cho, Complementary functions of vanadium in boosting electrocatalytic activity of CuCoNiFeMn high-entropy alloy for water splitting, Adv. Funct. Mater. 33 (2023) 2301153.
[345] H. Shi, X.-Y. Sun, S.-P. Zeng, Y. Liu, G.-F. Han, T.-H. Wang, Z. Wen, Q.-R. Fang, X.-Y. Lang, Q. Jiang, Nanoporous nonprecious high-entropy alloys as multisite electrocatalysts for ampere-level current-density hydrogen evolution, Small Struct. 4 (2023) 2300042.
[346] Q. Mo, W. Zhang, L. He, X. Yu, Q. Gao, Bimetallic $Ni_{2-x}Co_xP$/N-doped carbon nanofibers: solid-solution-alloy engineering toward efficient hydrogen evolution, Appl. Catal. B-Environ. 244 (2019) 620–627.
[347] D. Senthil Raja, Y.-C. Ting, T.-Y. Lin, C.-C. Cheng, P.-W. Chen, F.-Y. Yen, S.-Y. Lu, Quad-metallic MOF-derived carbon-armored pseudo-high entropy alloys as a bifunctional electrocatalyst for alkaline water electrolysis at high current densities, J. Mater. Chem. A 11 (2023) 25283–25297.
[348] H. Shi, X.-Y. Sun, S.-P. Zeng, Y. Liu, G.-F. Han, T.-H. Wang, Z. Wen, Q.-R. Fang, X.-Y. Lang, Q. Jiang, Nanoporous nonprecious high-entropy alloys as multisite electrocatalysts for ampere-level current-density hydrogen evolution, Small Struct. 4 (2023) 2300042.
[349] H. Liu, H. Qin, J. Kang, L. Ma, G. Chen, Q. Huang, Z. Zhang, E. Liu, H. Lu, J. Li, N. Zhao, A freestanding nanoporous NiCoFeMoMn high-entropy alloy as an efficient electrocatalyst for rapid water splitting, Chem. Eng. J. 435 (2022) 134898.
[350] Y.-H. Chang, C.-T. Lin, T.-Y. Chen, C.-L. Hsu, Y.-H. Lee, W. Zhang, K.-H. Wei, L.-J. Li, Highly efficient electrocatalytic hydrogen production by MoS_x grown on graphene-protected 3D Ni foams, Adv. Mater. 25 (2013) 756–760.
[351] M. Liu, Z. Sun, S. Li, X. Nie, Y. Liu, E. Wang, Z. Zhao, Hierarchical superhydrophilic/superaerophobic CoMnP/Ni_2P nanosheet-based microplate arrays for enhanced overall water splitting, J. Mater. Chem. A 9 (2021) 22129–22139.
[352] Y. Gong, L. Wang, H. Xiong, M. Shao, L. Xu, A. Xie, S. Zhuang, Y. Tang, X. Yang, Y. Chen, P. Wan, 3D self-supported Ni nanoparticle@N-doped carbon nanotubes anchored on NiMoN pillars for the hydrogen evolution reaction with high activity and anti-oxidation ability, J. Mater. Chem. A 7 (2019) 13671–13678.
[353] N. Shaikh, I. Mukhopadhyay, A. Ray, Heterointerfaces of nickel sulphides and selenides on Ni-foam as efficient bifunctional electrocatalysts in acidic environments, J. Mater. Chem. A 10 (2022) 12733–12746.
[354] R. Zhang, L. Xu, Z. Wu, L. Wang, J. Zhang, Y. Tang, L. Xu, A. Xie, Y. Chen, H. Zhang, P. Wan, Nitrogen doped carbon encapsulated hierarchical NiMoN as highly active and durable HER electrode for repeated ON/OFF water electrolysis, Chem. Eng. J. 436 (2022) 134931.
[355] J. Chen, Z. Hu, Y. Ou, Q. Zhang, X. Qi, L. Gu, T. Liang, Interfacial engineering regulated by CeO_x to boost efficiently alkaline overall water splitting and acidic hydrogen evolution reaction, J. Mater. Sci. Technol. 120 (2022) 129–138.
[356] B. Cao, Y. Cheng, M. Hu, P. Jing, Z. Ma, B. Liu, R. Gao, J. Zhang, Efficient and durable 3D self-supported nitrogen-doped carbon-coupled nickel/cobalt phosphide electrodes: stoichiometric ratio regulated phase- and morphology-dependent overall water splitting performance, Adv. Funct. Mater. 29 (2019) 1906316.
[357] B. Liu, Y.-F. Zhao, H.-Q. Peng, Z.-Y. Zhang, C.-K. Sit, M.-F. Yuen, T.-R. Zhang, C.-S. Lee, W.-J. Zhang, Nickel-cobalt diselenide 3D mesoporous nanosheet networks supported on Ni foam: an all-pH highly efficient integrated electrocatalyst for hydrogen evolution, Adv. Mater. 29 (2017) 1606521.
[358] Y. Yang, H. Yao, Z. Yu, S.M. Islam, H. He, M. Yuan, Y. Yue, K. Xu, W. Hao, G. Sun, H. Li, S. Ma, P. Zapol, M.G. Kanatzidis, Hierarchical nanoassembly of MoS_2/Co_9S_8/Ni_3S_2/Ni as a highly efficient electrocatalyst for overall water splitting in a wide ph range, J. Am. Chem. Soc. 141 (2019) 10417–10430.
[359] H. Zhao, X. Jiang, M. Jin, J. Song, M. Li, J. Zhou, X. Pan, Construction of urchin-like bimetallic phosphides induced by carbon dots for efficient wide pH hydrogen production, J. Colloid Interface Sci. 652 (2023) 1208–1216.
[360] W. Zhai, Y. Ma, D. Chen, J.C. Ho, Z. Dai, Y. Qu, Recent progress on the long-term stability of hydrogen evolution reaction electrocatalysts, InfoMat 4 (2022) e12357.
[361] T. Wu, M. Sun, H.H. Wong, C.H. Chan, L. Lu, Q. Lu, B. Chen, B. Huang, Recent advances and strategies of electrocatalysts for large current density industrial hydrogen evolution reaction, Inorg. Chem. Front. 10 (2023) 4632–4649.
[362] W. Xu, H. Wang, Earth-abundant amorphous catalysts for electrolysis of water, Chin. J. Catal. 38 (2017) 991–1005.
[363] B. Zhou, R. Gao, J.J. Zou, H. Yang, Surface design strategy of catalysts for water electrolysis, Small 18 (2022) 2202336.
[364] I.T. McCrum, M.T.M. Koper, The role of adsorbed hydroxide in hydrogen evolution reaction kinetics on modified platinum, Nat. Energy 5 (2020) 891–899.